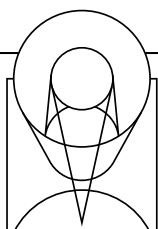


Westerlund 2

NASA, ESA, the Hubble Heritage Team (STScI/AURA),
A. Nota (ESA/STScI), and the Westerlund 2 Science Team

[2015] VOL [32] ISSUE [02]



NEWSLETTER

Space Telescope Science Institute

Hubble's 25th Anniversary and Beyond

Hussein Jirdeh, jirdeh@stsci.edu, and Carol Christian, carolc@stsci.edu

Introduction

In 2015, we marked the 25th year of the *Hubble Space Telescope's* journey of enabling scientific discovery and engagement of the public. Looking back to April 24, 1990, as the space shuttle *Discovery* lifted off from Earth with the *Hubble Space Telescope* nestled securely in its bay, followed by the telescope's release into space, anticipation was high for the success of the mission. Over its history, *Hubble* indeed has invigorated and reshaped our perception of the cosmos and uncovered a universe where almost anything within the laws of physics seems possible.

This year, we celebrated achievements of *Hubble* by reflecting on the properties of space and time the observatory revealed, showcasing brand new results in a wide range of astronomical topics, and sharing its accomplishments with the public. Today, we celebrate that *Hubble* continues to provide views of never-before-seen cosmic wonders, and has a bright future—remaining on the forefront of key scientific topics.

As part of *Hubble's* anniversary, the Institute partnered with NASA, the European Space Agency, and other institutions to highlight the observatory's 25 years of accomplishments. The series of events kicked off in January with the release

of a new multi-band image of the Eagle Nebula. This was followed by the annual science Spring Symposium and conference dinner, the showcasing of the spectacular anniversary image of the Westerlund 2 star cluster, a *Hubble* commemoration at the National Air and Space Museum, and other public activities such as education programs, exhibits, seminars, and multi-media and social media campaigns.

Science

In January, a new multi-wavelength image probing the Eagle Nebula from *Hubble's* newest instruments kicked off the anniversary year at the American Astronomical Society meeting. The Panchromatic *Hubble* Andromeda Treasury (PHAT) program, which sampled about 40% of M31 in 7,398 exposures taken over 411 individual multi-color pointings, was highlighted in a 30-foot mosaic panel, and underscored in several science talks. Other topics, such as the measurement of the Milky Way Galaxy's Fermi Bubble expansion, along with newest results on exoplanets and dark energy probes, filled out the rich science roster of the meeting.

Throughout the year, striking results from scientific studies ranged from the solar system and discovery of the chaotic nature of two of Pluto's moons, to detection of cloudy atmospheres on exoplanets, star formation and galaxy evolution, dark matter in galaxy cluster collisions, and new cosmic distance records. The 25th anniversary itself was celebrated with the Spring Symposium entitled "*Hubble* 2020: Building on 25 Years of Discovery." This Symposium not only looked at some of the notable advances made through *Hubble* investigations, but also underscored synergies with other missions. It also highlighted the future role of *Hubble* in relation to the promise of the *James Webb Space Telescope* and upcoming facilities such as *WFIRST/AFTA* and the next generation of large UV optical telescopes in space.

The dramatic anniversary image of the star cluster Westerlund 2 was unveiled in Washington D.C. by NASA on the last day of the symposium. This was followed by events at the Institute with panel discussions populated by astronauts, the



Figure 1: These images by *Hubble* reveal how different the iconic Pillars of Creation appear in visible and in near-infrared light.

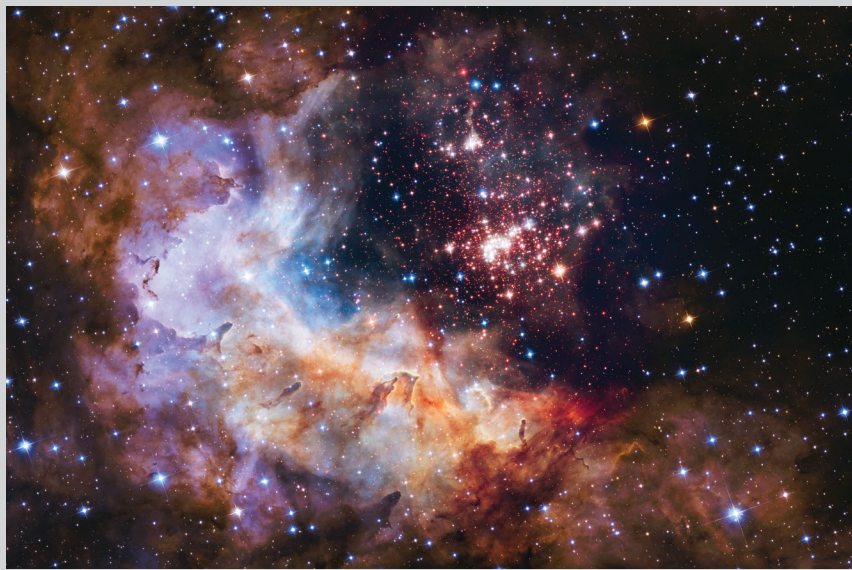


Figure 2: Westerlund 2 cluster and star-forming region.

NASA administrator, and other individuals reflecting on the fabrication, launch, and refurbishment of *Hubble* over the years. The annual Bahcall Lecture, given by Prof. Robert Kirshner (Harvard-Smithsonian Center for Astrophysics) as part of the 25th Anniversary celebration, punctuated the afternoon. A conference dinner followed, with participation by *Hubble* astronauts, as well as key individuals from industry and the science community who have played a major role in the design, construction, launch, and in-orbit repair of the telescope. Senator Barbara Mikulski completed the festivities with a congratulatory address.

Classroom education

The core of *Hubble*'s success is breakthrough science, often demonstrated through dramatic imagery and widely disseminated through the literature, as well as the news media, social media, and public information channels. These results are adapted to trusted and resilient educational resources through a proven model for science, technology, engineering, and math (STEM) education. Partnerships between scientists and educational specialists result in relevant, effective, and field-tested educational tools disseminated to classrooms affecting millions of youths at a time. While supported with only a small percentage of the *Hubble* budget, the program enhances STEM education initiatives for over 500,000 teachers in the classrooms of over 6 million students nationwide *each year*.

Accordingly, *Hubble*'s celestial silver milestone was celebrated during anniversary week through a special nationwide teach-in program that was aired on social media and was accessible to every classroom in the nation. Students and teachers joined educators and astronomers for an online exploration of the remarkable history and bright future of the telescope to learn how astronomy and our understanding of the universe have been transformed by *Hubble* research.

Public exhibits

The anniversary provided a perfect opportunity to widely showcase *Hubble*'s scientific achievements and the vision for its future in the context of *Webb* and beyond. The Gallery Walk at Reagan National Airport and the Gateway Gallery at Washington Dulles International Airport now greet visitors the world over, momentarily transporting their imaginations across the universe. The Institute provided the collection of images, artifacts, and student artwork for the displays.

From a distance, the images convey an impression of the great variety of astronomical subjects observed by *Hubble*. Viewing them close-up, visitors are able to enjoy the great beauty of the images and learn more about their scientific significance. The display cases at Gallery Walk also house artifacts that illustrate how *Hubble* has become the "People's Telescope." The cases include tools astronauts used to service the observatory, technological spinoffs, student artwork, and elements of *Hubble* incorporated into popular culture. Exhibits were also ingeniously created for the captive audiences at baggage claim areas at Baltimore/Washington International Thurgood Marshall, Reagan National, and Washington Dulles International airports.

To enable numerous other sites to share in the celebration and create their own custom exhibits, the Institute created a website with source material including the "Visions of the Universe" imagery, as well as slides and images for public lectures for the general public.

A list of all the events, activities, and products in celebration of *Hubble*'s 25th anniversary is available at <http://hubble25th.org>.



Figure 3: OPO produced airport exhibit.

Examples of other 25th anniversary activities	
25th Anniversary Website	The website http://hubble25th.org lists the anniversary events, videos, images, and activities
Seminars & Lectures	Seminars and lectures held around the world to celebrate the anniversary
Social Media	A social-media campaign for the anniversary
Electronic Book	An electronic book "A Quarter-Century of Discovery with the <i>Hubble Space Telescope</i> " with images and videos, https://itunes.apple.com/us/book/quarter-century-discovery/id983709653?mt=11
Videos	A series of videos dedicated to science and the people behind the telescope are being released; one a month throughout 2015, http://hubble25th.org/videos/6
Images	Two images: one at the 2015 AAS, and one on the anniversary date, were released
Resources	A resource page was created for downloading logos, banners, exhibit material, videos and presentations http://hubble25th.org/resources/7
Education Products	A set of special education products was prepared for the anniversary

From Cosmic Birth to Living Earths: The Future of UVOIR Space Astronomy

Jason Tumlinson, tumlinson@stsci.edu; Sara Seager, seager@mit.edu, Julianne Dalcanton, jd@astro.washington.edu, and Marc Postman, postman@stsci.edu

The Associated Universities for Research in Astronomy (AURA) recently published a new vision for the 2030s entitled *From Cosmic Birth to Living Earths: The Future of UVOIR Space Astronomy*. The report caps a two-year AURA-chartered study of how the ambitious goals of exoplanet and cosmic origins science can be combined into a single flagship general observatory dubbed the “High-Definition Space Telescope” (*HDST*).

Led by co-chairs Julianne Dalcanton (University of Washington) and Sara Seager (MIT), the study panel defines *HDST* as a flagship 12-meter general observatory with broadband (0.1–3 micron) sensitivity, several novel modes of instrumentation such as high-performance optical/near infrared (NIR) coronagraphy and far-UV multi-object spectroscopy (MOS), and unprecedented stability in support of high-precision astrometry, spectroscopy, and exoplanet characterization. *HDST*’s headline science goals are to: (1) detect and characterize dozens of Earth-like planets in the habitable zones of nearby stars, looking for biosignature gases in their optical/NIR spectra; and (2) to revolutionize studies of stars, galaxies, and the ultimate ingredients of life in the cosmos with high-resolution imaging and spectroscopy across the full Ultraviolet-Optical-Infrared (UVOIR) bandpass.

HDST builds on NASA and ESA’s foundation of missions for exoplanet discovery and characterization: *Kepler*, *Webb*, *TESS*, and *Plato* have or are expected to make fundamental advances in finding and

studying planets around other stars. But even if all these missions exhaust their full potential, they will not be able to find and examine the atmospheres of dozens of Earth-like planets in the habitable zones of nearby stars.

Webb in particular will excel at detecting the atmospheres of planets larger than Earth transiting stars smaller than the Sun (i.e., super-Earths orbiting M-dwarfs) where conditions are more favorable for an infrared telescope with coronagraphic contrast at only the 10^{5-6} level. Reaching the atmospheres of dozens of Earth-twin planets typically requires contrast ratios of order 10^{10} , and so is beyond even the future generations of giant ground-based telescopes, which might reach a handful of Earth-size planets by surveying up to a few dozen M stars.

NASA’s *WFIRST* will advance key starlight-suppression technologies and search for giant planets and SuperEarths (1.25–2 Earth masses) at the $\sim 10^9$ level, but again will not reach dozens of Earth-twin planets. A large stride toward characterizing dozens of Earth-twin planets and searching them for biosignatures requires 10-billion-fold (10^{10}) starlight suppression and a collecting area large enough to obtain revealing exoplanet spectra, which in turn require a large telescope with an extremely stable wavefront coupled with advanced starlight-suppression technology (a coronagraph and/or starshade).

The AURA study advocates that NASA and its community and industrial partners take steps to meet these technological challenges while the array of current and near-future missions lays the groundwork for *HDST*’s search for “Living Earths.”

HDST also promises revolutionary gains in capability that will make tremendous advances in our understanding of astrophysical objects and processes from the smallest stars to the most massive black holes. As a flagship in the mold of the Great Observatories, *HDST* will unleash the widespread creativity of the astronomical community with transformative capabilities: it will have 25 times the pixel density per area as *Hubble* in the optical, 4 times better resolution than *Webb* in the NIR, and up to 100 times the point-source UV spectroscopic sensitivity.

It also will be designed to have multi-object UV spectroscopy for up to 100 sources in a ~ 3 arcmin field of view, and extremely stable wavefronts to provide precise point-spread functions over long timelines. *HDST*’s optical-band spatial resolution corresponds to ~ 100 pc or finer physical scales *at all redshifts*, which will reveal the internal structure of high-*z* galaxies that even *Webb* will not resolve (Fig 1).

HDST will also have the UV sensitivity to map the weak emission from metals in the circumgalactic medium of galaxies at $z < 2$, where gas flows drive galaxy fueling and transformation. This same UV MOS

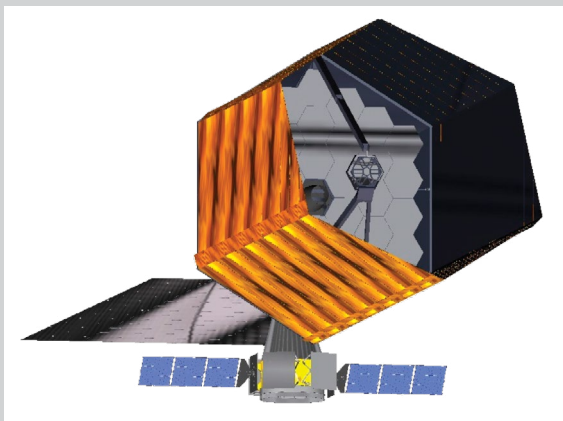


Figure 1: This is an artist’s concept of *HDST*, which will be a flagship 12-meter general observatory that combines exoplanet and cosmic origins science. It will feature broadband sensitivity, high-performance optical/NIR coronagraphy, far-UV multi-object spectroscopy, and unprecedented stability in support of high-precision astrometry, spectroscopy, and exoplanet characterization.

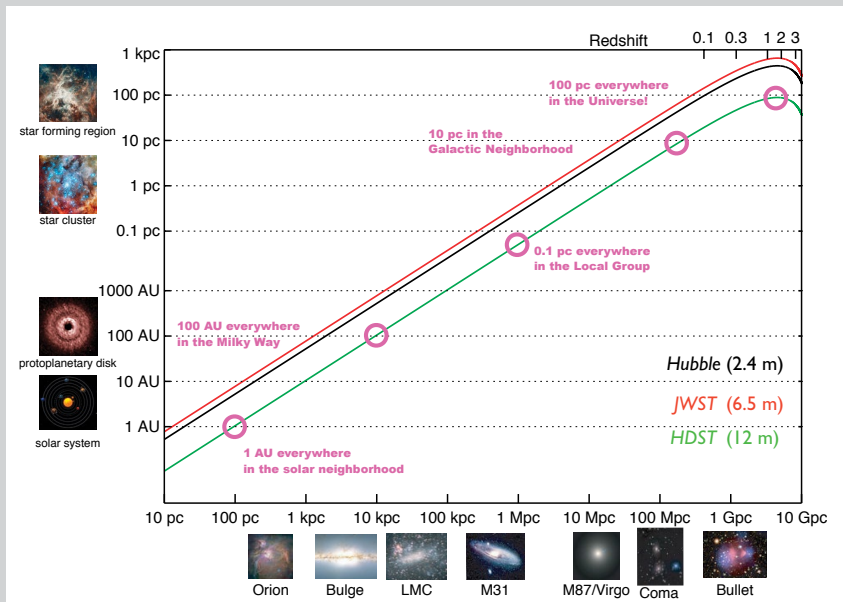


Figure 2: The physical size of *HDST*'s diffraction-limited spatial resolution element, as a function of distance/redshift. Note that the *HDST* resolution element is <100 AU anywhere in the Milky Way and <100 pc anywhere in the observable universe.

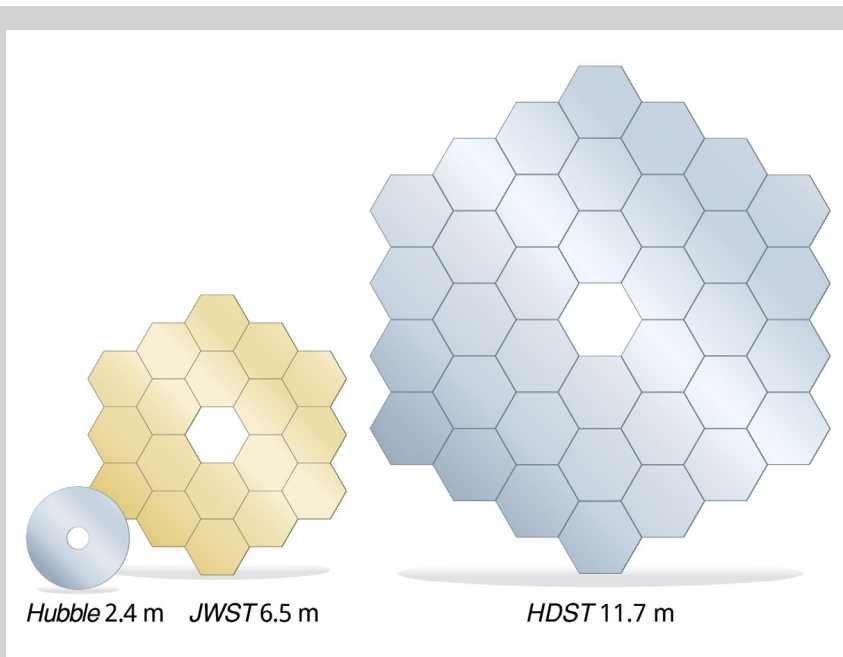


Figure 3: This is a direct, to-scale, comparison between the primary mirrors of *Hubble*, *JWST*, and *HDST*. In this concept, the *HDST* primary is composed of 36 1.7-meter segments. Smaller segments could also be used. An 11-meter class aperture could be made from 54 1.3-meter segments.

capability will enable detailed dissection of star-formation and AGN-driven feedback source-by-source in nearby galaxies. These new UVOIR capabilities promise to transform our understanding galaxies, stars, and the origins of the chemical elements.

The AURA study also carefully examined the technology requirements for *HDST* and concluded that, with the proper investments this decade, *HDST* will be feasible and affordable for a new start in the next decade and launch in the 2030s. The high degree of starlight suppression required for *HDST*'s exoplanet science is the greatest technology challenge, but new designs for coronagraphy are advancing rapidly. For cosmic origins science, the greatest technology needs are for large-format and high-quantum efficiency UV and optical detectors and UV coatings that support sensitivity down to 0.1 micron while minimally affecting the optical wavefront. The report makes specific recommendations on these points that the committee believes should be used to prioritize technology development funding in the next few years.

The AURA study committee is now engaging in discussions about *HDST* with the astronomical community at large, and with NASA and its international and industry partners. We welcome further discussions of *HDST* science and technology; more details and contact information are available at www.hdstvision.org.

Hubble Cycle 23 Proposal Selection

Lou Strolger, strolger@stsci.edu, **Brett Blacker**, blacker@stsci.edu, **Claus Leitherer**, leitherer@stsci.edu, and **Neill Reid**, inr@stsci.edu

This year we celebrate *Hubble*'s outstanding 25 years in orbit, recognizing both the tremendous achievements made with the observatory over the years, and the discoveries yet to come. *Hubble*'s 23rd cycle of science observations promises to carry on that legacy, with scientific demand remaining as high as it has ever been. We received a total of 1,115 proposals by the phase I deadline in April, including 182 in Archival, Archival Legacy, and Theory categories, requesting a total of 19,303 orbits. These proposals include investigators from 44 U.S. states (and the District of Columbia), and investigators from 42 countries.

The international members of the proposal review panels and the Time Allocation Committee (TAC) met in June to provide recommendations to the Director, who approved 261 proposals totaling 3,563 awarded orbits, which will start executing at the beginning of Cycle 23 in October. Here, we give an overview of the construction and outcome of the Cycle 23 review.

The review process

The *Cycle 23 Call for Proposals (CP)* was released on January 7, 2015, announcing observing opportunities with *Hubble*'s current instrumentation: the Advanced Camera for Surveys (ACS), the Cosmic Origins Spectrograph (COS), the Fine Guidance Sensors (FGS), the Space Telescope Imaging Spectrograph (STIS), and the Wide Field Camera 3 (WFC3). The *CP* also announced opportunities to request funding for archival and theoretical research. The *Cycle 23 CP* carried over three important opportunities from previous cycles. Medium Proposals continued as a separate proposal category for programs requesting between 35 and 75 orbits, to improve the success rate of programs in this historically challenging orbit range.

Recognizing the unique and limited availability of *Hubble*'s ultraviolet (UV) capabilities, the UV Initiative was continued to encourage the community (and the TAC) to increase the fraction of time and awards dedicated to wavelengths below 3200 Å. Following the highly favorable mid-term review, the Institute Director also decided to proceed with the final two clusters of the Frontier Fields, encouraging the community to develop archival, theory, and supplementary observing programs that maximize the scientific return on the data from all six clusters.

Members of the review panels and the TAC were recruited several months prior to the proposal deadline, and asked to serve on one of the 14 panels organized by science category, consisting of two panels on cosmology, three on galaxies, two panels covering active galactic nuclei and the intergalactic medium, two on stellar populations, three on stars, and two covering planets and solar-system objects. Each panel has at least one "mirror" panel, covering similar topics and expertise, allowing proposals to be transferred as needed to avoid conflicts of interest within a given panel.

1,115 proposals were received electronically via the ASTRONOMER'S PROPOSAL TOOL by the phase I proposal deadline on April 10, 2015. Each was sorted by science category and organized into the review panels described above. Each review panel subsequently received between 70 to 90 small (<35 orbits) and medium (35 to 74 orbits) proposals to grade in preparation for the in-person discussion in June.

To decrease the burden on the panelists, each was only assigned about two-thirds of the proposals in their panel. These grades were collected a few weeks before the meeting, and sorted into a preliminary rank order within each panel. Proposals ranking in the bottom 40% were triaged, and generally not discussed further in the TAC process unless raised for discussion by a non-conflicted panelist. The Large and Treasury proposals (>75 orbits) were reviewed by the TAC members for discussion in their meeting following the panel reviews.

The review panels met over three days in Baltimore, MD, to deliberate and regrade the proposals, and produce a final rank order for the non-triaged proposals in each panel. Members of the TAC were also assigned to these panels to serve as non-voting chairs, guiding the discussion and carrying forward opinions (should they be necessary) from the panels to the TAC. Each panel was provided a nominal orbit allocation to help guide decisions, especially for proposals critically ranked at or near the potential award boundary.

Medium proposals were ranked amongst the Small proposals, allowing a gauge of their relative importance in the competition for the pool set aside for the Medium category. A panel could optionally identify Medium proposals to award from its nominal allocation, essentially ensuring the proposal's success, albeit at the expense of a large fraction of that panel's awardable time. Panelists were also asked to review the Large and Treasury proposals pertinent to their panel science category. Comments on the Medium and Large proposals were provided to the panel chairs for the TAC review.

Immediately following the panel review, the TAC met for an additional two days to review the panels' recommendations, and to decide the final rank orders for the Medium, and Large and Treasury programs, within those respective orbit pools. Prof. Bradley Peterson of the Ohio State University served as chair of the Cycle 23 TAC, and Dr. Catherine Cesarsky of Commissariat à l'Énergie Atomique, Dr. Mark Dickinson of National Optical Astronomy Observatory, and Prof. Rogier Windhorst of Arizona State University served as TAC members at large. The Institute Director completed the final review of the TAC recommendations in the week following the TAC meeting, and the Cycle 23 results were announced shortly thereafter.

Ensuring an impartial review

We continue to strive for impartiality and fairness in the *Hubble* review process. Conflicts of interest for each reviewer are identified based on institution and publication record, and mirror panels are used to avoid conflicts when possible.

Once the proposals are initially distributed to the panel, each panelist must identify any remaining strong conflicts of interest, including competing proposals, mentorship relationships, and close collaborations. Panelists are not permitted to grade proposals for which they are conflicted, and for strong conflicts, e.g., any in which they themselves or their institutions would directly benefit from, panelists are not permitted to participate in the discussion.

Additionally, the Institute has taken steps to address the unconscious gender bias of the *Hubble* TAC process, which has resulted in small but statistically significant over-representation of male PIs relative to female PIs in each of the last 23 *Hubble* cycles.

Continuing the practice from last cycle, PI names were removed from the cover page and proposal IDs, and only the initials for the PI's and Col's first names were given. The *Hubble* TAC orientation also included a presentation of the historical over-representation of male *Hubble* PIs and the issue of unconscious bias.

Results

With 261 of 1,115 proposals accepted, the average *Hubble* Cycle 23 acceptance rate was 23.4%, negligibly higher than the 23.1% acceptance rate from the last cycle. Similarly, the oversubscription ratio for all General Observer (GO) programs remained level, at 5.4:1 by orbit, or 4.4:1 by proposal. The estimated oversubscription of Archival and Theory proposals by nominal funding dipped slightly from the last two cycles, down by about 10% to 3.71:1. PIs from ESA member countries lead 24% of the accepted Cycle 23 programs, about the same rate as with last cycle.

Medium proposals have shown a notable increase in their success rates over the last few cycles. Cycle 23 sees an average success rate of 19% (by proposal), representing the third consecutive 40–50% increase in success rate in as many cycles.

WFC3 remains the most requested instrument, with 46% of the awarded time utilizing this instrument in its various modes on primary targets (18% WFC3/IR imaging, 11% WFC3/IR spectroscopy, 16% WFC3/UVIS imaging, and 1% WFC3/UVIS spectroscopy). COS is now the

second most utilized instrument, with 23% of the awarded time going to FUV (19%) and NUV (4%) spectroscopy. STIS was awarded 16% of available orbits, almost evenly split across the spectroscopic modes, and ACS completes the allocation, with 15% of the time going to the WFC (13%) and SBC (2%) imaging modes. Approximately 40% of the proposals received under the UV Initiative were awarded time.

The Cycle 23 time allocation was well-matched to the proposal pressure in each of the science categories, with each approved for a similar fraction of the requested orbits. Cosmology programs make up the largest allocation in this cycle (23%), with Quasar Absorption Lines and IGM at 12%, and Extra-Solar Planets at 11%.

Acknowledgments

We thank all of the *Hubble* TAC members, review panelists, and external reviewers for their service on the *Hubble* Cycle 23 TAC. Numerous Institute personnel contributed to the support of review process.

Science Policies Group astronomers Andy Fruchter, Janice Lee, Claus Leitherer, Jennifer Lotz, Neill Reid, and Lou Strolger were responsible for selecting the panelists, assigning the proposals to panels and panelists, coordinating policy, and providing oversight during the review.

Technical Manager Brett Blacker received, organized, and distributed the proposals, oversaw the proposal database, announced the results, and prepared the statistical summaries and figures provided here.

The TAC logistics were devised and coordinated by Sherita Hanna, with administrative support from Tania Anderson, Robin Auer, Geoff Carter, Kelly Coleman, Martha Devaud, Brian Fincham, Sarah Flores, Flory Hill, Shaquintay Johnson, Linda Kaiser, Tracy Lamb, Alisa Meizlish, Karen Petro, Karyn Poletis, Darlene Spencer, Rolanda Taylor, and Loretta Willers.

Panel support was provided by Michael Dulude, Meredith Durbin, Lisa Frattare, Katie Gosmeyer, Olivia Jones, Miranda Link, Crystal Mannfolk, Tala Monroe, Camilla Pacifici, Maria Peña-Guerrero, Karla Peterson, Tony Roman, Russell Ryan, John Stansberry, and Laura Watkins.

Instrument expertise was provided by Marco Chiaberge, Linda Dressel, Norman Grogan, Matt Lallo, John MacKenty, Ed Nelan, Cristina Oliveira, Charles Proffitt, Julia Roman-Duval, and Elena Sabbi.

IT support was provided by Val Ausherman, Romeo Gourgue, Jay Grimes, Craig Hollinshead, Craig Levy, Jessica Lynch, Thomas Marufu, Greg Masci, Glenn Miller, Corey Richardson, Patrick Taylor, Calvin Tullos, and Shane Wolfe.

Ray Beaser, Vickie Bowersox, Margie Cook, Roosevelt Davis, Karen Debelius, Cathy Donellan, Adia Jones, Lisa Kleinwort, Amy Power, Val Schnader, Paula Sessa, and Sarah Shin provided support from the Business Resources Center. Pam Jeffries provided support from the Office of Public Outreach, and Zak Concannon provided assistance from the Copy Center.

Finally, we thank Andre Deshazo, Rob Franklin, Rob Levine, Glenn Martin, Greg Pabst, Frankie Schultz, Mike Sharpe, Trevor Thompson, Mike Venturella, and G Williams of Facilities, and Prof. Dan Reich and the Bloomberg facilities staff.

Summary of Cycle 23 Results

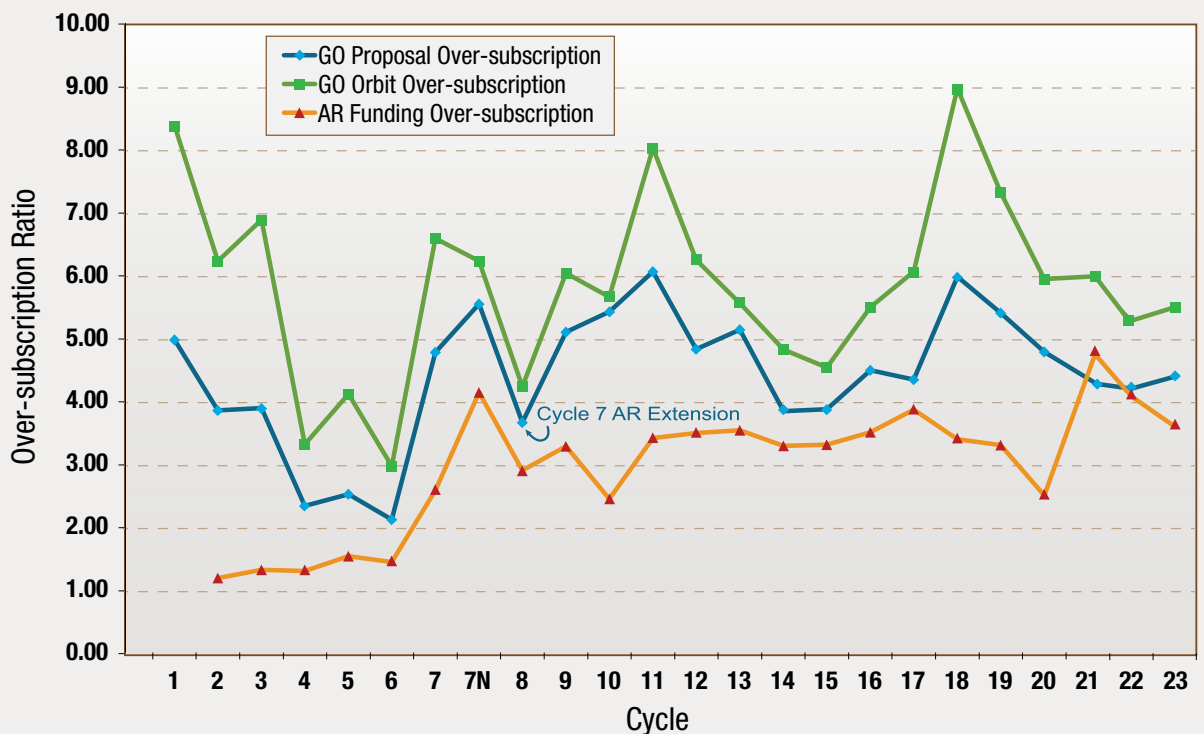
Proposals	Requested	Approved	% Accepted	ESA Accepted	ESA % Total
General Observer	891	202	22.7%	56	27.7%
Snapshot	42	10	23.8%	3	30.0%
Archival Research	96	28	29.2%	0	
AR Legacy	11	3	27.3%	0	
Theory	75	18	24.0%	0	
Total	1115	261	23.4%	59	27.8%
Primary Orbits	19301	3563	18.5%	1041	29.2%

Primary Orbits category does not include 2 Calibration Orbits

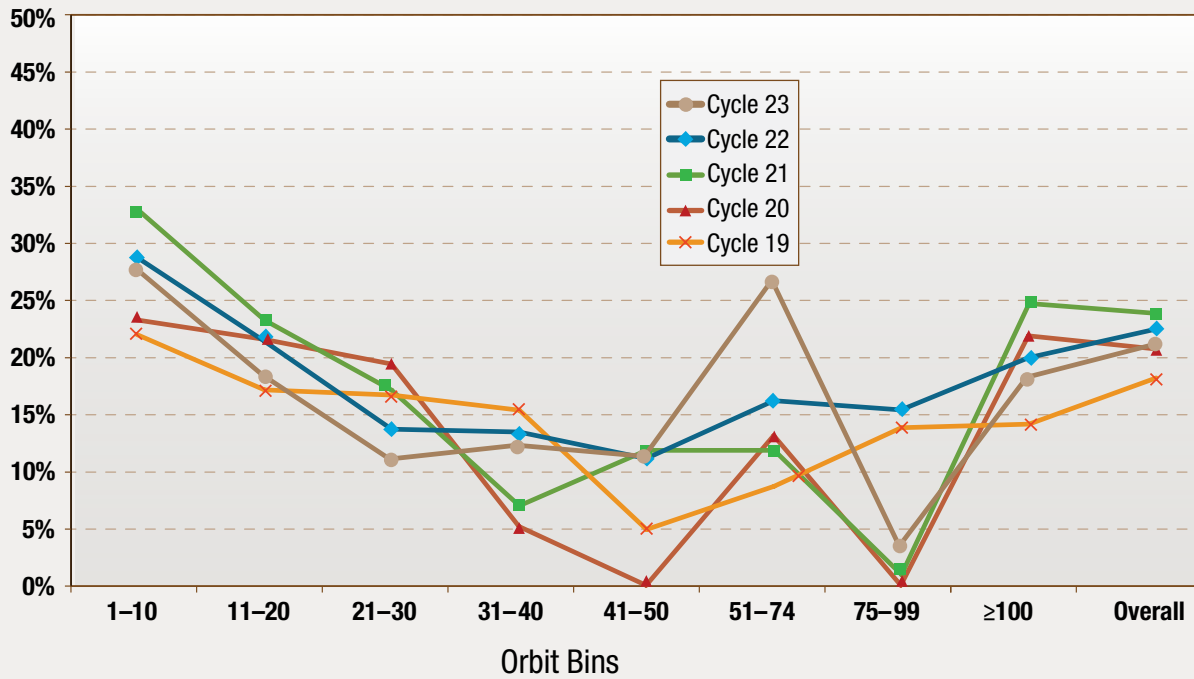
Proposal Breakdown by PI Country

Country	Submitted	Approved	Country	Submitted	Approved
Australia	15	5	Korea	1	0
Austria	5	0	Mexico	1	0
Brazil	2	0	Norway	1	0
Canada	15	2	Poland	1	1
Chile	12	3	Portugal	2	0
China	10	3	Russia	3	0
Columbia	1	0	Spain	13	6
Czech Republic	1	1	Sweden	11	3
Denmark	5	1	Switzerland	11	5
Finland	2	0	The Netherlands	13	2
France	25	6	Turkey	1	0
Germany	41	6	United Kingdom	74	20
Ireland	4	1	United States	803	187
Israel	8	3	Uruguay	1	0
Italy	23	5			
Japan	10	1	ESA Proposals	242	59

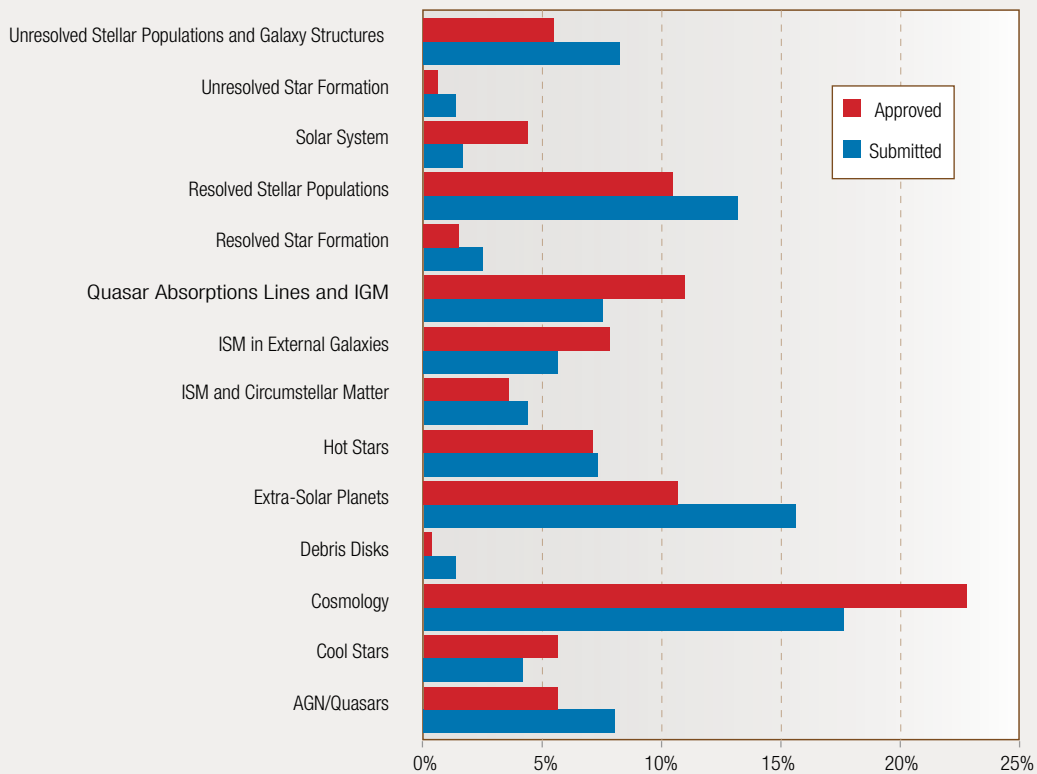
Proposal Acceptance Ratio: Over-subscription by Cycle



Proposal Success Rate as a Function of Orbit Request, Cycles 19–23



Orbits by Science Category



Cycle 23 Instrument Statistics

Configuration	Mode	Prime	Coordinated Parallel	Total	Instrument Prime Usage	Instrument Prime + Coordinated Parallel Usage	Pure Parallel Usage	Snap Usage
ACS/SBC	Imaging	2.0%	0.0%	1.7%			0.0%	0.0%
ACS/SBC	Spectroscopy	0.2%	0.0%	0.2%			0.0%	0.0%
ACS/WFC	Imaging	12.7%	52.0%	18.2%			0.0%	16.0%
ACS/WFC	Ramp Filter	0.0%	0.0%	0.0%	15.0%	20.2%	0.0%	0.0%
ACS/WFC	Spectroscopy	0.1%	0.0%	0.1%			0.0%	0.0%
COS/FUV	Spectroscopy	19.4%	0.0%	16.7%			0.0%	6.0%
COS/NUV	Imaging	0.0%	0.0%	0.0%	22.9%	19.7%	0.0%	0.0%
COS/NUV	Spectroscopy	3.5%	0.0%	3.0%			0.0%	0.0%
FGS	POS	0.0%	0.0%	0.0%	0.0%	0.0%	0.0%	0.0%
FGS	TRANS	0.0%	0.0%	0.0%			0.0%	0.0%
STIS/CCD	Imaging	0.1%	0.0%	0.1%			0.0%	0.0%
STIS/CCD	Spectroscopy	4.4%	0.0%	3.8%			0.0%	6.0%
STIS/FUV	Imaging	1.5%	0.0%	1.3%	16.5%	14.2%	0.0%	0.0%
STIS/FUV	Spectroscopy	3.9%	0.0%	3.3%			0.0%	0.0%
STIS/NUV	Imaging	0.1%	0.0%	0.1%			0.0%	0.0%
STIS/NUV	Spectroscopy	6.6%	0.0%	5.6%			0.0%	0.0%
WFC3/IR	Imaging	17.8%	15.8%	17.5%			40.0%	43.0%
WFC3/IR	Spectroscopy	10.6%	0.0%	9.1%	45.6%	45.9%	23.0%	0.0%
WFC3/UVIS	Imaging	15.7%	32.2%	18.0%			37.0%	29.0%
WFC3/UVIS	Spectroscopy	1.5%	0.0%	1.3%			0.0%	0.0%
		100.0%	100.0%	100.0%	100.0%	100.0%	100.0%	100.0%
Imaging	49.9%	ACS	13.0%					
Spectroscopy	50.1%	COS	22.9%					
		FGS	0.0%					
		STIS	16.5%					
		WFC3	45.6%					

TAC Members and Panelists

Name	Institution
TAC Members	
Bradley M. Peterson, TAC Chair	Ohio State University
Catherine Cesarsky, At Large	Commissariat à l'Energie Atomique
Mark Dickinson, At Large	National Optical Astronomy Observatory
Rogier A Windhorst, At Large	Arizona State University
Extragalactic Panel Members	
Roberto G. Abraham, Chair	University of Toronto
Aaron J. Barth	University of California–Irvine
Matthew Bayliss	Harvard University
John P. Blakeslee	Dominion Astrophysical Observatory, NRCC/HIA
Tamara Bogdanovic	Georgia Institute of Technology
Adam S. Bolton	University of Utah
Sanchayeeta Borthakur	The Johns Hopkins University
Tereasa Brainerd, Chair	Boston University
Rebecca E. A. Canning	Stanford University
Michele Cappellari	University of Oxford
Rupali Chandar, Chair	University of Toledo
Stéphane Charlot	CNRS, Institut d'Astrophysique de Paris
Françoise Combes, Chair	Observatoire de Paris
Michael Cooper	University of California–Irvine
Duilia F. de Mello	Catholic University of America
Harald Ebeling	University of Hawaii
Eiichi Egami	University of Arizona
Jayanne English	University of Manitoba
Michael Eracleous, Chair	Penn State University
Sarah Gallagher	University of Western Ontario
Rajib Ganguly	University of Michigan
Karl Gebhardt	University of Texas at Austin
Eilat Glikman	Middlebury College
Bradford Holden	University of California–Santa Cruz
Ikuru Iwata	NAOJ, Subaru Telescope
Regina Jorgenson	Willamette University
Neal S. Katz	University of Massachusetts
Guinevere Kauffmann, Chair	Max-Planck-Institut für Astrophysik
Brian Keeney	University of Colorado–Boulder
Dale D. Kocevski	Colby College
Steven Kraemer	Catholic University of America
James T. Lauroesch	University of Louisville
Kyoung-Soo Lee	Purdue University
Adam Leroy	Ohio State University
Yuxing Li	Penn State University
Xin Liu	University of California–Los Angeles

Name	Institution
Britt Lundgren	University of Wisconsin–Madison
Claudia Maraston	University of Portsmouth
Richard J. Massey	University of Durham
Daniel McIntosh	University of Missouri–Kansas City
John S. Mulchaey	Carnegie Institute of Washington
Richard Mushotzky	University of Maryland
Adam D. Myers	University of Wyoming
John M. O'Meara	Saint Michaels College
Brian W. O'Shea	Michigan State University
Pascal Oesch	Yale University
Polychronis Papaderos	University do Porto
Laura Pentericci	INAF, Osservatorio Astronomico di Roma
Mari Polletta	INAF, Istituto di Astrofisica Spaziale e Fisica Cosmica, Milano
Ryan Quadri	Texas A & M University
David J. Radburn-Smith	University of Washington
Steven A. Rodney	The Johns Hopkins University
Gwen C. Rudie	Carnegie Institute of Washington
Barbara S. Ryden	Ohio State University
David B. Sanders	University of Hawaii
Sandra Savaglio	University of Calabria
Hee-Jong Seo	Ohio University
Keren Sharon	University of Michigan
Kartik Sheth	National Radio Astronomy Observatory
J. Michael Shull	University of Colorado–Boulder
Aneta Siemiginowska	Smithsonian Astrophysical Observatory
John T. Stocke, Chair	University of Colorado–Boulder
Todd Tripp	University of Massachusetts
Jonathan R. Trump	Penn State University
Monica Valluri	University of Michigan
Arjen van der Wel	Max-Planck-Institut für Astronomie, Heidelberg
Julie Wardlow	University of Copenhagen, Niels Bohr Institute
Greg Zeimann	Penn State University
Wei Zheng	The Johns Hopkins University
Adi Zitrin	California Institute of Technology
Planetary Panel Members	
Daniel Apai	University of Arizona
Susan D. Benecchi	Planetary Science Institute
Esther Buzenli	Max-Planck-Institut für Astronomie, Heidelberg
David Ehrenreich	Observatoire de Genève

TAC Members and Panelists

Name	Institution
Catherine Espaillat	Boston University
William M. Grundy	Lowell Observatory
Renyu Hu	Jet Propulsion Laboratory
Erich Karkoschka	University of Arizona
Alain Lecavelier des Etangs	CNRS, Institut d'Astrophysique de Paris
Mercedes Lopez-Morales, Chair	Smithsonian Astrophysical Observatory
Melissa A. McGrath	SETI Institute
Arielle Moullet	National Radio Astronomy Observatory
Philip Nicholson	Cornell University
Darin Ragozzine	Florida Institute of Technology
William Reach	Universities Space Research Association
Aki Roberge	NASA Goddard Space Flight Center
Lorenz Roth	Royal Institute of Technology
Hilke E. Schlichting	Massachusetts Institute of Technology
Britney E. Schmidt	Georgia Institute of Technology
David Kent Sing, Chair	University of Exeter
Angelle Tanner	Mississippi State University
Galactic Panel Members	
Francesca Bacciotti	INAF, Osservatorio Astrofisico di Arcetri, Firenze
Jeremy Bailin	University of Alabama
You-Hua Chu, Chair	Academia Sinica
Romano L.M. Corradi	Instituto Astrofísico de Canarias
Trent J. Dupuy	University of Texas at Austin
Christopher J. Evans, Chair	Royal Observatory, Edinburgh
John J. Feldmeier	Youngstown State University
Christopher R. Gelino	Jet Propulsion Laboratory
Michael D. Gregg	University of California–Davis
Aaron Grocholski	Louisiana State University A & M
Brad M. Hansen	University of California–Los Angeles
Lee W. Hartmann, Chair	University of Michigan
Suzanne L. Hawley, Chair	University of Washington
Todd J. Henry	Georgia State University
Jay B. Holberg	University of Arizona
Rémy Indebetouw	National Radio Astronomy Observatory
Anne Jaskot	Smith College
Saurabh W. Jha	Rutgers State University of New Jersey
Lex Kaper	Universiteit van Amsterdam
David L. Kaplan	University of Wisconsin–Milwaukee
Gillian R. Knapp	Princeton University
Kaitlin Kratter	University of Arizona
Adam L. Kraus	University of Texas–Austin

Name	Institution
Andrew J. Levan	University of Warwick
Emily Levesque	University of Colorado–Boulder
Thomas J. Maccarone	Texas Tech University
Andrew Withycombe Mann	University of Texas at Austin
Marcella Marconi	INAF, Osservatorio Astronomico di Capodimonte
Jason Nordhaus	Rochester Institute of Technology
Evan Patrick O'Connor	North Carolina State University
Lida Oskinova	Universität Potsdam
Veronique Petit	Florida Institute of Technology
Luke Roberts	California Institute of Technology
Raghvendra Sahai	Jet Propulsion Laboratory
David J. Sand	Texas Tech University
Anil C. Seth	University of Utah
Jay Strader	Michigan State University
Silvia Torres-Peimbert	Universidad Nacional Autónoma de México
Dean Townsley	University of Alabama
Eleonora Troja	University of Maryland
Kim A. Venn, Chair	University of Victoria
Eva Villaver	Universidad Autónoma de Madrid
Serena Viti	University College London
Ted von Hippel	Embry-Riddle Aeronautical University
Matthew G. Walker	Carnegie Mellon University
Benjamin F. Williams	University of Washington
Brian E. Wood	Naval Research Laboratory
Guy Worthey	Washington State University
David R. Zurek	American Museum of Natural History

Accepted Proposals

Name	Institution	ESA Member	Type	Title
Extragalactic Programs				
Angela Adamo	Stockholm University	Yes	GO	Hi-PEEC, <i>Hubble</i> Imaging Probe of Extreme Environments and Clusters
Chris Ahn	University of Utah		GO	Searching for a Supermassive Black Hole in the Brightest Ultracompact Dwarf Galaxy
Nahum Arav	Virginia Polytechnic Institute and State University		GO	Deep Multiwavelength Campaign on an AGN Outflow: Absolute Abundances and the Warm Absorber Connection
Vivienne Baldassare	University of Michigan		GO	Studying the Nuclear Morphology of a Dwarf Galaxy with a 50,000 Solar-mass Black Hole
Robert Barrows	University of Colorado at Boulder		GO	Resolving the Nuclear Regions of Confirmed Offset AGN
Aaron Barth	University of California–Irvine		GO	Bulge Structure and Kinematics in an Extreme Spiral Galaxy Hosting Megaparsec-Scale Radio Jets
Eric Bell	University of Michigan		AR	A Model-Independent Assessment of the Effects of Dust Attenuation at $0.5 < z < 1$ on <i>HST</i> -derived F814W Galaxy Morphologies, Structures and Luminosities
Danielle Berg	University of Wisconsin–Milwaukee		GO	Stellar Populations and Physical Conditions at ~ 100 pc Resolution in a Lensed Galaxy at $z \sim 4$
John Biretta	Space Telescope Science Institute		GO	High-precision Proper Motions in the M87 Jet
John Blakeslee	Dominion Astrophysical Observatory		GO	Homogeneous Distances and Central Profiles for MASSIVE Survey Galaxies with Supermassive Black Holes
Adam Bolton	University of Utah		GO	Quantifying Cold Dark Matter Substructure with a Qualitatively New Gravitational Lens Sample
Gabriel Brammer	Space Telescope Science Institute	Yes	SNAP	Calibrating the Dusty Cosmos: Extinction Maps of Nearby Galaxies
Jarle Brinchmann	Leiden Observatory	Yes	GO	He II Emission as a Tracer of Ultra-low Metallicity and Massive Star Evolution
James Bullock	University of California–Irvine		AR	Simulating Ultra-faint Dwarf Galaxies: The Hallmark of Reionization at the Threshold of Galaxy Formation
Nell Byler	University of Washington		AR	Detangling Galaxy Spectra: A Baseline Calibration Using Resolved Stars
Edward Cackett	Wayne State University		GO	Probing the Accretion Disk in the Seyfert 1 NGC 4593
Benjamin Cain	University of California–Davis		AR	Measuring the Subhalo Mass Function with Flexion
Daniela Calzetti	University of Massachusetts–Amherst		AR	The Young Star Groups in Dwarf Galaxies
Marios Chatzikos	University of Kentucky		AR	Deciphering the Fossil Record in Quasar Ionization Echoes
Hsiao-Wen Chen	University of Chicago		GO	Characterizing Circumgalactic Gas around Passive Galaxies
Ena Choi	Rutgers the State University of New Jersey		AR	Triggering and Quenching: Simulations and Mock Observations of Active Galactic Nuclei and their Hosts
Yumi Choi	University of Washington		AR	A New Method to Measure the UV Escape Fraction from Galaxies
Lise Christensen	University of Copenhagen, Niels Bohr Institute	Yes	GO	Unveiling Stellar Populations in Absorption-selected Galaxies
James Colbert	Jet Propulsion Laboratory		GO	Does All The Lyman Continuum Emission Escape From Young, Low Mass Starbursts?
Michael Cooper	University of California–Irvine		AR	The Faint Galaxy Frontier: Galaxy Formation at the Extremes of Mass and Density in the Deep Fields
D. Crenshaw	Georgia State University Research Foundation		AR	What is the Impact of Narrow-Line Region Outflows on AGN Feedback?

Accepted Proposals

Name	Institution	ESA Member	Type	Title
Arlin Crotts	Columbia University in the City of New York		GO	Light Echoes and Environment of SN 2014J in M82
Neal Dalal	University of Illinois at Urbana–Champaign		AR	Backsplash as a Probe of Cosmology
Harald Ebeling	University of Hawaii		SNAP	Beyond MACS: A Snapshot Survey of the Most Massive Clusters of Galaxies at $z > 0.5$
Eiichi Egami	University of Arizona		GO	Near-IR Imaging of Three Spectacular Lensed Submillimeter Galaxies Discovered by the <i>Herschel</i> Lensing Survey
Claude-André Faucher-Giguère	Northwestern University/CIERA		AR	Metallicity and Azimuthal Angle Diagnostics of Inflows and Outflows: Interpreting <i>HST</i> Measurements of Circumgalactic Gas Flows
Brenda Frye	University of Arizona		GO	The Planck Dusty Gravitationally Enhanced submillimeter Sources (GEMS)
Michele Fumagalli	University of Durham	Yes	GO	First Measurement of the Small-scale Structure of Circumgalactic Gas via Grism Spectra of Close Quasar Pairs
Pierre Guillard	CNRS, Institut d'Astrophysique de Paris	Yes	GO	Hot Gas Cooling and Turbulence in the 3C326N Radio Galaxy
Matthew Hayes	Stockholm University	Yes	GO	Unveiling the Dark Baryons II: the First Sample of $0 < v_l$ Emission Imaging
Alex Hill	Haverford College		AR	Gaseous Infall and Star Formation from Redshift 2 to the Milky Way
John Hughes	Rutgers the State University of New Jersey		GO	Measuring the Mass of El Gordo to Near the Virial Radius
Jimmy Irwin	University of Alabama		GO	Confirmation of an Intermediate-mass Black Hole in an Extragalactic Globular Cluster
Knud Jahnke	Max-Planck-Institut für Astronomie, Heidelberg	Yes	GO	Are the Fastest Growing Black Holes at $z = 2$ Caused by Major Galaxy Mergers?
Anne Jaskot	Smith College		GO	LyC, Ly- α , and Low Ions in Green Peas: Diagnostics of Optical Depth, Geometry, and Outflows
Glenn Kacprzak	Swinburne University of Technology		GO	A New Dual Perspective of Multi-phase Galaxy Outflows
Jeyhan Kartaltepe	National Optical Astronomy Observatory		AR	What Drives Star Formation in Galaxies?: Combining the Strengths of <i>HST</i> and <i>Herschel</i>
Neal Katz	University of Massachusetts–Amherst		AR	A New Galactic Wind Model to Better Understand the Implications of QSO Absorption Lines
Patrick Kelly	University of California–Berkeley		GO	Refsdal Redux: Precise Measurements of the Reappearance of the First Supernova with Multiple Resolved Images
Tae-Sun Kim	INAF, Osservatorio Astronomico di Trieste	Yes	GO	Crossing the Redshift Desert: Ionizing Background Radiation and Intergalactic Hydrogen at $z \sim 1$
Michael Koss	Eidgenössische Technische Hochschule	Yes	GO	Studying Dual AGN Activity in the Final Merger Stage
Gerard Kriss	Space Telescope Science Institute		GO	Measuring Absolute Abundances in NGC 5548 and Definitively Linking the UV and X-ray Outflows
Nicolas Lehner	University of Notre Dame		GO	Just the BASICS: Linking Gas Flows in the Circumgalactic Medium to Galaxies
Claus Leitherer	Space Telescope Science Institute		GO	The II Zw 40 Supernova: 30 Doradus on Steroids
Adam Leroy	The Ohio State University		GO	An Ionizing Photon Rate Map of NGC 6946
Rachael Livermore	University of Texas at Austin		AR	Searching for Faint High- z Galaxies in the <i>Hubble</i> Frontier Fields

Accepted Proposals

Name	Institution	ESA Member	Type	Title
Jingzhe Ma	University of Florida		GO	Revealing the Host Galaxy of a Strong Milky Way-type 2175 Å Absorber at $z = 2.12$
Walter Maksym	University of Alabama		GO	Mapping the Radiative and Kinetic History of Fading AGNs
Walter Maksym	University of Alabama		GO	Long-term Ultraviolet Spectroscopy of a Tidal Disruption Event at only 90 Mpc
Sangeeta Malhotra	Arizona State University		GO	Lyman α Escape in Green Pea Galaxies (Give Peas a Chance)
Eileen Meyer	Space Telescope Science Institute		GO	Mapping the kpc-scale Velocity Structure of Jets with <i>HST</i>
Eileen Meyer	Space Telescope Science Institute		GO	Monitoring an Internal Shock Collision in Action in 3C 264
Bahram Mobasher	University of California–Riverside		AR	Multi-waveband Photometric Catalogs for the <i>Hubble</i> Frontier Field Clusters and their Parallel Fields
Mireia Montes	Yale University		AR	The Intra-cluster Light as Seen by the <i>Hubble</i> Frontier Fields
Leonidas Moustakas	Jet Propulsion Laboratory		AR	Nonlinear Evolution Predictions for Dark Matter Substructure, and Predictions for Gravitational Lensing Probes
Andrew Newman	Carnegie Institution for Science		GO	Early Quiescent Galaxies Under the Magnifying Glass
John O'Meara	Saint Michaels College		GO	A 100 Million-fold Increase in the Measured Sizes of Neutral Gas Reservoirs in the Early Universe
Siang Oh	University of California–Santa Barbara		AR	Turbulent Mixing and Thermal Instability in the Circumgalactic Medium
Benjamin Oppenheimer	University of Colorado at Boulder		AR	Characterizing Group Baryons and Galaxies Through EAGLE Zoom Simulations
Ivana Orlitová	Astronomical Institute, Academy of Sciences of the Czech Republic	Yes	GO	Origin of Double Peaks in Lyman- α Spectra: Diffuse Halos or Lyman Continuum Leakage?
Mark Peacock	Michigan State University		GO	The Spatial Distribution of Hot Stellar Populations in M31's Globular Clusters
Ismael Perez-Fournon	Instituto de Astrofísica de Canarias	Yes	GO	The Nature and Environment of the Most Luminous Starburst Galaxies at Redshift > 5
Thomas Puzia	Pontificia Universidad Católica de Chile		GO	The Coma Cluster Core Project
Swara Ravindranath	Space Telescope Science Institute		GO	Spectral Diagnostics for the Reionization Era: Exploring the Semi-Forbidden C III Emission in Low Metallicity Green Pea Galaxies
Amy Reines	University of Michigan		SNAP	The Structures of Dwarf Galaxies Hosting Massive Black Holes
Gordon Richards	Drexel University		GO	Are High-redshift Spectroscopic Black Hole Mass Estimates Biased?
Philipp Richter	Universität Potsdam	Yes	GO	Circumgalactic Gas at its Extreme—The Absorption Properties of Interacting Galaxies
Adam Riess	The Johns Hopkins University		GO	A New Threshold of Precision, 30 Micro-arcsecond Parallaxes and Beyond
Mickaël Rigault	Humboldt Universität zu Berlin	Yes	SNAP	Honing Type Ia Supernovae as Distance Indicators, Exploiting Environmental Bias for H_0 and w
Jane Rigby	NASA Goddard Space Flight Center		GO	The Ultimate Emission Line Diagnostics Study at $z = 1.4$
Steven Rodney	The Johns Hopkins University		GO	Frontier Fields Supernova Search
Gregory Rudnick	University of Kansas Center for Research, Inc.		AR	The Role of Quenching and Merging in Shaping the Passive Galaxy Population in Distant Clusters
David Rupke	Rhodes College		GO	A Local Benchmark for High-redshift Feedback

Accepted Proposals

Name	Institution	ESA Member	Type	Title
Claudia Scarlata	University of Minnesota–Twin Cities		AR	Emission Line Galaxy Constraints from <i>HST</i> : Towards Accurate Forecasts for <i>WFIRST</i> and <i>Euclid</i>
Jan-Torge Schindler	University of Arizona		AR	Constraining the Merger Fraction of Quasars with High-resolution <i>HST</i> Imaging
Stella Seitz	Universitäts-Sternwarte München	Yes	GO	Revealing the Largest Gravitational Lens PLCK G287.0+32.9
Anil Seth	University of Utah		AR	Black Holes and Central Mass-to-Light Ratios in Low Mass Early-type Galaxies
Tom Shanks	Durham University	Yes	GO	Tracing the CMB Cold Spot Supervoid Using H _I Gas Clouds
Edward Shaya	University of Maryland		GO	Draining the Local Void
Yue Shen	Carnegie Institution of Washington		GO	Host galaxy Properties of $z \sim 0.3$ Broad-line AGN With Direct Black Hole Masses from Reverberation Mapping
J. Shull	University of Colorado at Boulder		AR	Spatial Modeling of the Topology of He II Reionization
Devin Silvia	Michigan State University		AR	Can Thermal Instabilities Drive Galactic Precipitation and Explain Observed Circumgalactic Structure?
Russell Smith	University of Durham	Yes	GO	Improved Masses for Two New Low-redshift Strong Lens Galaxies: Do Giant Ellipticals Really Have a Heavy IMF?
Roberto Soria	Curtin University		GO	Diagnosing the Super-Eddington Accretion/Outflow Regime Using the Microquasar MQ1 in M83
Elizabeth Stanway	The University of Warwick	Yes	GO	Understanding the Star Formation Environment of a Very Low Redshift, Low Luminosity, Long γ -ray Burst
Daniel Stark	University of Arizona		GO	COS Views of He II Emitting Star-forming Galaxies: Preparing for the <i>JWST</i> Era
John Stocke	University of Colorado at Boulder		GO	Probing Hot Gas in Spiral-Rich Galaxy Groups
Lorrie Straka	Universiteit Leiden	Yes	GO	Damped Lyman- α Systems in the Disks of Low- z SDSS Galaxies on Top of QSOs
Veronica Strazzullo	Universitäts-Sternwarte München	Yes	GO	Environmental Signatures on Galaxy Populations in the Most Massive Clusters at $z \sim 1.5$
Nial Tanvir	University of Leicester	Yes	GO	Identifying and Studying γ -ray Bursts at Very High Redshifts
Elisa Toloba	University of California–Santa Cruz		AR	The Nature of Compact Stellar Systems in Massive Galaxy Clusters Using the <i>Hubble</i> Frontier Fields
Christy Tremonti	University of Wisconsin–Madison		GO	Direct Imaging of Galactic Winds in Extreme Starburst Galaxies
Tommaso Treu	University of California–Los Angeles		GO	Accurate Cosmography From Gravitational Time Delays: 2.3% on H ₀ from Deep WFC3 Images of Lensed Quasars
Ignacio Trujillo	Instituto de Astrofísica de Canarias	Yes	GO	The Pristine Globular-cluster Population of the Primordial Relic Galaxy NGC1277
Kohji Tsumura	FRIS, Tohoku University		GO	Absolute Measurement of the Cosmic Near-Infrared Background Using Eclipsed Galilean Satellites as Occulters
Pieter van Dokkum	Yale University		GO	A Wide-Field WFC3 Imaging Survey in the COSMOS Field
Schuyler Van Dyk	California Institute of Technology		GO	A Search for a Light Echo from Supernova 2013ej
Sjoert van Velzen	The Johns Hopkins University		GO	A First Look at the Late Stages of Accretion in Tidal Disruption Flares
Eros Vanzella	INAF, Osservatorio Astronomico di Bologna	Yes	GO	Unveiling the Lyman Continuum Morphology with <i>HST</i>
Bart Wakker	University of Wisconsin–Madison		GO	Mapping the Circumgalactic Medium of Two Large Spiral Galaxies

Accepted Proposals

Name	Institution	ESA Member	Type	Title
Ran Wang	KIAA, Peking University		GO	Imaging the Extended Star Formation in the Host Galaxy of a Millimeter Bright Quasar at $z = 6.13$
John Wise	Georgia Tech Research Corp.		AR	Observational Diagnostics for High-redshift Galaxies with Massive Black Hole Seeds
Guy Worthey	Washington State University		SNAP	NGSL Extension 1. Hot Stars and Evolved Stars
Eva Wuyts	Max-Planck-Institut für Extraterrestrische Physik	Yes	GO	A Complete Census: Mapping the Ly- α Emission and Stellar Continuum in a Lensed Main-Sequence Galaxy at $z = 2.39$ Hosting an AGN-driven Nuclear Outflow
Guangtun Zhu	The Johns Hopkins University		GO	Characterizing the Circumgalactic Medium of Luminous Red Galaxies
Planetary Programs				
Daniel Apai	University of Arizona		AR	Scanning Red Skies: Contribution Functions for Interpreting <i>HST</i> Multi-layer Observations of Ultracool Atmospheres
Gilda Ballester	University of Arizona		GO	New FUV Diagnostics of the Atmosphere of the Hot-Jupiter HD 209458b with <i>HST</i> /COS
Susan Benecchi	Planetary Science Institute		GO	Collisional Processing in the Kuiper Belt and Long-range KBO Observations by <i>New Horizons</i>
Zachory Berta-Thompson	Massachusetts Institute of Technology		GO	The Atmospheres of Two Low-mass, Low-density Exoplanets Transiting a Young Star
Beth Biller	University of Edinburgh, Institute for Astronomy	Yes	GO	Exometeorology: Characterizing Weather on a Young Free-floating Planet
Dennis Bodewits	University of Maryland		GO	Far-UV Spectroscopic Measurements of the Deuterium Abundance of Comets
Vincent Bourrier	Observatoire de Genève	Yes	GO	Probing the Nature and Evolution of the Oldest Known Planetary System Through Lyman-alpha Observations
Vincent Bourrier	Observatoire de Genève	Yes	GO	Characterization of the Extended Atmosphere and the Nature of the Hot Super-Earth 55 Cnc e and the Warm Jupiter 55 Cnc b
Brendan Bowler	California Institute of Technology		GO	Imaging Accreting Protoplanets in the Young Cluster IC 348
Imke de Pater	University of California–Berkeley		GO	Giant Impacts on Giant Planets
Michał Drahus	Uniwersytet Jagielloński	Yes	GO	<i>Hubble</i> Close-Up of the Disrupting Asteroid P/2012 F5
David Ehrenreich	Observatoire de Genève	Yes	GO	<i>HST</i> Confirmation and Characterization of a Potentially Habitable World
David Ehrenreich	Observatoire de Genève	Yes	GO	Full <i>HST</i> Coverage of a Comet-like Exoplanet in Transit
Thomas Evans	University of Exeter	Yes	GO	Measuring the L-T Transition for a Warm Saturn Exoplanet
Yanga Fernandez	University of Central Florida		AR	Characterizing Outbursts and Nucleus Properties of Comet 29P/Schwassmann-Wachmann 1
Kevin France	University of Colorado at Boulder		GO	A Direct Imaging Experiment to Determine the Origin of H ₂ Emission from M-dwarf Exoplanetary Systems
Boris Gänsicke	The University of Warwick	Yes	SNAP	The Frequency and Chemical Composition of Rocky Planetary Debris Around Young White Dwarfs: Plugging the Last Gaps
John Gizis	University of Delaware		GO	Cloud Evolution on Uranus with K2 and <i>HST</i>
Gregory Herczeg	Peking University		GO	The Very Low-mass Object FW Tau b: An Edge-on Brown Dwarf Disk or a Planet Caught in Formation?

Accepted Proposals

Name	Institution	ESA Member	Type	Title
Dean Hines	Space Telescope Science Institute		GO	Post-perihelion Imaging Polarimetry of the 67P/Churyumov-Gerasimenko with ACS: Continued Support of the <i>Rosetta</i> Mission
Mark Hollands	The University of Warwick	Yes	GO	The Dawn of Rocky Planet Formation
David Jewitt	University of California–Los Angeles		GO	<i>Hubble</i> Imaging of a Newly Discovered Active Asteroid
Paul Kalas	University of California–Berkeley		GO	First Imaging Polarization Study of Fomalhaut's 140 AU Dust Belt
Laurent Lamy	Observatoire de Paris–Section de Meudon	Yes	GO	The Grand Finale: Probing the Origin of Saturn's Aurorae with <i>HST</i> Observations Simultaneous to <i>Cassini</i> Polar Measurements
Jian-Yang Li	Planetary Science Institute		GO	Born Small or Gone Small–Determining the Evolutionary State of Comet 252P/LINEAR during its Close Approach to Earth
Christopher Manser	The University of Warwick	Yes	GO	A Highly Dynamical Debris Disk in an Evolved Planetary System
Carl Melis	University of California–San Diego		GO	Down the Tubes: Vetting the Apparent Water-rich Parent Body Being Accreted by the White Dwarf GD 16
Jonathan Nichols	University of Leicester	Yes	GO	Observing Jupiter's FUV Auroras Near Juno Orbit Insertion
Alex Parker	Southwest Research Institute		AR	A High-Precision Archival Measurement of the Kuiper Belt Luminosity Function
David Polishook	Weizmann Institute of Science		GO	Establishing an Evolutionary Sequence for Disintegrated Minor Planets
Aki Roberge	NASA Goddard Space Flight Center		GO	Inventing Gas in Debris Disks: UV Spectroscopy of Eta Tel
Lorenz Roth	Royal Institute of Technology	Yes	GO	Probing Ceres' Exosphere and Water Vapor Outgassing
Mark Showalter	SETI Institute		GO	Neptune's Evolving Inner Moons and Ring-arcs
Bruno Sicardy	Observatoire de Paris	Yes	GO	Search for Material Around Chiron
David Sing	University of Exeter	Yes	GO	Characterizing the Atmosphere of the Enlarged Neptune-mass Planet HAT-P-26b
William Sparks	Space Telescope Science Institute		GO	Monitoring the Ice Plumes of Europa
Lawrence Sromovsky	University of Wisconsin–Madison		GO	Methane Distribution and Transport in the Active Atmosphere of Uranus
Margaret Turnbull	SETI Institute		AR	Characterizing the Galactic and Extragalactic Background of Exoplanet Direct-imaging Targets
Hannah Wakeford	University of Exeter	Yes	GO	Measuring the Absolute H ₂ O Abundance of WASP-39b's Atmosphere
Paul Wilson	CNRS, Institut d'Astrophysique de Paris	Yes	GO	Far-UV Observations of H, C, N and O in Exocomets of Beta Pic
Siyi Xu	European Southern Observatory– Germany	Yes	GO	A Young White Dwarf with an Infrared Excess: Dust Disk or Substellar Companion?
Galactic Programs				
Loïc Albert	Université de Montréal		GO	Direct Test of the Brown Dwarf Evolutionary Models through Secondary Eclipse Spectroscopy of LHS 6343
Heddy Arab	Space Telescope Science Institute		GO	Mapping Dust Extinction Properties Across the IC 63 Photodissociation Region
Nate Bastian	Liverpool John Moores University	Yes	GO	Searching For Multiple Populations in Massive Young and Intermediate-age Clusters

Accepted Proposals

Name	Institution	ESA Member	Type	Title
Philip Bennett	Eureka Scientific Inc.		GO	A Red Supergiant Mass Accurate to 1%
Luciana Bianchi	The Johns Hopkins University		SNAP	Understanding Stellar Evolution of Intermediate-mass Stars from a New Sample of Sirius B-like Binaries
Howard Bond	The Pennsylvania State University		GO	The Nature of SPIRITS Mid-Infrared Extragalactic Transients
Martha Boyer	NASA Goddard Space Flight Center		GO	Assessing the Impact of Metallicity on Stellar Dust Production
Martha Boyer	NASA Goddard Space Flight Center		GO	The Evolution of Metal-rich Asymptotic Giant Branch Stars
Alyson Brooks	Rutgers the State University of New Jersey		AR	Small Statistics No More: a Suite of Simulated Dwarf Galaxies to Interpret Observations
Peter Brown	Texas A & M University		GO	An Ultraviolet View of Overluminous Type Ia Supernovae
Nuria Calvet	University of Michigan		GO	Trickles of Accretion: Catching a Final Glimpse of Gas in the Disk
Deirdre Coffey	University College Dublin	Yes	GO	True Jet Rotation Probed in NUV Jet Core
Roger Cohen	Universidad de Concepción		GO	Opening the Window on Galaxy Assembly: Ages and Structural Parameters of Globular Clusters Towards the Galactic Bulge
Andrew Cole	University of Tasmania		GO	The Star-formation History and Proper Motion of NGC 6822
Matteo Correnti	Space Telescope Science Institute		GO	Pushing to Sub-Gyr Globular Cluster Ages: the IR CMD of NGC 6397
Denija Crnojevic	Texas Tech University		GO	Resolved Halo Substructures Beyond the Local Group: the Assembly Histories of NGC 253 and NGC 5128
Matthew Darnley	Liverpool John Moores University	Yes	GO	A Remarkable Recurrent Nova in M31: The Leading Single Degenerate Supernova Ia Progenitor Candidate (?)
Cody Dirks	Northwestern University		AR	Investigating the Gas within the Planck Galactic Cold Clumps
Hui Dong	Instituto de Astrofísica de Andalucía	Yes	GO	Opening a New Window towards the Nuclear Star Cluster in the Milky Way
Trent Dupuy	University of Texas at Austin		GO	Mapping the Substellar Mass-Luminosity Relation Down to the L/T Transition
Zachary Edwards	Louisiana State University and A & M College		GO	Startlingly Fast Evolution of the Stingray Nebula
Catherine Espaillat	Boston University		GO	Footprints of the Magnetosphere: the Star-disk Connection in T Tauri Stars
Nancy Evans	Smithsonian Institution Astrophysical Observatory		GO	Precision Masses and Distances of Classical Cepheids
Steven Federman	University of Toledo		GO	A Multiwavelength Study of the Nature of Diffuse Atomic and Molecular Gas
Alex Filippenko	University of California–Berkeley		AR	The Local Environments of Supernovae from Archival <i>HST</i> Images
Alex Filippenko	University of California–Berkeley		SNAP	Continuing a Snapshot Survey of the Sites of Recent, Nearby Supernovae
Ryan Foley	University of Illinois at Urbana–Champaign		AR	Archival Investigations of the Local Environments of Supernovae
Ryan Foley	University of Illinois at Urbana–Champaign		GO	Possible Stellar Donor or Remnant for the Type Ia SN 2008ha
Ori Fox	University of California–Berkeley		GO	Long-lost Companions: A Search for the Binary Secondaries of Three Nearby Supernovae

Accepted Proposals

Name	Institution	ESA Member	Type	Title
Morgan Fraser	University of Cambridge	Yes	GO	Searching for the Disappearance of the Progenitor of the Unique SN 2009ip
Anna Frebel	Massachusetts Institute of Technology		GO	Constraining Pop III Supernova Energies and the Formation of the First Low-mass Stars with the Iron-poor Star HE1327-2326 (with $[\text{Fe}/\text{H}] = -5.4$)
Boris Gänsicke	The University of Warwick	Yes	GO	An <i>HST</i> Legacy Ultraviolet Spectroscopic Survey of the 13pc White Dwarf Sample
Avishay Gal-Yam	Weizmann Institute of Science		GO	Explosions in Real Time: Ultra-rapid UV Flash Spectroscopy of Infant Core-collapse Supernovae
Carme Gallart	Instituto de Astrofísica de Canarias	Yes	GO	The Lowest Mass Galaxies with Extended Star Formation History: a New Cosmological Challenge
Miriam Garcia	Centro de Astrobiología (CSIC/INTA)	Yes	GO	The Winds of the Most Fe-poor Massive Stars of the Local Group: Sextans-A
Douglas Gies	Georgia State University Research Foundation		GO	The Fastest Rotating Stars
Karl Gordon	Space Telescope Science Institute		GO	Small Magellanic Cloud Ultraviolet Dust Extinction: A Focused Study of Four Sightlines near a Molecular Cloud with Variable 2175 Å Bumps
Paul Goudfrooij	Space Telescope Science Institute		GO	Probing Extended Star Formation in the Young Massive Star Cluster NGC 1850
Paul Goudfrooij	Space Telescope Science Institute		GO	Resolving the Nature of the Stellar Halo of the Sombrero, the Nearest Giant Early-type Spiral Galaxy
Jonathan Hargis	Haverford College		GO	New Faint Galaxies at the Local Group's Edge: Antlia B and Five Candidate Ultra-faint Dwarfs
Christian Johnson	Smithsonian Institution Astrophysical Observatory		GO	NGC 6273: Towards Understanding a New Class of Galactic Globular Clusters
Jason Kalirai	Space Telescope Science Institute		GO	Using Stellar Evolution as a Clock to Watch the Dynamical Evolution of a Globular Cluster
Oleg Kargaltsev	George Washington University		GO	Establishing the Nature of the Far-UV Emission from the Double Pulsar
C. Kochanek	The Ohio State University		GO	Confirming NGC 6946 BH1—A Black Hole Formed in a Failed Supernova
Shrinivas Kulkarni	California Institute of Technology		GO	UV Spectroscopy of Supernova-companion Interaction in a Type Ia Supernova
Thierry Lanz	Observatoire de la Côte d'Azur	Yes	GO	Probing Supernovae Chemical Yields in Low-metallicity Environments with UV Spectroscopy of Magellanic Cloud B-type Stars
Andrew Levan	The University of Warwick	Yes	GO	The Late Time Behaviour and Environments of the First Gravitational-wave Transients
Chun-Fan Liu	Academia Sinica, Institute of Astronomy and Astrophysics		GO	Identifying Ionization Mechanisms through Spatially-resolved Neon Emission in the Jets of Sz 102
Kevin Luhman	The Pennsylvania State University		GO	Testing Model Atmospheres with the Coldest Known Brown Dwarf
Thomas Madura	NASA Goddard Space Flight Center		AR	A Robust Method for Modeling 3-D <i>HST</i> /STIS Data Cubes Using Time-dependent 3-D Simulations
Jesús Maíz-Apellániz	Centro de Astrobiología (CSIC/INTA)	Yes	GO	The Optical-UV Extinction Law in 30 Doradus
Dan Maoz	Tel Aviv University–Wise Observatory		GO	Connecting White Dwarf Rotation and Debris Accretion

Accepted Proposals

Name	Institution	ESA Member	Type	Title
Derck Massa	Space Science Institute		GO	FUVB Flat Fields for the COS FUV Blue Modes
Derck Massa	Space Science Institute		GO	The Wind of ksi Per: A Tomographic View of Stellar Wind Dynamics
Justyn Maund	University of Sheffield	Yes	GO	Stellar Forensics VII: A Post-explosion View of the Progenitors of Core-collapse Supernovae
Roberto Mignani	INAF, Istituto di Astrofisica Spaziale e Fisica	Yes	GO	The Old Pulsar PSR J0108-1431, a Key Target to Understand the Long-term Evolution of Neutron Stars
Roberto Mignani	INAF, Istituto di Astrofisica Spaziale e Fisica	Yes	GO	The Ultraviolet Light Curve and Spectrum of PSR B0540-69, the Crab Twin
Dan Milisavljevic	Smithsonian Institution Astrophysical Observatory		GO	The Unprecedented Supernova Metamorphosis of SN 2014C
James Miller-Jones	Curtin University		GO	Confirmation of the First Ultracompact Black Hole X-ray Binary
Antonino Milone	Australian National University		GO	Multiple Stellar Populations in Two Young Large Magellanic Cloud Clusters: NGC 1755 and NGC 1866
Katja Poppenhaeger	Smithsonian Institution Astrophysical Observatory		GO	The Magnetic Activity Puzzle of the Super-Earth Host Star KOI-314
Blagoy Rangelov	George Washington University		GO	The Intermediate-age Cluster GLIMPSE-C01
John Raymond	Smithsonian Institution Astrophysical Observatory		GO	Thermal Equilibration and Cosmic-ray Acceleration in Astrophysical Shocks: UV Spectra of the SN1006 Remnant
Seth Redfield	Wesleyan University		GO	Connecting Earth with its Galactic Environment: Probing Our Interstellar Past Along the Historical Solar Trajectory
Armin Rest	Space Telescope Science Institute		GO	Spectral Time Series of the Cas A Supernova
Mark Reynolds	University of Michigan		GO	Characterizing a Magnetic CV Associated with a PNe via COS UV Spectroscopy
Ian Roederer	University of Michigan		GO	The First Detections of Phosphorus, Sulphur, and Zinc in a Bona-fide Second-generation Star
Ian Roederer	University of Michigan		GO	STIS Observations of Metal-poor Stars: Direct Confrontation with Nucleosynthetic Predictions
Elena Sabbi	Space Telescope Science Institute		GO	The Primordial Binary Fraction in Trumpler 14: Frequency and Multiplicity Parameters
John Salzer	Indiana University System		GO	The Intriguing Case of the (Almost) Dark Galaxy AGC 229385
Ata Sarajedini	University of Florida		GO	Exploring the Nature and Synchronicity of Early Cluster Formation in the Local Group
Adam Schneider	University of Toledo		GO	Taming the Tepid Three
Benjamin Shappee	Carnegie Institution of Washington		GO	Whimper of a Bang: Documenting the Final Days of the Nearby Type Ia Supernova 2011fe
Joshua Simon	Carnegie Institution of Washington		GO	The Lowest Luminosity Star-forming Galaxy
Edward Sion	Villanova University		GO	The SN Ia Candidate T Pyxidis: The Mystery of its High Accretion Rate
Nathan Smith	University of Arizona		AR	Are LBVs in Andromeda as Isolated as LMC LBVs? Critical Test of a Massive Star Paradigm
Sangmo Sohn	The Johns Hopkins University		GO	The First Proper Motions of Ultra-faint Dwarf Galaxies: Probing Reionization and Planar Associations of Satellites

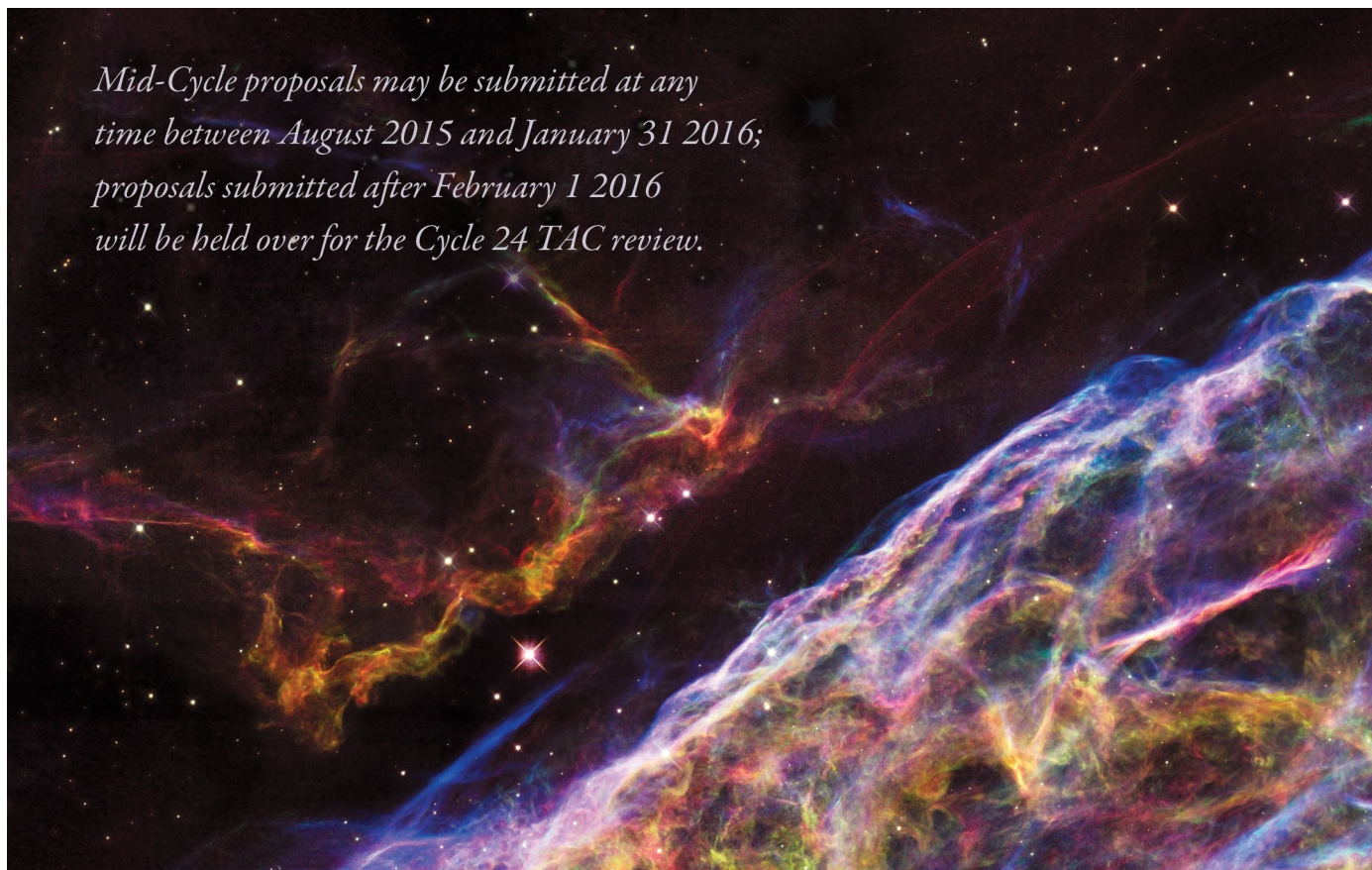
Accepted Proposals

Name	Institution	ESA Member	Type	Title
Sangmo Sohn	The Johns Hopkins University		GO	Globular Cluster Orbits from <i>HST</i> Proper Motions: Constraining the Formation and Mass of the Milky Way Halo
Karl Stapelfeldt	NASA Goddard Space Flight Center		SNAP	A Snapshot Imaging Survey of <i>Spitzer</i> -selected Young Stellar Objects in Nearby Star-formation Regions
Jay Strader	Michigan State University		GO	Dynamical Confirmation of a Stellar-mass Black Hole in the Globular Cluster M62
Katalin Takats	Universidad Andrés Bello		GO	Verifying the Progenitor Identification of the Type II-P Supernova 2009ib
Jonathan Tan	University of Florida		AR	The Orion Experiment
Nial Tanvir	University of Leicester	Yes	GO	r-process Kilonova Emission Accompanying Short-duration GRBs
Pier-Emmanuel Tremblay	Space Telescope Science Institute		GO	The Suppression of Convection in Magnetic White Dwarfs
Pier-Emmanuel Tremblay	Space Telescope Science Institute		GO	Defining New IR-Bright Flux Standards for Cosmology Applications
Eleonora Troja	University of Maryland		GO	Identify the Signature of Neutron-star Mergers Through Rapid <i>Hubble</i> Observations of a Short GRB
R. Tully	University of Hawaii		AR	Exploiting the Archive for TRGB Distances
Jeff Valenti	Space Telescope Science Institute		AR	Improving UV Continuous Opacities and Model Spectra for Cool Stars
Schuyler Van Dyk	California Institute of Technology		GO	The Stellar Origins of Supernovae
Lifan Wang	Texas A & M University		GO	Imaging Polarimetry of Light Echoes around SN 2014J
Laura Watkins	Space Telescope Science Institute		AR	Finding Needles in Haystacks: Intermediate-mass Black Holes in Galactic Globular Clusters
Daniel Welty	University of Chicago		AR	An Archival Survey of Trace Neutral Interstellar Species: Comparing Diagnostics of Physical Conditions
Jessica Werk	University of California–Santa Cruz		GO	Using UV-bright Milky Way Halo Stars to Probe Star-formation Driven Winds as a Function of Disk-scale Height
Benjamin Williams	University of Washington		AR	Finding and Aging the Population of High-mass X-ray Binaries in M33
Benjamin Williams	University of Washington		AR	Measuring the Upper End of the Supernova Progenitor Mass Distribution in M83
Large Programs				
Luigi Bedin	Osservatorio Astronomico di Padova	Yes	GO	The End of the White Dwarf Cooling Sequences of Omega Centauri
Sanchayeeta Borthakur	The Johns Hopkins University		GO	How are H I Disks Fed? Probing Condensation at the Disk-halo Interface
Drake Deming	University of Maryland		GO	A Metallicity and Cloud Survey of Exoplanetary Atmospheres Prior to <i>JWST</i>
Robert Kirshner	Harvard University		GO	RAISIN2: Tracers of Cosmic Expansion with SN IA in the IR
Nicolas Lehner	University of Notre Dame		GO	Project AMIGA: Mapping the Circumgalactic Medium of Andromeda
S. Megeath	University of Toledo		SNAP	A Snapshot WFC3 IR Survey of <i>Spitzer/Herschel</i> -identified Protostars in Nearby Molecular Clouds
Casey Papovich	Texas A & M University		GO	The CANDELS Lyman-alpha Emission At Reionization (CLEAR) Experiment

Accepted Proposals

Name	Institution	ESA Member	Type	Title
Treasury Programs				
Daniel Apai	University of Arizona		GO	Cloud Atlas: Vertical Cloud Structure and Gravity in Exoplanet and Brown Dwarf Atmospheres
Dan Coe	Space Telescope Science Institute	Yes	GO	RELICS: Reionization Lensing Cluster Survey
Ruth Peterson	SETI Institute		GO	The Intersection of Atomic Physics and Astrophysics: Identifying UV Fe I Lines from Metal-poor Turnoff Stars
Brian Siana	University of California–Riverside		GO	The Final UV Frontier: Legacy Near-UV Imaging of the Frontier Fields
Pure Parallel Program				
Matthew Malkan	University of California–Los Angeles		GO	WFC3 Infrared Spectroscopic Parallel Survey: The WISP Deep Fields
AR Legacy Programs				
Maruša Bradač	University of California–Davis		AR	Breaking Cosmic Dawn: Observing the $z \gtrsim 7$ Universe through Cosmic Telescopes
Danilo Marchesini	Tufts University		AR	A Legacy Archive Program Providing Optical/NIR-selected Multiwavelength Catalogs and High-level Science Products of the <i>HST</i> Frontier Fields
Eric Murphy	California Institute of Technology		AR	Enhancing the Frontier Field Legacy by Combining the Power of <i>HST</i> and the Jansky VLA

Mid-Cycle proposals may be submitted at any time between August 2015 and January 31 2016; proposals submitted after February 1 2016 will be held over for the Cycle 24 TAC review.



Lyman- α : The Many Applications and Challenges of This Powerful Emission Line

Jeffrey L. Linsky, jlinsky@jila.colorado.edu

The atomic hydrogen Lyman- α line centered at 1215.67 Å has proven to be extremely valuable for studying stellar mass loss, fluorescent excitation of molecular hydrogen in the environments of very young stars, the deuterium/hydrogen ratio in the Galaxy, and mass loss and photochemical processes in exoplanet atmospheres. These powerful applications result from Lyman- α being the strongest emission line in the ultraviolet spectrum of solar-type stars and as strong as the entire ultraviolet spectrum of cooler stars. The UV-sensitive Space Telescope Imaging Spectrograph and Cosmic Origins Spectrograph on the *Hubble Space Telescope* have been very effective tools for studying these diverse phenomena, despite the challenges posed by Lyman- α 's extreme opacity and the absorption of most of its flux by interstellar hydrogen.

The anatomy of the Lyman- α line

The observed Lyman- α emission line of the nearby star α Centauri B shown in Figure 1 highlights the challenges and opportunities for using this spectral line as a probe of stars and interstellar gas. Even though this star is only 4 light-years away, the optical depth at the center of the interstellar absorption exceeds 100,000, and the amount of interstellar absorption in the line center is difficult to analyze. Except for the very few rapidly moving stars like Kapteyn's star (radial velocity 245 km s⁻¹), interstellar absorption removes the entire stellar emission-line core, requiring some technique for reconstructing the intrinsic stellar emission line.

Fortunately, the deuterium Lyman- α absorption line is located at -81.55 km s⁻¹ relative to the hydrogen Lyman- α line. D and H have nearly the same excitation and ionization in the warm interstellar medium, but different thermal broadening and abundance. For many stars located within the low-density interstellar gas extending to roughly 300 light-years from the Sun, known as the Local Cavity, interstellar absorption in the D line is not saturated. As a result, one can infer the interstellar H absorption profile by fitting the D-line profile assuming the present-day cosmic abundance ratio with the heavier singly ionized iron and magnesium ions, providing information on the interstellar velocity dispersion along the line of sight.

Using this technique, Wood et al. (2005a) have reconstructed the Lyman- α emission lines of 40 stars. France et al. (2013) have developed another reconstruction technique useful for lines of sight with simple interstellar gas velocity structures. Even for the nearest stars, the intrinsic stellar flux is at least twice the observed value and often much larger. With these reconstructed Lyman- α fluxes, Linsky et al. (2013) have identified correlations with other stellar emission lines and stellar activity parameters that provide estimates of the intrinsic Lyman- α fluxes of stars like the Sun or cooler, including exoplanet host stars.

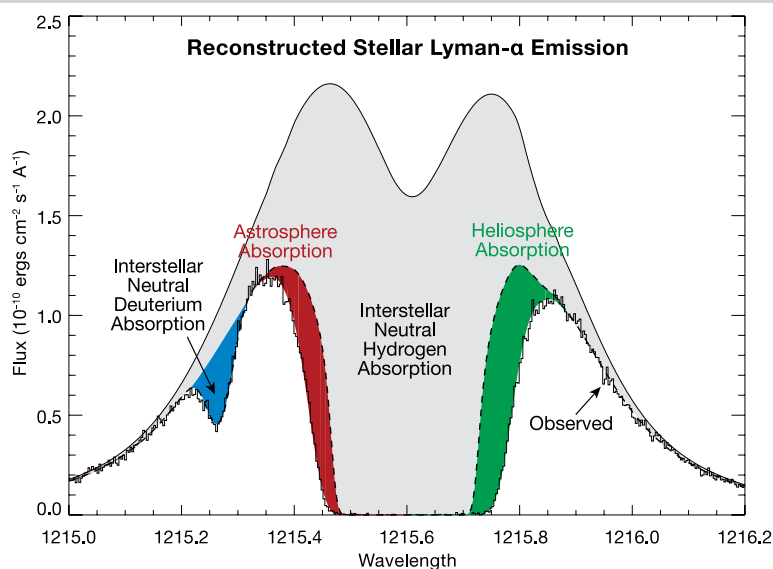


Figure 1: The Lyman- α line profile of the middle-aged K1 V star α Centauri B (thick line) observed with the echelle grating (resolution $\lambda/\Delta\lambda = 90,000$) of *Hubble*'s first generation instrument, the High Resolution Spectrograph. The unabsorbed Lyman- α emission line emitted by the stellar chromosphere (thin line) has been reconstructed from the deuterium absorption line, the present-day D/H ratio, and kinematic information on the interstellar medium from heavy ions. The light gray shading indicates absorption by interstellar hydrogen, and the blue shading centered at 1215.3 Å (-81.55 km s⁻¹ from the center of the hydrogen absorption) is absorption by interstellar deuterium. Extra absorption (green) on the long wavelength side of the interstellar hydrogen absorption is produced by hydrogen in the solar hydrogen wall. Extra absorption (red) on the short wavelength side of the interstellar absorption is produced by hydrogen in the stellar hydrogen wall. The original figure is from Linsky & Wood (1996).

Deuterium in the local Galactic disk

The deuterium Lyman- α line also plays a critical role in measuring the deuterium-to-hydrogen number ratio (D/H), which is an important test of the density of ordinary matter and the creation of H, D, and He in the very early Universe. Since, the observed D/H ratios in the Galactic disk gas are altered by many competing processes, sorting out these processes requires accurate D/H measurements for a variety of sight lines through different regions of the Galaxy.

For sight lines to the very closest stars, the interstellar D and H Lyman- α lines measure the D/H ratio, but for longer lines of sight in the Galaxy, Lyman- β and the higher lines in the Lyman series provide the required range of optical depths in both the D and H lines to accurately measure the D/H ratio. Analysis of these higher Lyman lines along many lines of sight observed with the *Far Ultraviolet Spectrograph Explorer* (FUSE) satellite allowed Linsky et al. (2006) to infer a D/H ratio of 15.6 ± 0.4 parts per million (ppm) in the gas located within about 300 light-years of the Sun.

At further distances, the large range in interstellar gas D/H ratios between 4 and 23 ppm can be explained by different amounts of D gas depletion onto dust grains along these lines of sight. This technique has allowed Cooke et al. (2014) and others to infer D/H ratios in very metal-poor gas toward quasars using the Lyman series lines redshifted into the *Hubble* spectral range.

Mass loss from solar-like and cooler stars

Unexpectedly, the deuterium Lyman- α interstellar absorption has also provided a critical clue for measuring stellar mass-loss rates, a measurement needed to calculate the erosion of planetary atmospheres. The slowing down of cool-star rotation rates with age requires that these stars lose mass, but there has been no reliable technique for measuring these mass-loss rates. A critical clue to finding a mass-loss rate diagnostic was provided by the velocity separation between the D and H Lyman- α lines, which is fixed by atomic physics at -81.55 km s $^{-1}$, but is often significantly different from the predicted value.

The likely cause is charge exchange between outflowing stellar-wind protons and interstellar H atoms that produces a pileup of heated-decelerated H atoms forming a hydrogen wall in the outer heliosphere and in its stellar analog, the astrosphere. As shown in Figure 1, the heliospheric hydrogen wall produces absorption on the long wavelength side of the interstellar H absorption, and the astrospheric hydrogen wall produces absorption on the short wavelength side. Depending on which absorption feature is stronger, the separation of the interstellar D and H absorption-line centers can be either larger or smaller than the atomic physics value.

The breakthrough in finding a useful spectral diagnostic for stellar mass loss occurred when Wood et al. (2005b) showed that the observed Lyman- α profiles are well matched by models of the interaction between stellar winds and the interstellar medium. These models predict that the astrospheric absorption feature moves to shorter wavelengths (more negative velocities) relative to the interstellar H absorption with increasing stellar mass-loss rate. Figure 2 shows an example of using the shape of the astrospheric absorption feature to infer the stellar

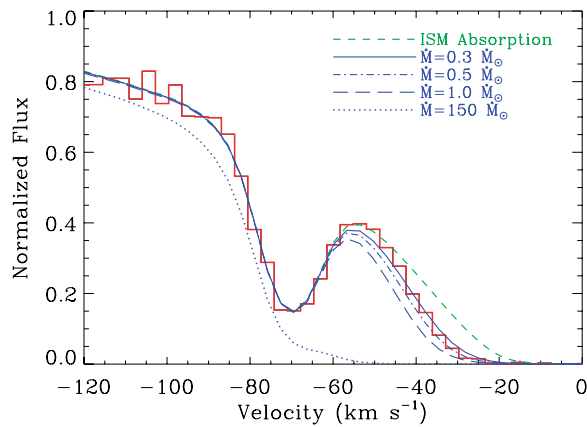


Figure 2: A portion of the Lyman- α line of π^1 UMa, a rapidly rotating young G1.5 V star, observed with the Space Telescope Imaging Spectrograph's E140M grating (resolution $\lambda/\Delta\lambda = 45,000$). The observed profile (red) is compared with astrospheric models with different mass-loss rates in units of the solar mass-loss rate ($2 \times 10^{-14} M_{\odot}/\text{yr}$). Increasing mass-loss rate extends the astrospheric absorption to more negative velocities. Figure from Wood et al. (2014).

mass-loss rate, in this case for the young, solar-like star π^1 Ursa Majoris.

Accurate measurements of the astrospheric Lyman- α absorption require high-resolution spectra observed through a narrow slit to suppress geocoronal emission (solar Lyman- α photons scattered by H atoms in the Earth's outer atmosphere). Only the high-resolution modes of the STIS instrument can obtain the Lyman- α spectra needed to measure cool star mass-loss rates. New observations are needed while STIS is still operating to measure the mass-loss rates of stars that are very active, very cool, and very young.

Fluorescence of H $_2$ and CO in the circumstellar disks of very young stars

For very young stars with circumstellar disks, generally called classical T Tauri stars (CTTS), reconstructed stellar Lyman- α emission lines are the background light sources that pump the rich cluster of fluorescent H $_2$ emission lines in their ultraviolet spectra. These fluorescent processes provide a unique tracer of small amounts of residual gas near the surfaces of protoplanetary disks left behind during planetary formation. Herczeg et al. (2004) found that for TW Hya, a prototypical CTTS, the fluorescing H $_2$ gas is located in a circumstellar disk at temperatures near 2500 K.

There are also UV emission lines of CO seen in *Hubble* COS spectra that are pumped by Lyman- α in CTTS (France et al. 2011). The *Hubble* Cycle 17 large observing program "The Disks, Accretion, and Outflows (DAO) of T Tau Stars" (P.I. Gregory Herczeg) has provided a wealth of observations of these stars, including many examples of Lyman- α fluorescence.

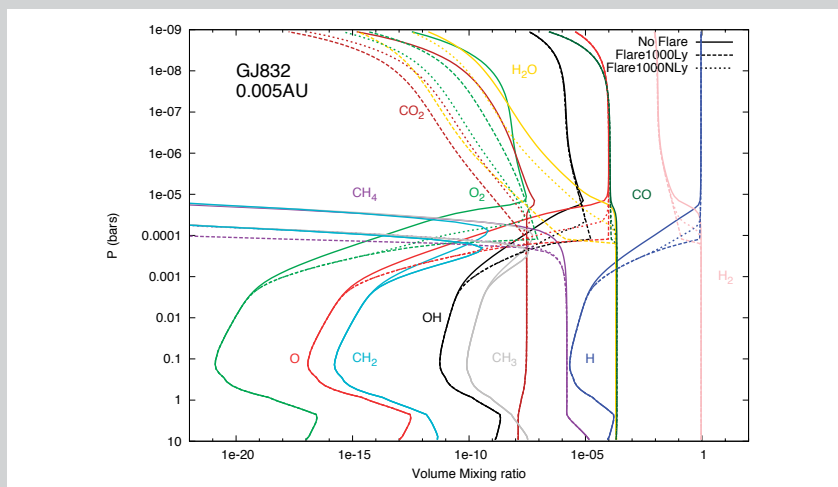


Figure 3: Mixing ratios for important molecules and atoms in the atmosphere of a hypothetical hot Jupiter exoplanet located close to the star GJ 832. These simulations include the ultraviolet fluxes of the quiescent M1 V host star, a flare with 1000 times the quiescent Lyman- α flux, and a flare with no increase in the Lyman- α flux. The effect of increased Lyman- α flux is to dissociate water and carbon dioxide high in the atmosphere where the gas pressure is 0.0001 bars, producing increased abundances of atomic hydrogen and oxygen. Figure courtesy of Yamila Miguel.

Hot exoplanets with Lyman- α tails

Reconstructed stellar Lyman- α emission lines are also the background light sources for studying exoplanet atmospheres during transits. The discovery of significantly more Lyman- α line absorption during the transit of the exoplanet HD 209458b compared to STIS observations outside of transit led Vidal-Madjar et al. (2003) to conclude that this hot-Jupiter exoplanet is losing mass.

Subsequent observations by this group and others (see the recent review by Fossati 2015) showed that other gas giant exoplanets are also losing H and other elements from their outer atmospheres through hydrodynamic outflows (also known as hydrodynamic “blow-off”), ion pickup by the stellar wind, and Roche lobe overflow (Bourrier & Lecavelier des Etangs 2013). Absorption seen in H Lyman- α and other lines after transit egress (e.g., Kulow et al. 2014) indicates planetary mass loss in a comet-like tail, and absorption seen prior to ingress has been interpreted as absorption by a shock ahead of the planet in its orbit.

Photochemistry in exoplanet atmospheres

Finally, reconstructed stellar Lyman- α emission lines also control the photochemistry in exoplanet atmospheres. The peak photodissociation cross-sections of water, carbon dioxide, and methane are located in the 1000–1700 Å spectral region. Since the stellar Lyman- α emission line is the strongest emission feature in the UV spectra of G and K stars and is as strong as the entire 1200–3200 Å region in M dwarfs (France et al. 2013), Lyman- α plays a critical role in the photochemistry of these molecules.

Figure 3 shows a simulation of the effects of Lyman- α radiation on several molecular species in the atmosphere of a hypothetical hot Jupiter located close to its cool host star. In this simulation and in simulations for the mini-Neptune GJ 436b (Miguel et al. 2015), an increase in the Lyman- α flux by a factor of 1000, as could occur during a flare or continuously in very active stars, reduces the H₂O and CO₂ mixing ratios by factors of 10–100 at atmospheric levels above 0.0001 bars.

At the same time, the mixing ratios of atomic H and O and O₂ are increased by the same factors between pressure levels 0.0001 and 0.00001 bars. This simulation demonstrates that O, O₂, and O₃ can be produced abiotically (e.g., Domagal-Goldman et al. 2014; Tian et al. 2014). Also, the production of atomic H and O by Lyman- α photodissociation of H₂O and their ionization by extreme-ultraviolet radiation from the host star can lead to mass loss by ion pickup in the stellar wind. This process may explain the loss of the atmosphere of Mars (Brain et al. 2009).

Acknowledgements

The author thanks Kevin France for suggestions and Yamila Miguel for her unpublished figure. I also thank NASA and the Space Telescope Science Institute for the efficient operation of the *Hubble Space Telescope* that is the source of the data presented here.

Continued
page 28

References

- Bourrier, V., & Lecavelier des Etangs, A. 2013, A&A, 557, 124
Brain, D., et al. 2009, Icarus, 2006, 139
Cooke, R. J., Pettini, M., Jorgenson, R. A., Murphy, M. T., & Steidel, C. C. 2014, AJ, 781, 31
Domagal-Goldman, S. D., et al. 2014, ApJ, 792, 90
Fossati, L., et al. 2015, arXiv:1503.01278
France, K., et al. 2011, ApJ, 734, 31
France, K., et al. 2013, ApJ, 763, 149
Herczeg, G. J., Wood, B. E., Linsky, J. L., Valenti, J. A., & Johns-Krull, C. M. 2004, ApJ, 607, 369
Kulow, J. R., France, K., Linsky, J. L., & Parke Loyd, R. O. 2014, ApJ, 786, 132
Linsky, J. L., & Wood, B. E. 1996, ApJ, 463, 254
Linsky, J. L., et al. 2006, ApJ, 647, 1106
Linsky, J. L., France, K., & Ayres, T. 2013, ApJ, 766, 69
Miguel, Y., Kaltenegger, L., Linsky, J. L., & Rugheimer, S. 2015, MNRAS, 446, 345
Tian, F., France, K., Linsky, J. L., Mauas, P. J. D., & Viejtes, M. C. 2014, EPSL, 385, 22
Vidal-Madjar, A., Lecavelier des Etangs, A., Désert, J.-M., Ballester, G. E., Ferlet, R., Hébrard, G., & Mayor, M. 2003, Nature, 422, 143
Wood, B. E., Müller, H.-R., Redfield, S., & Edelman, E. 2014, ApJ, 781, L33
Wood, B. E., Müller, H.-R., Zank, G. P., Linsky, J. L., & Redfield, S. 2005b, ApJ, 628, L143
Wood, B. E., Redfield, S., Linsky, J. L., Müller, H.-R., & Zank, G. P. 2005a, ApJS, 159, 118

Up and Down! A Third Lifetime Position for COS/FUV

Julia Roman-Duval, duval@stsci.edu, and the COS/STIS Instrument Team

Introduction

The Cosmic Origins Spectrograph (COS) far-ultraviolet (FUV) channel uses three stacked photon-counting micro-channel plate (MCP) detectors to convert incoming photons into clouds of ten million or so electrons. Cross-delay line (XDL) anodes located at the bottom of the MCPs measure the time and location of incident photons, as well as the size of the electron clouds, called the pulse height (PH) or gain.

The number of electrons that can be extracted from a pixel is limited and corresponds to about 2.7×10^4 photons (Sahnou et al. 2013). Therefore, the extraction of charge from the MCPs during COS/FUV detector use causes the instrument to lose its ability to convert incoming photons into detectable electron clouds. The peak of the PH distribution, or modal gain, consequently decreases, a process called gain-sag (Figure 1, top panel).

When the modal gain drops below 3, some electron clouds become too small for detection by the electronics, causing a local loss of 5% or more in recorded flux (Figure 1, bottom panel). The gain-sag effect is seen throughout the spectrum owing to continuum sources, but is worst in regions where the high count-rate Ly α airglow line is recorded (Figure 2). Flux loss incurred by gain-sag resembles spectral absorption features and compromises the spectral quality of COS/FUV spectra.

To ensure that the lifespan of COS/FUV extends out to 2020, and to optimize its scientific return, a gain-sag management strategy has been implemented. The response of the detector declines with usage, but increases when the operating high-voltage (HV) of the MCPs is increased (Figure 2). Therefore, the COS/FUV HV is periodically increased to avoid gain-sag induced flux loss.

When the maximum operational HV values are reached and spectral information can no longer be recovered by increasing the HV, the location of science spectra on the detector, called the lifetime position, needs to be moved to a pristine region of the detector. Figure 3 shows the G130M/1291 locations of the five different lifetime positions that are available, constrained by the aperture mechanism to fit within $\pm 6''$ about the position used initially for operations (LP1). Each lifetime position typically lasts 2–3 years, depending on usage.

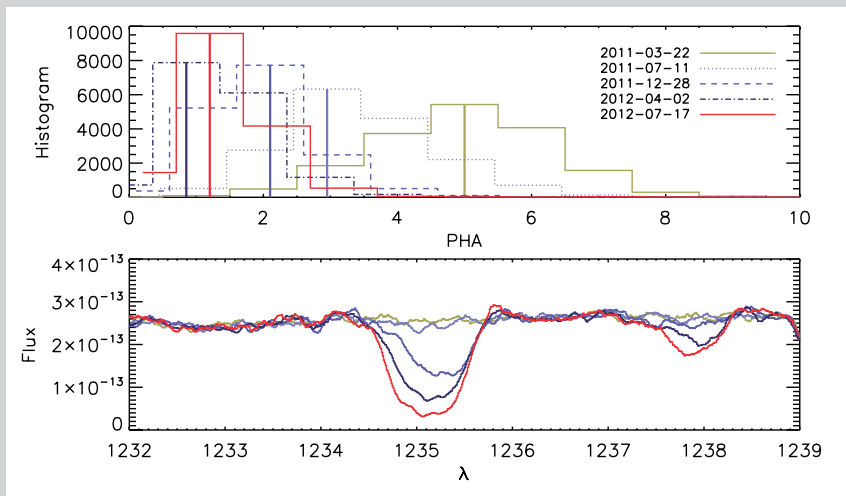


Figure 1: (Top) Pulse height distribution in an airglow region as a function of time. As the detector is used and charge extracted, the size of the electron clouds or pulse height (histograms) and corresponding modal gain (solid lines) decreases. (Bottom) Spectra in the same airglow region as a function of time. When the modal gain decreases below 3 due to usage-induced gain-sag, flux loss resembles spectral lines.

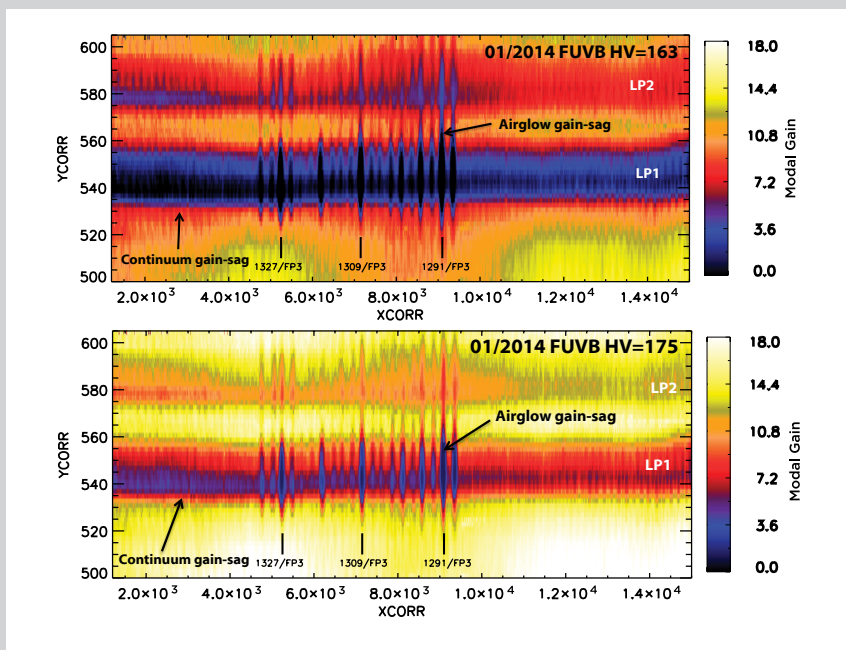


Figure 2: Modal gain maps on FUVB obtained during LP2 operations in January 2014 at HV numeric settings of 163 (top) and 175 (bottom). The modal gain increases with HV. The trenches in the modal gain incurred by Lyman α airglow are clearly visible as vertical stripes, and are indicated in the Figure for the FP-POS = 3 setting of the 1291, 1309, and 1327 central wavelengths. Gain-sag in the continuum covers most of the footprint of lifetime position 1.

COS/FUV operations initially started at LP1, which lasted until July 23, 2012. On that date science spectra were moved to lifetime position 2 (LP2), about +3.5'' or 41 pixels above LP1 in the cross-dispersion direction. The HV was increased twice (on June 24, 2013 and on July 21, 2014) on the FUVB detector to mitigate gain-sag effects. The HV was increased once on FUVB. Monitoring of the COS/FUV usage and modal gain showed that, by February 2015, the modal gain at LP2 at the maximum operational HV would reach the critical value of 3 in two or more airglow regions, incurring flux losses not recoverable by dithering with multiple FP-POS. As a result, the move to the COS/FUV lifetime position 3 (LP3) was planned for February 2015, and preparations for the LP3 move were started in September 2013.

Continued
page 30

Optimization of the LP3 location

Since LP2 was located *above* LP1, LP3 was to be placed *below* LP1 (Figure 3). While maximizing the spectral resolution and lifetime of COS/FUV implied that LP3 should be located as close to LP1 as possible, ensuring that COS/FUV spectra at LP3 maintain their excellent spectral quality imposed some major constraints on how much LP3 spectra could overlap with the deep gain-sag holes left at LP1, and therefore how small the LP1–LP3 separation could be.

Simulations of data taken at various locations between $-2''$ and $-3.5''$ below LP1 showed that, for all modes except the “blue modes” G130M/1055 and 1096 which have very wide cross-dispersion profiles, no significant ($>2\%$) flux loss would occur if LP3 were to be located farther than $2.1''$ from LP1. The wide 1222 central wavelength would have to operate at 4 HV levels higher than other modes in order to minimize the impact of gain-sag from LP1.

The simulations made use of our knowledge of the gain at LP1 at the end of LP1 operations, of the flux loss as a function of modal gain, as well as the knowledge of the footprint (or profiles) of each COS/FUV central wavelength on the detector. It was therefore decided to leave the “blue modes” (1055 and 1096) operating at LP2 and to move all other modes to LP3. Since the move to LP3 was scheduled before gain-sag holes occurred, the blue modes are not impacted by gain-sag, and do not incur continuum gain-sag due to their wide spectral profiles, induced by the extreme specialized grating rotation angles and corresponding focus values for those modes.

Based on the results from the simulations, on-orbit data at $-2.06''$ and $-2.33''$ below LP1 were taken with the G130M/1291, G130M/1222, and G140L/1280 as part of program 13618. The goal of this program was to verify that the flux accuracy and spectral quality of spectra taken this close to LP1 was consistent with the expectations from the simulations. The 1291, 1222, and 1280 cenwaves have

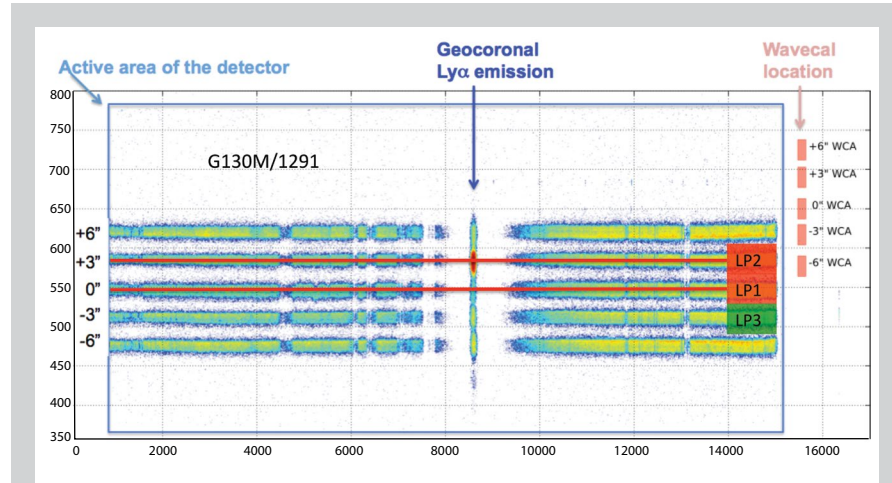


Figure 3: The five lifetime positions available for COS/FUV. The aperture mechanism constrains the different lifetime positions to fit within $\pm 6''$ about LP1.

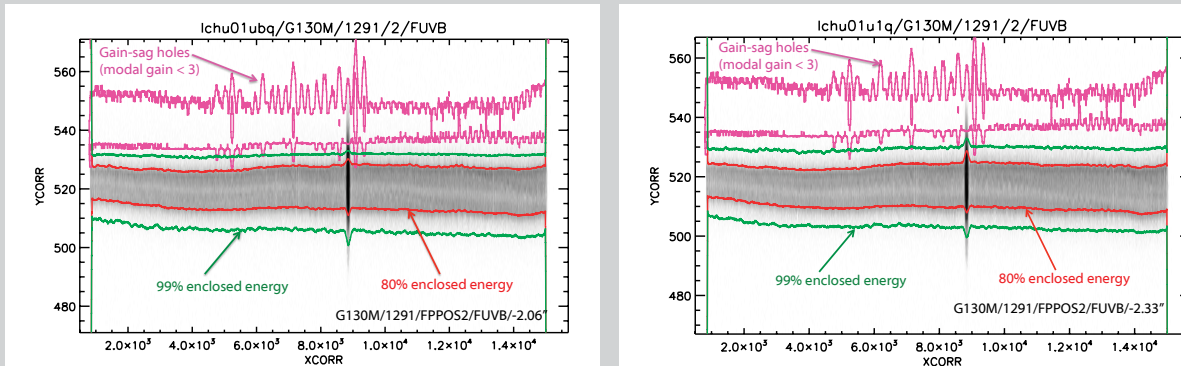


Figure 4: G130M/1291/FP-POS2 exposures on FUVB taken as part as 13618, at $-2.06''$ below LP1 (*left*) and $-2.33''$ below LP1 (*right*). The gray scale corresponds to the flat-fielded image in detector coordinates. The red and green lines correspond to the 80% and 99% enclosed energy contours of the spectral profiles. The pink contours show the gain-sag holes from LP1 where the modal gain is lower than 3. At $-2.06''$, the 80% enclosed energy contour of the 1291 spectra (red) overlap slightly with gain-sag holes, while at $-2.33''$ below LP1, gain-sag holes only affect the wings (outer 10%) of the spectral profiles and do not incur flux loss $>2\%$.

the widest cross-dispersion profiles and fall the closest to the LP1 gain-sag regions and therefore represent the limiting cases for the smallest possible LP1–LP3 separation.

Analysis of the 13618 data showed that at $-2.06''$, the inner 80% enclosed energy core of the G130M profiles slightly (by 1 pixel) overlapped with the gain-sag holes at LP1 (Figure 4), although no flux loss $>2\%$ could be observed in FP-POS-combined spectra. At $-2.33''$, the LP1 gain-sag holes lay well above the core of the LP3 G130M profiles, and no flux loss could be observed in individual FP-POS exposures. To ensure that all science spectra are properly calibrated even with the maximum centering error of the target acquisition (± 3 pixels), LP3 was therefore located at $-2.5''$ below LP1 with a safe margin of 4 pixels from the edges of the gain-sag holes.

The shorter separation between LP1 and LP3 compared to LP1–LP2 required major changes to the extraction algorithm in CALCOS. The “two-zone” extraction was implemented in CALCOS 3.0 and 3.1 to support science at LP3. Proffitt et al. describe this in a companion *Newsletter* article.

Calibration of COS/FUV lifetime position 3

The cross-dispersion profiles, flat-field, flux calibration, and spectral resolution of COS/FUV depend on detector location. Three programs were executed to calibrate the COS/FUV instrument at LP3. Program 13932 (PI Debes) executed in September 2014 and achieved several calibration goals. These deep observations of *Hubble* standard stars WD0308-565 and GD71 allowed us to derive precise cross-dispersion profiles and centroid traces at LP3 to be used in the two-zone extraction (see *Newsletter* article by Proffitt et al.).

Flat-fields and sensitivity curves at LP3 were also established. The L-flats at LP3 are grating-dependent and different from previous lifetime positions (Figure 5). The corresponding LP3 reference files were implemented in the CALCOS pipeline in July 2015 and achieve 2% and 5% accuracies in the relative and absolute flux calibrations, respectively.

Program 13933 (PI Fox) executed in February 2015 with the goal of verifying the performance of COS/FUV observations at LP3 with the bright object aperture (BOA) and measuring its spectral resolution. A preliminary analysis of those data shows that the spectral resolution of the BOA has decreased slightly compared to LP2 (by $\sim 20\%$) and is now similar to the spectral resolution at LP1.

Finally, program 13931 (PI Roman-Duval) executed in July 2015 and acquired observations of SMC star AzV 75 to measure the zero-point offset of the wavelength solution and characterize the spectral resolution of COS/FUV at LP3. As expected, the spectral resolution at LP3 is $<5\%$ lower than at LP2 (and 10–15% lower than at LP1).

Impact for observers

The move of COS/FUV from LP2 to LP3 has been transparent to users. New calibration products (e.g., flat-field and flux calibration) were delivered recently, and users were advised to re-retrieve their data in an STScI Analysis Newsletter (July 2015 STAN). The spectral resolution of COS/FUV decreased by $<5\%$ between LP2 and LP3. Each target is observed at only one LP.

Future of COS/FUV

If the usage of COS/FUV remains steady, LP3 will suffer from gain-sag effects in the summer of 2017. Spectra will need to be moved to yet another lifetime position, LP4. The location of LP4 has not yet been determined.

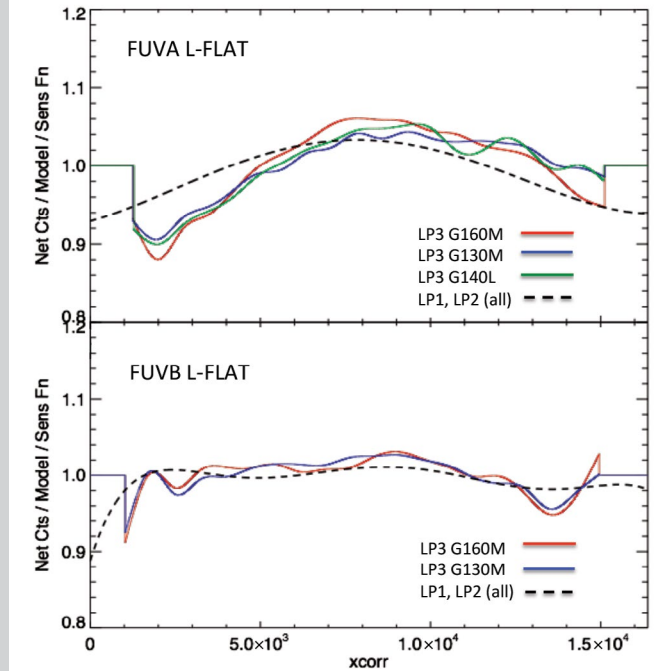


Figure 5: COS/FUV L-flats for FUVA (top) and FUVB (bottom). The LP1 and LP2 L-flats were identical, while the LP3 L-flat is grating dependent and is different from previous lifetime positions.

Squeezing Together: A New Procedure for Extracting Spectra at the Third COS/FUV Lifetime Position

Charles R. Proffitt, proffitt@stsci.edu, and the COS/STIS Team

Introduction

The micro-channel plates of the Cosmic Origins Spectrograph (COS) far-ultraviolet (FUV) detector have a limited lifetime. A high voltage gradient across the detector's micro-channel plates (MCPs) creates a cascade of electrons in response to each detected FUV photon. However, only so many electrons can be extracted from a given location of each MCP, and once a given detector pixel has been exposed to about 2.7×10^4 photons, the number of electrons produced per photon, i.e., the gain, gets too low to reliably locate the original photon.¹ This localized "gain sag" on the MCP makes it necessary to adjust the COS FUV aperture locations and *Hubble* pointing every few years to shift the spectra to a fresh part of the detector. These adjustments are referred to as "Lifetime Position" moves.

As detailed in the accompanying article by Roman-Duval et al., the second such move, from Lifetime Position 2 (LP2) to Lifetime Position 3 (LP3), was made on February 9, 2015. At current usage rates, each Lifetime Position should give good quality data for about 2½ years. Up to five total positions are potentially available. This should allow the COS FUV channel to continue operation well past 2020 with only minor compromises in its performance.

To maximize spectral resolution and the lifetime of COS, it was decided to locate LP3 at a location as close as possible to the original LP1 position. An offset from LP1 of only $-2.5''$ was adopted, significantly smaller than the $+3.5''$ offset adopted for LP2. Because this places new spectra very close to the worn-out regions near LP1, it complicates the extraction of 1D spectra from the 2D spectral images.

The COS detector format is long and narrow, with each of the two detector segments being divided into 16,384 pixels in the *X* or dispersion direction, but only 1024 in the *Y* direction perpendicular to the dispersion. When a spectrum of an external point-source target is taken, the 2D spectral image occupies only a small part of this vertical range (typically less than 30 pixels in the cross-dispersion direction). The exact location and height of the footprint of each COS mode on the detector vary with the grating and central wavelength setting, (as shown in Figure 1).

To extract the flux observed at each wavelength, it is first necessary to sum the detected counts at each wavelength (*X* location), over the illuminated cross-dispersion profile (*Y* direction). For a given

central wavelength setting, the older "BOXCAR" extraction algorithm, which COS uses for data taken at LP1 and LP2, adopts a fixed extraction region that is generously sized to include all of the flux from a point-source target even after allowing for typical centering errors in the aperture. If any "bad" pixels at all are included in the region being used for the sum, the entire column is marked as bad and these regions are excluded when combining different exposures.

At the new LP3 position, this can create problems, as illustrated in Figure 1. The overlap of the large

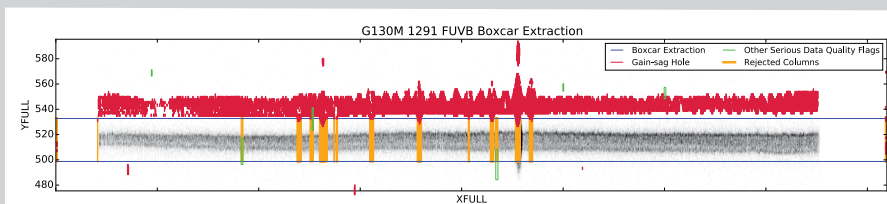


Figure 1: This illustrates how the BOXCAR algorithm would operate at LP3. The grayscale image shows the observed distribution of light on the FUVB detector segment for an observation of a hot standard star done using the 1291 setting of the COS G130M grating. The wavelength increases with the XFULL coordinate, while YFULL is the spatial direction perpendicular to the dispersion. The red regions show the areas of the detector damaged from earlier usage. The blue lines mark the edges of the region used in the BOXCAR extraction. At any location where the bad pixels fall in between the blue lines, the entire wavelength bin is flagged as bad. These regions are marked in yellow. As can be seen here, many wavelength bins are being rejected for rather minor overlap with the damaged regions.

¹Note that the COS NUV and the STIS FUV and NUV Multi-Anode Micro-channel plate Array (MAMA) detectors use crossed sets of anode wires to detect and locate events. This allows them to operate at significantly lower gain than does the long-format COS FUV delay line detector. Because of this design difference, degradation from gain sag is not expected to be a concern during the lifetime of the MAMA detectors.

extraction box with the previously damaged regions of the detector can result in several wavelength bins being discarded. However, the LP3 location was chosen so that these bad detector regions fall at the edge of the spectral profiles, where the loss of flux is negligible (see article by Roman-Duval). What is therefore needed is an algorithm that can decide when a “bad” pixel impacts the profile enough that it might significantly compromise the measured flux.

The new extraction procedure

The new TWOZONE extraction algorithm was developed for this purpose. The observed spectral image is first straightened by a new calibration step to remove residual optical and detector distortions in the cross-dispersion direction (see Fig. 2) and then shifted in the cross-dispersion direction to align with a point-source template reference profile (see Fig. 3). This reference profile is then “shrink-wrapped” to define two different regions for the extraction—an “inner” zone containing about 80% of the enclosed profile energy and an “outer” zone containing about 99% of the enclosed energy (see Fig. 4). The observed counts are summed over the full 99% enclosed energy region, but columns are rejected only if bad pixels are found in the inner zone.

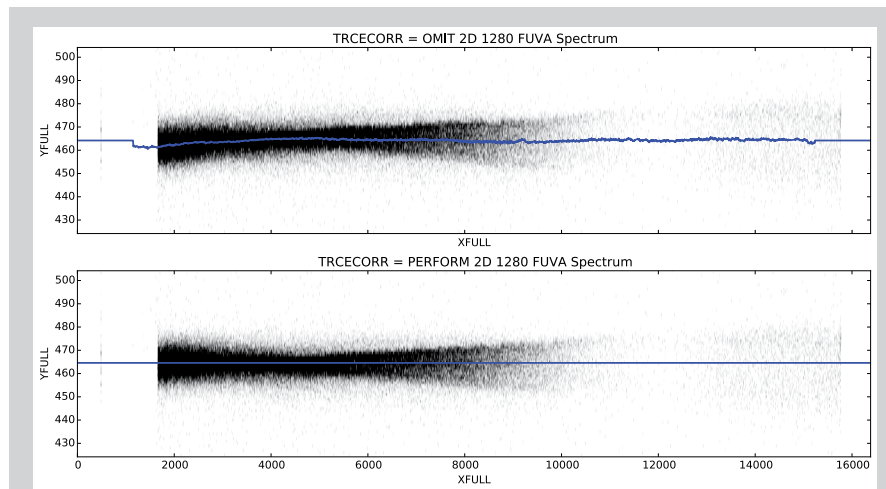


Figure 2: This figure shows how the new distortion correction in the revised algorithm removes optical and detector distortions, yielding a straighter spectrum that is easier to compare and align with reference profiles. The *top* panel shows the uncorrected spectral image for a G140L 1280 FUV observation, while the *bottom* panel shows the image after the correction has been applied.

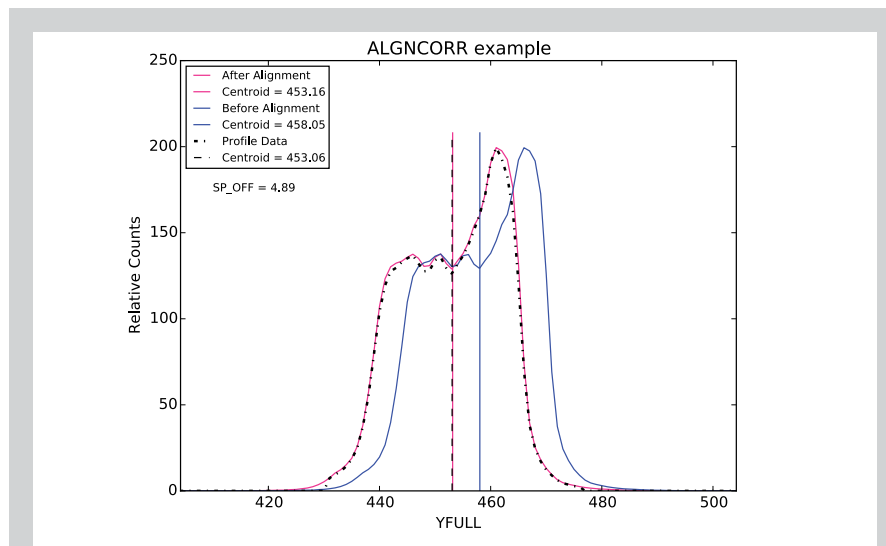


Figure 3: This figure shows the collapsed cross-dispersion profile, summed over all wavelengths, of a G130M 1222 FUV observation before (blue line) and after (pink line) the data have been aligned. For COS FUV observations, each pixel in the cross-dispersion direction corresponds to about 0.1" on the sky. The broken line shows the collapsed cross-dispersion reference profile to which the observed profile was aligned. The flux-weighted centroid values for each of the profiles are also marked by a vertical line.

*Continued
page 34*

A library of standard reference profiles, one for each of the available central wavelength settings, has been tabulated and is included with the reference files used to calibrate COS data. Using the reference template profiles rather than the observed data from each individual observation to define the inner and outer zones allows reliable calibration for even very faint and noisy observations. Another reference file contains the library of residual distortion corrections used to straighten the images prior to alignment with the profiles. This correction not only results in smoother profiles, but it ensures that the centering in the cross-dispersion direction is done consistently, regardless of the shape of the source spectral energy distribution.

In Figure 5, we show how this new algorithm is applied to the data shown in Figure 1. The columns are only rejected when a pixel in the inner 80% of the enclosed energy is marked as bad. This dramatically reduces the number of gaps in the extracted 1D spectrum without leading to the introduction of any artifacts from the gain-sag holes.

In the absence of bad detector regions, and when observing point sources, the new algorithm gives results very close to that of the old BOXCAR algorithm. If, instead of developing the TWOZONE algorithm, we had simply adopted a smaller BOXCAR extraction region and corrected the flux for the reduced enclosed energy fraction, the results would have been unacceptably sensitive to minor misalignments

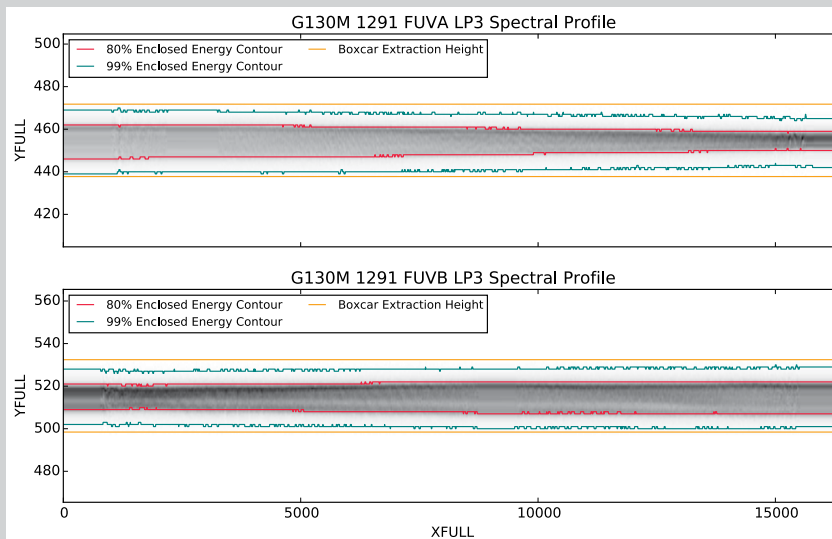


Figure 4: The point-source template reference profiles for both the FUVA (*top*) and FUVB (*bottom*) segments of the G130M 1291 setting at LP3 are shown by the grayscale images. Three sets of contours are also shown. The outermost yellow contours approximate the extraction region used in the BOXCAR algorithm. The blue curves mark the 99% enclosed energy contour, while the red curves show the 80% enclosed energy contour.

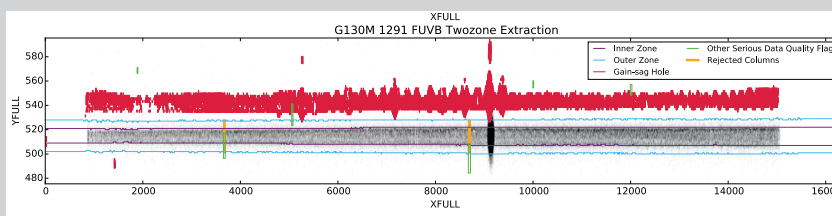


Figure 5: This figure illustrates the application of the new TWOZONE extraction algorithm. The annotations are as in Figure 1, except that instead of marking the large extraction region used for the BOXCAR algorithm, we show the boundaries of the inner (pink line, 80% enclosed energy) and outer (blue line, 99% enclosed energy) zones used in the TWOZONE extraction algorithm. Note that when using the TWOZONE algorithm, there are far fewer rejected regions (yellow) than there are when using the BOXCAR algorithm (Fig. 1)

of the source profile with the narrow extraction region. Summing over the 99% enclosed energy region of the spectral image allows the TWOZONE algorithm to be tolerant of such minor misalignments or changes in the profile's shape. Another advantage of the new algorithm is that by reducing the height over which spectra are extracted, the amount of detector background included is also reduced. This will improve the signal-to-noise for observations of very faint sources.

Because the new extraction region is narrower in the cross-dispersion direction than is the region used by the BOXCAR algorithm, the results for spatially extended sources calibrated using the TWOZONE algorithm may show larger artifacts than would have been the case for the older algorithm. Sources with an angular diameter larger than about 0.6 arcseconds may require a customized extraction to yield the best results.

This new TWOZONE extraction algorithm is currently being used by default for calibration of all COS FUV data taken at LP3, and is applied to all such data retrieved from the Milkulski Archive for Space Telescopes (MAST). Data from earlier lifetime positions continue to be calibrated using the BOXCAR algorithm. Full details are given in Instrument Science Report COS ISR 2015-02 by Proffitt et al., which is available on the COS instrument web pages, and in version 3.0 of the *COS Data Handbook* (Fox et al. 2016).

Preparing for *James Webb* *Space Telescope* Science

Jason Kalirai, jkalirai@stsci.edu

The fall of 2015 marks the three-year countdown to the launch of the *James Webb Space Telescope*, and the two-year countdown to the Cycle 1 *Call for Proposals*!

On schedule and budget

The development, integration, and testing of *Webb* hardware and software systems continued in 2015, and the project remains on schedule and budget for its October 2018 launch.

Progress towards several major mission milestones began in the past year. Following years of planning, the pathfinder (i.e., a test model) to the *Webb* backplane, which holds the primary mirrors, was moved into NASA's giant thermal vacuum chamber at the Johnson Space Center. Chamber A has a diameter of almost 20 meters and a height of 36 meters, and will serve as the primary testing ground for *Webb*'s optics and instruments in 2017.

Earlier this year, the first pathfinder test was performed in the fully deployed configuration, and was used to perform an end-to-end checkout of the optical test equipment in the Chamber to verify that future alignment and thermal tests of the flight structure will work as intended (Figure 1). The test also included an alignment of two engineering (i.e., spare) *Webb* mirrors mounted on the pathfinder backplane, a first for the mission. Using actuators, the two mirrors were aligned to better than 1/1000th diameter of a human hair, at -400°F ! A second optical pathfinder test in Chamber A will also include the Tertiary and Fine Steering Mirrors, and utilize special optical sources that simulate real star images.

The flight backplane of *Webb*, which will hold its 18 primary mirror segments, was delivered from Northrop Grumman Aerospace Systems to a clean room in NASA's Goddard Space Flight Center (GSFC) in August 2015. This delivery represents a major milestone for the project, and sets up the next crucial phase of assembling the 6.5-meter *Webb* primary mirror for the first time. The first mirror segments were successfully installed late in 2015, this process can be watched live on the NASA Webb-cam, <http://www.jwst.nasa.gov/webcam.html> (Figure 2). We will soon see what the biggest space telescope ever made looks like!

The year 2015 also marked the beginning of the third and final cryo-vacuum test (CV3) of the *Webb* science instruments at GSFC (Figure 3). The Integrated Science Instrument Module (ISIM) has already successfully passed two complementary cryogenic tests. This last, crucial set of comprehensive performance tests and calibration data acquisitions will verify that all science instruments are ready

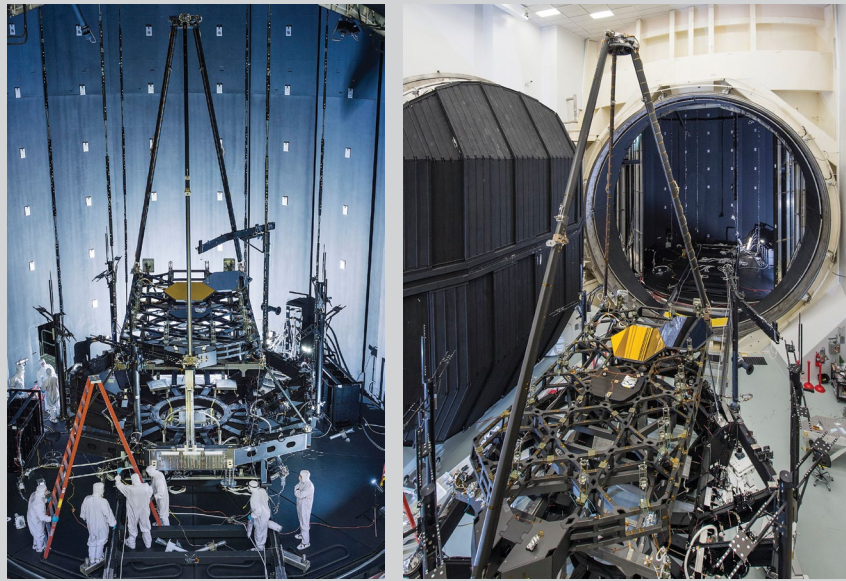


Figure 1: The testing of the *Webb* pathfinder backplane, with two spare mirrors, in Chamber A at NASA's Johnson Space Center.

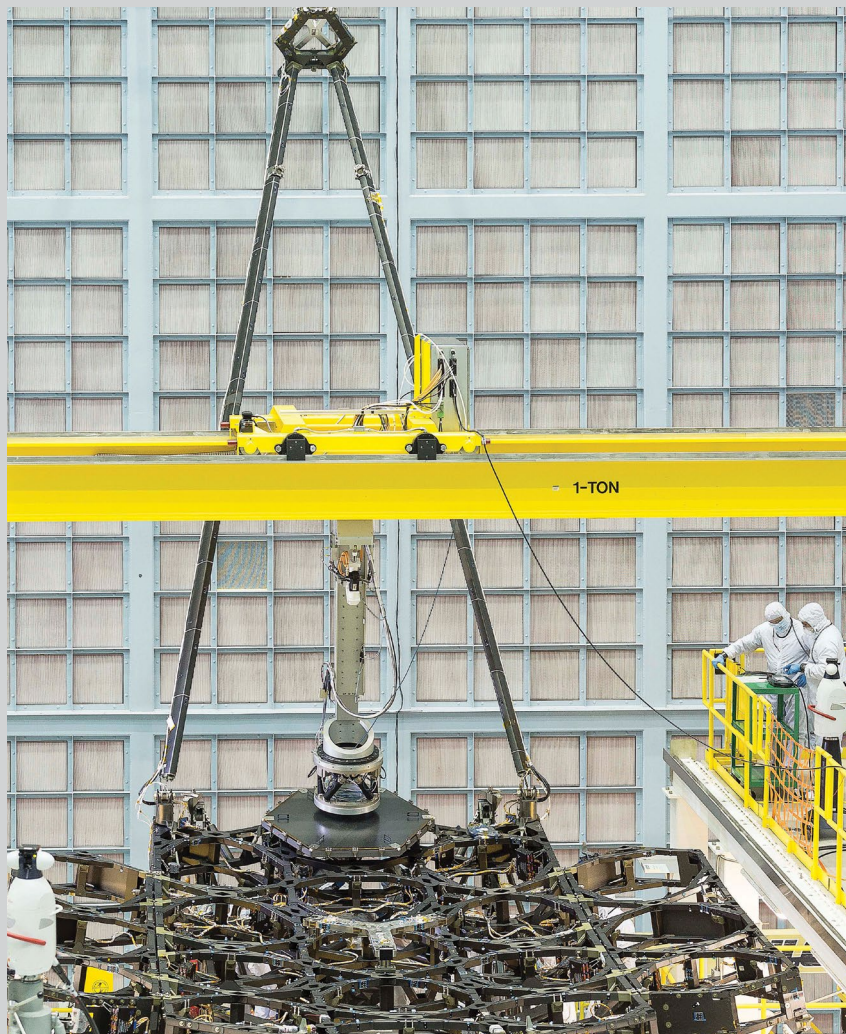


Figure 2: Engineers install the first mirror segment onto the *Webb* backplane at NASA GSFC (late 2015).

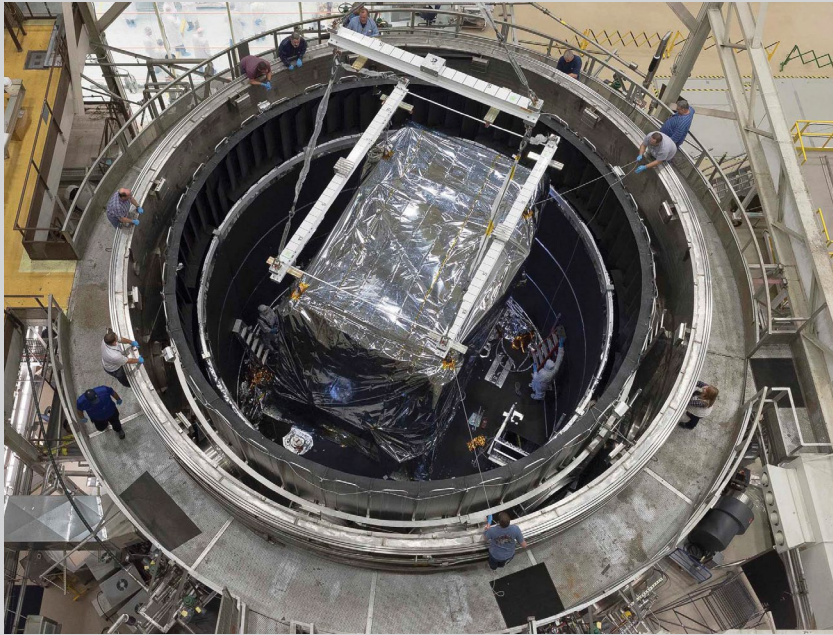


Figure 3: The *Webb* science instruments entering a thermal chamber at GSFC for their final cryotesting campaign.

for flight. STScI's commanding system for *Webb* science observations will also be tested during CV3. For example, "Day in the Life" tests will begin with the proposal planning system software and route commands through to the data management and calibration system pipelines.

Other *Webb* milestones in 2015 include the manufacturing of two of the five *Webb* flight sunshield layers, the flight cryocooler compressor assembly (used by the Mid-Infrared Instrument, MIRI) moving to acceptance testing, and the spacecraft bus structure being delivered to integration and testing.

The science timeline and Early Release Science Program

During the past few years, *Webb*-related discussions have largely focused on hardware, schedule, and budget. In October 2015, ESA organized and hosted a major international science conference, "Exploring the Universe with *JWST*" (Figure 4). Over two hundred scientists from the international community came together at ESTEC in the Netherlands to highlight how *Webb* would affect major themes in astronomical research today.

Based on contributions from a broad range of science communities, including: solar system exploration; exoplanet characterization; stellar populations in the Local Volume; and the distant Universe, there was a strong sense that the science case for *Webb* is stronger than it has ever been.

For many fields in astronomy, the discoveries over the past 10 years motivate future capabilities exactly matching those of *Webb*: high sensitivity, combined with high-resolution imaging in the near- and mid-infrared part of the spectrum; sensitive spectroscopy in integral fields; slit, slitless, and multi-object modes; and both near- and mid-infrared coronagraphs (see Table 1).

The first General Observer (GO) science observations with *Webb* are likely to be scheduled six months after launch, in April 2019. The preparations for those observations must start much earlier, as illustrated in Figure 5, which shows the current science timeline. The call for GO Proposals for Cycle 1 will be issued by the Institute in November 2017, just two years from now! Guaranteed Time Observers (GTOs), including the PI-led instrument teams and the interdisciplinary scientists, will have submitted their observing proposals earlier that year, finalizing their Cycle 1 observations by June 2017. Those specific observations are protected from duplication, and the list will be published and available to the GO community. The proposal deadline for Cycle 1 GO proposals will be in February 2018, with the Telescope Allocation Committee (TAC) meeting in May 2018 to recommend the final program.

The Cycle 2 proposal schedule is more condensed. The GO *Call for Proposals* will be issued in September 2019, with the proposal deadline set for December 2019 and the TAC meeting in February 2020. With the proposal deadline only 7 months into the cycle, many members of the GO community could be faced with very limited access to *Webb* science data.



Figure 4: The "Exploring the Universe with *JWST*" conference at ESTEC in October 2015 brought leading scientists from the community together to discuss *Webb*.

Webb Imaging Modes

Mode	Instrument	Wavelength (microns)	Pixel Scale (arcsec)	Field of View
Imaging	NIRCam	0.6–2.3	0.032	2.2 x 4.4'
	NIRCam	2.4–5.0	0.065	2.2 x 4.4'
	NIRISS	0.9–5.0	0.065	2.2 x 2.2'
	MIRI	5.0–28	0.11	1.23 x 1.88'
Aperture Mask Interferometry	NIRISS	3.8–4.8	0.065	2.2 x 2.2'
Coronagraphy	NIRCam	0.6–2.3	0.032	20 x 20"
	NIRCam	2.4–5.0	0.065	20 x 20"
	MIRI	10.65	0.11	24 x 24"
	MIRI	11.4	0.11	24 x 24"
	MIRI	15.5	0.11	24 x 24"
	MIRI	23.0	0.11	30 x 30"

Webb Spectroscopy Modes

Mode	Instrument	Wavelength (microns)	Resolving Power ($\lambda/\Delta\lambda$)	Field of View
Slitless Spectroscopy	NIRISS	1.0–2.5	150	2.2 x 2.2'
	NIRISS	0.6–2.5	700	single object
	NIRCam	2.4–5.0	2000	2.2 x 2.2'
Multi-Object Spectroscopy	NIRSpec	0.6–5.0	100, 1000, 2700	3.4 x 3.4' with 250k 0.2 x 0.5" microshutters
Single Slit Spectroscopy	NIRSpec	0.6–5.0	100, 1000, 2700	slits with 0.4 x 3.8" 0.2 x 3.3" 1.6 x 1.6"
	MIRI	5.0–~14.0	~100 at 7.5 microns	0.6 x 5.5" slit
IFU Spectroscopy	NIRSpec	0.6–5.0	100, 1000, 2700	3.0 x 3.0"
	MIRI	5.0–7.7	3500	3.0 x 3.9"
	MIRI	7.7–11.9	2800	3.5 x 4.4"
	MIRI	11.9–18.3	2700	5.2 x 6.2"
	MIRI	18.3–28.8	2200	6.7 x 7.7"

Table 1

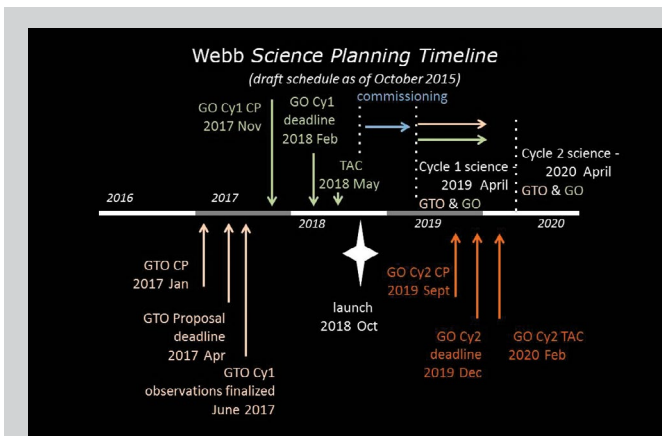


Figure 5: The General Observer (GO) proposal schedule for *Webb* cycles 1 and 2.

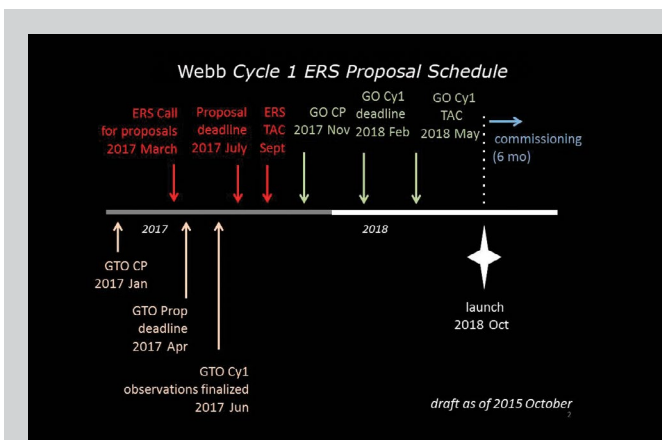


Figure 6: The draft schedule for Early Release Science program.

Following the recommendation of the *JWST* Advisory Committee (JSTAC; <http://www.stsci.edu/jwst/advisory-committee>), the Institute intends to create an Early Release Science (ERS) program, undertaken relatively early in Cycle 1, and using up to 500 hours of Director's Discretionary Time. This program is the first opportunity for the GO community to apply for *Webb* time. Data obtained as part of the ERS program will be non-proprietary, so that the full GO community will get access to a broad range of *Webb* data in time to inform Cycle 2 proposals. The successful proposal teams will also produce science-enabling data products for the community.

The ERS program will comprise a suite of science-driven observing programs, designed by the community and selected through proposal peer review. Programs will be competitively selected over a range of science areas, will span key *Webb* observing modes (see Table 1), and will have requirements to solve technical challenges that are essential to achieving broad *Webb* science objectives.

The anticipated timeline for the ERS program is shown in Figure 6. The *Call for Proposals* will be issued in March 2017, and may be preceded by a call for mandatory *Notices of Intent* to allow appropriate planning. The proposal deadline will be after the GTO Cycle 1 observations have been finalized and published, followed by a peer-reviewed selection in September 2017. The ERS results will be publicized prior to the GO Cycle 1 Call being released in November 2017.

The ERS program offers a fantastic opportunity for the community to quickly gain expertise on *Webb* through hands-on analysis of scientifically compelling data sets using a broad range of its complex observing modes. More information on the *Webb* ERS program will be posted at <http://www.stsci.edu/jwst/science/ers> and presented at the *Webb* Town Hall at the January 2016 American Astronomical Society meeting (Wednesday, January 6th at 6:30 pm).

Webb user tools

The first direct contact most observers will have with the *Webb* ground system is through the front end of the *Proposal and Planning*

Improving *Webb* Coronagraphic Performance with Small-Grid Dithers

Charles-Philippe Lajoie, lajoie@stsci.edu, Rémi Soummer, soummer@stsci.edu,
Laurent Pueyo, pueyo@stsci.edu, and the *JWST* Coronagraphs Working Group

Introduction

The *James Webb Space Telescope* will be equipped with a suite of coronagraphs allowing observers to hunt for faint point sources or extended structures around bright stars and galaxies. For example, the *Webb* coronagraphs will allow for the imaging and characterization of exoplanets orbiting bright stars within tens of astronomical units of the Sun, as well as disks around quasars and young stars. Coronagraphic observations typically rely on subtracting a reference star Point Spread Function (PSF) from the science target in order to remove the bright stellar scattered light (also called “speckles”) and reveal any faint surrounding objects. In recent years, coronagraphic observations have greatly benefited from advances in post-processing techniques, i.e., new methods that perform the aforementioned PSF subtraction using an optimal combination of reference stars. Here, we discuss the results of simulations aimed at demonstrating a possible new *Webb* mode that utilizes many subpixel dithered reference images, called Small-Grid Dithers, to optimize coronagraphic PSF subtraction.

Small-Grid Dithers simulations

PSF subtraction works best when the science target and the reference PSFs are positioned in the same way with respect to the occulting mask. The main reason is that small offsets, even of a few milliarcseconds in the case of the Mid-Infrared Instrument (MIRI), can drastically affect the speckle pattern, therefore limiting the efficiency of the PSF subtraction. However, because the *Webb* observatory slew accuracy is currently estimated to be ~ 5 milliarcseconds (1-sigma/axis), exactly matching the science target and the reference behind the coronagraphic masks cannot be done accurately.

Small-Grid Dithers are designed to circumvent this problem by providing a library of uniformly sampled PSFs from which an optimized synthetic PSF can be constructed to perform an improved subtraction (see Figure 1). The sampling of the PSF across the grid provides speckle diversity that is used to reconstruct an optimal reference PSF. Once the reference star is acquired, a small grid of observations is performed around its nominal position using Fine Steering Mirror offsets under fine guidance closed loop. These small dithers produce almost no overhead cost other than the additional exposure times. For technical guiding reasons, the maximum offset available for such dithers is limited to one Fine Guidance Sensor (FGS) pixel, i.e., ~ 69 milliarcseconds.

We have simulated Small-Grid Dithers for both the MIRI four-quadrant phase masks and the Near-Infrared Camera’s (NIRCam’s) round occulter and bar occulters using square grids of varying step sizes. Simulated PSFs are generated for the target as well as the reference at each grid point (e.g., Soummer & Makidon 2010; Perrin et al. 2011, 2012). We also include various noise sources as well as jitter (7 mas 1-sigma/axis) in our simulated images in order to create realistic scenes. Figure 2 illustrates the steps involved in our Small-Grid Dithers approach, where the end product is an image of the residuals from the PSF subtraction.

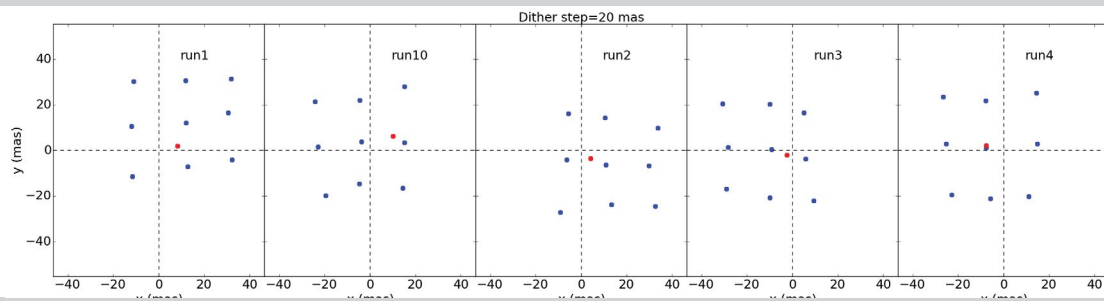


Figure 1: Multiple examples of Small-Grid Dithers for the reference star (blue dots) relative to an assumed science target star (red). The intersection of the dashed line represents the center of the coronagraphic mask and the target and references are positioned behind the mask using the expected observatory slew accuracy (5 mas at 1-sigma/axis). In general, the target and the reference stars will not be exactly collocated behind the mask, but the grid encompasses the target star location.

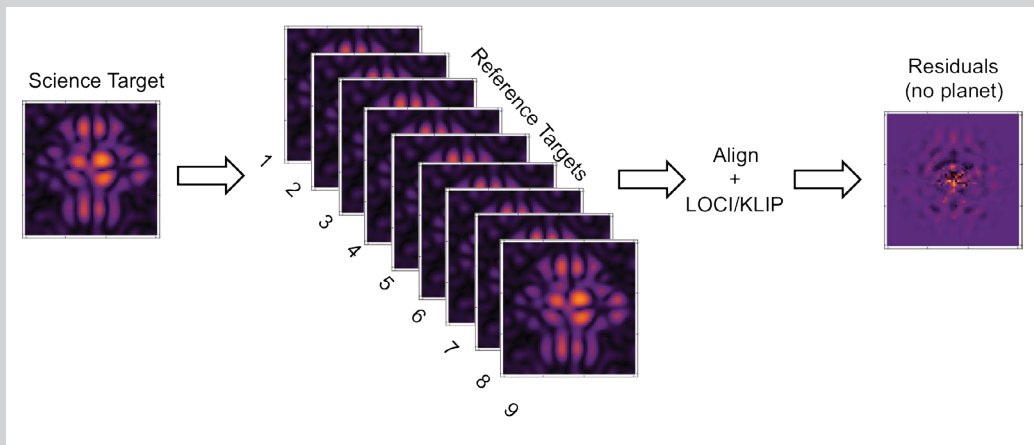


Figure 2: Cartoon illustrating the Small-Grid Dither technique. A science target image is first acquired, followed by a square grid of reference images. Post-processing then aligns the reference PSFs to the target PSF and performs a local optimization to build an improved synthetic PSF, which is used for the final PSF subtraction (e.g., Locally Optimized Combination of Images [LOCI] algorithm or KL Image Projection [KLIP] algorithm; see Lafrenière et al. 2007 and Soummer et al. 2012 respectively).

Contrast performance

We have run multiple stochastic simulations of Small-Grid Dithers from which we derive average azimuthal profiles at the 5-sigma level (see Figure 3). Our results suggest that Small-Grid Dithers can yield a gain in contrast compared to classical subtraction ranging from 2 to 6 for NIRCcam and greater than 10 for MIRI. Although the absolute contrast curves may vary based on different assumptions in our simulations (e.g., wavefront error, slew accuracy), our main result here is that *the relative gain between Small-Grid Dithers and Classical subtraction is significant for both NIRCcam and MIRI*. Note that, for completeness, we have explored the effect of larger wavefront error in our simulations and our conclusions remain unchanged.

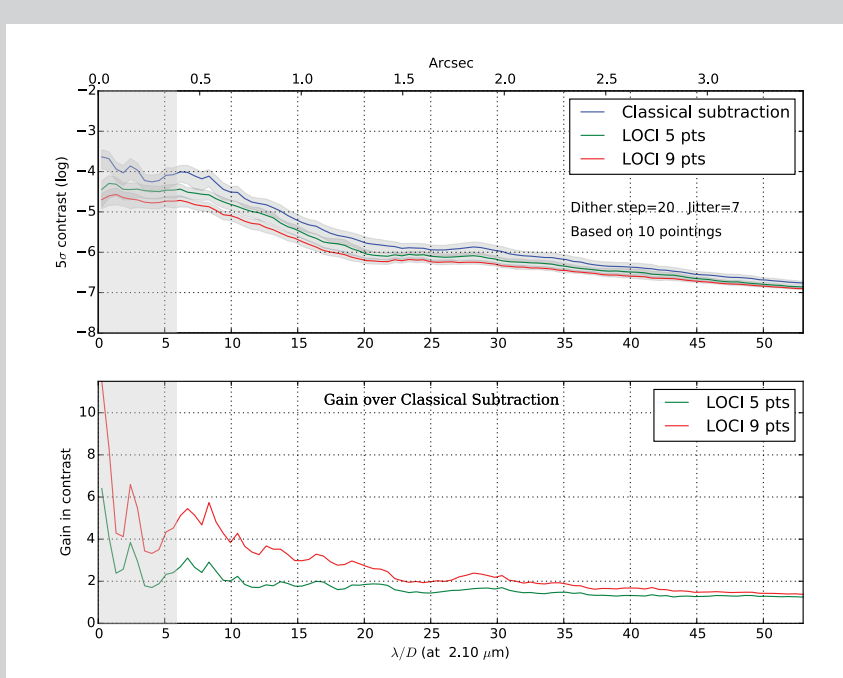


Figure 3: *Top panel:* Azimuthally averaged 5-sigma contrast curves for the NIRCcam round coronagraph mask at 2.10 μm (F210M + MASK 210R). The Classical subtraction refers to the subtraction of one target and one reference whereas the LOCI curves refer to our Small-Grid Dithers approach (using 5- and 9-point grids). *Bottom panel:* Contrast gain between Classical subtraction and Small-Grid Dithers. The shaded area represents the approximate size of the coronagraphic mask ($6 \lambda/D$, where λ is the wavelength and D is the diameter of Webb's primary mirror).

Continued
page 42

Moreover, our simulations suggest that a grid step size of ~ 10 to 20 milliarcseconds will yield optimal contrast performance, although the actual pointing performance on orbit may affect the optimal grid step. Finally, our results show that the gain in contrast is further improved as the number of reference PSFs is increased, albeit more finely sampled grids also lead to an increase in total exposure time. We therefore recommend using either 5- or 9-point grids as a baseline for Small-Grid Dithers. The use of brighter reference stars for Small-Grid Dither processing will also increase the overall efficiency of the technique.

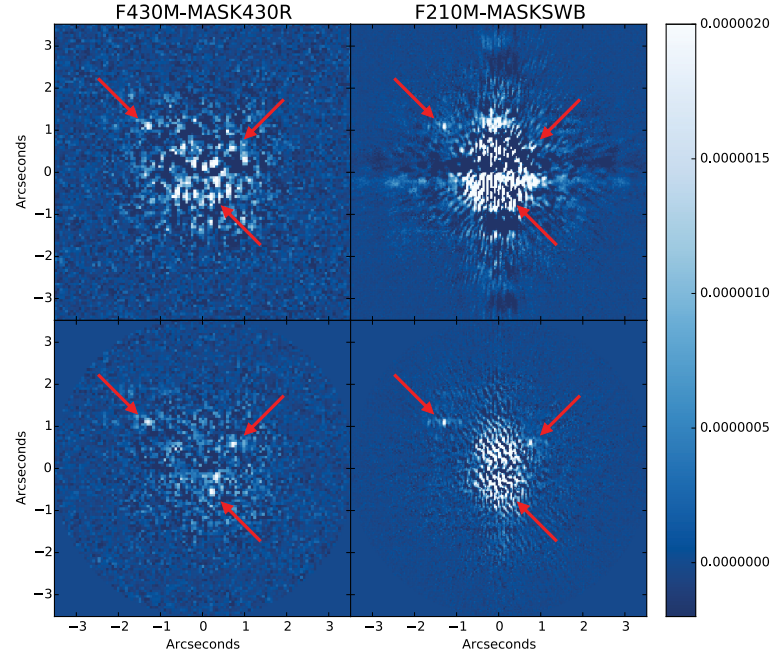


Figure 4: A simulated case showing the relative performance of Classical subtraction (*top row*) and Small-Grid Dithers (*bottom row*) for the NIRCcam F430M+MASK430R (*left*) and F210M+MASKSWB (*right*) coronagraphs using fake planets with a large difference in magnitude of 14.

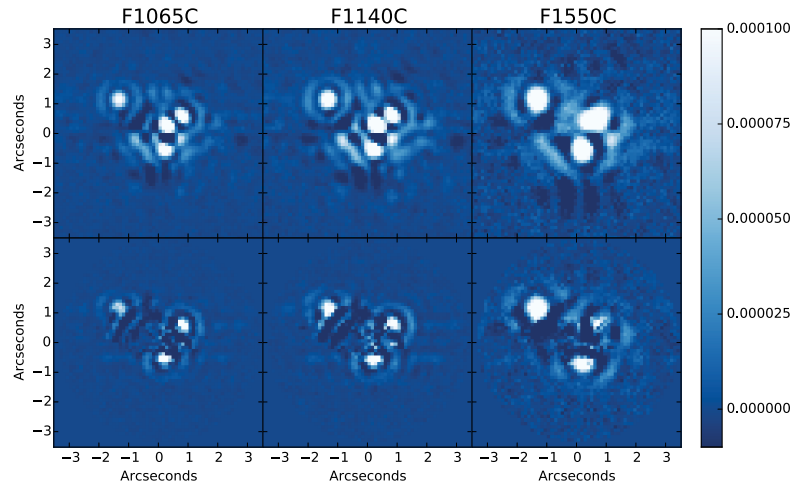


Figure 5: A simulated case showing the relative performance of Classical subtraction (*top row*) and Small-Grid Dithers (*bottom row*) for all three of MIRI's Four-Quadrant Phase Masks using fake planets with differences in magnitude of ~ 10 (see Boccaletti et al. 2015).

Although Classical subtraction is expected to reveal faint planets around bright stars, our simulations suggest that Small-Grid Dithers will consistently remove speckles to a level allowing for the detection of even fainter planets. This is illustrated in Figure 4 for NIRCcam, where very faint simulated planets are barely resolved with Classical subtraction but clearly visible with Small-Grid Dither processing. Figure 5 shows the improved performance with fake planets for the MIRI Four-Quadrant Phase Mask coronagraphs.

Following our conclusions, the Coronagraphs Working Group is currently formalizing recommendations to offer Small-Grid Dithers to general *Webb* coronagraph observers as an option in the Astronomer Proposal Tool (APT), <http://www.stsci.edu/hst/proposing/apt>.

Conclusion

With the Fine Steering Mirror offsets now available for science observations, *Webb* coronagraphs will readily benefit from Small-Grid Dithers and post-processing techniques such as LOCI or KLIP. Our simulations of Small-Grid Dithers show that a gain in contrast relative to classical PSF subtraction can be expected with all NIRCcam and MIRI coronagraphs. However, observers wishing to use Small-Grid Dithers will have to weigh the benefits of increased contrast against the overhead associated with the additional exposure time. The *JWST* Coronagraphs Working Group is now investigating how this new mode can be offered to the general user community and how to implement it in the Astronomers Proposal Tool. Further optimization of the technique should also be possible; for example, we will be investigating rectangular and offset grids for NIRCcam's bar occulters.

Acknowledgements

The authors wish to thank members of the *JWST* Coronagraphs Working Group for contributions to the Small-Grid Dithers project and this article.

References

- Boccaletti, A., et al. 2015, "The Mid-Infrared Instrument for *JWST*, V: Predicted Performance of the MIRI Coronagraphs," *PASP*, 127, 633
- Lafrenière, D., et al. 2007, "A New Algorithm for Point-Spread Function Subtraction in High-Contrast Imaging: A Demonstration with Angular Differential Imaging," *ApJ*, 660, 770
- Perrin, M., et al. 2011, "Simulating Point Spread Functions for the James Webb Space Telescope with *WebbPSF*," *Proceedings of the SPIE*, Volume 8442
- Perrin, M., et al. 2012, "Improved PSF Simulations for *JWST*: Methods, Algorithms, and Validation," STScI *JWST* Technical report JWST-STScI-002469
- Soummer, R., & Makidon, R. 2010, "Simulations of MIRI Coronagraphic Images," STScI *JWST* Technical report JWST-STScI-001952
- Soummer, R., et al. 2012, "Detection and Characterization of Exoplanets and Disks Using Projections on Karhunen-Loève Eigenimages," *ApJ*, 755, L28

NIRCam Ready for the Next Cryo Test

Armin Rest, arest@stsci.edu, John Stansberry, jstans@stsci.edu, David Golimowski, golim@stsci.edu, Massimo Robberto, robberto@stsci.edu, Bryan Hilbert, hilbert@stsci.edu, Gerard Kriss, gak@stsci.edu, Karl Misselt, misselt@as.arizona.edu, and Marcia Rieke, mrieke@as.arizona.edu



Engineers lower NIRCam into the Integrated Science Instrument Module (ISIM) at NASA's Goddard Space Flight Center.

Abstract: *NIRCam hardware testing and science-support development have progressed significantly since the last 2011 update that appeared in the STScI Newsletter. The instrument has been re-fitted with 10 new detectors and the entire instrument suite was tested in its flight configuration for the first time. NIRCam meets or exceeds all of its optical and detector performance requirements, and will be able to fulfill its dual roles as primary sensor for commissioning of the James Webb Space Telescope and 0.6–5 micron imager.*

NIRCam is the workhorse imager of the *Webb* telescope for the wavelength range 0.6–5 microns. With its powerful imaging capabilities it will open new frontiers in a wide range of science areas from planet formation to stellar physics and cosmology.

One of its primary science goals is the detection of “first light objects”: as the universe expanded and cooled, hydrogen molecules formed, enabling the formation of the first individual stars. These stars are thought to be 30 to 300 times as massive as the Sun and millions of times as bright, each burning for only a few million years before meeting a violent end as a core-collapse supernova or mini-quasar, which should be observable with NIRCam.

Another goal is the study of galaxy assembly. Theory and observations suggest that galaxies form through a process of the hierarchical merging of dark matter clumps: small objects formed first and were drawn together to form larger ones. Many details of this process are still unknown—what determines the final mass and shape of a galaxy; what is the role of the environment vs., for example, the central supermassive black hole; when and where do the first stellar clusters appear?

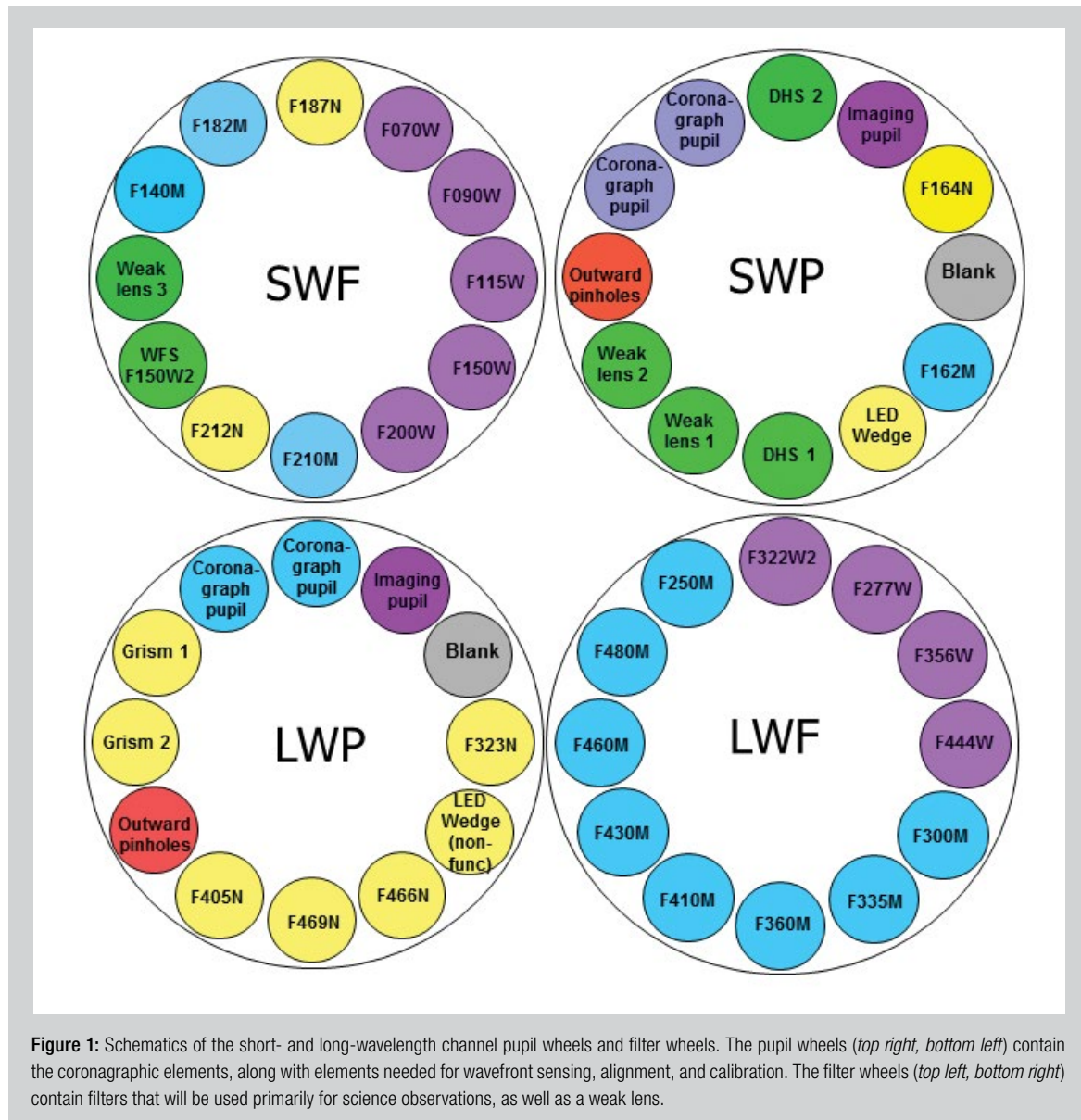
The formation and evolution of stars and planetary systems represent another key science theme. Broad- and medium-band imaging with NIRCam can trace star formation in the early metal-poor universe and establish the link with young stellar clusters in the local universe spanning a wide range of metallicities. Thanks to its sensitivity and spatial resolution, NIRCam can map the internal structure of pre-stellar cores through extinction mapping, reconstructing their composition (e.g., ices) and structure. Exoplanet characterization will be possible via direct imaging (using any of the five Lyot coronagraphic masks and multiple filters), and transit photometry or spectroscopy exploiting the exquisite stability of the space environment.

Technical capabilities

NIRCam is designed as a double instrument with two independent and redundant modules, mirror images of each other, pointing to adjacent fields separated by about 45". This redundancy not only guards against potential failures, but also doubles the field of view (FOV) for science observations. Each module has a short-wavelength (0.6–2.3 microns) and long-wavelength (2.4–5 microns) channel, observing the same field through a dichroic beam-splitter. Observations are typically carried out in parallel on both channels, doubling the observing efficiency.

The short- and long-wavelength detectors have image scales of 32 and 65 mas/pixel, Nyquist sampling the diffraction limited PSF at 2.0 and 4.0 microns, respectively. The long-wavelength channel uses a single HgCdTe Hawaii-IIIRG $2k \times 2k$ detector with 5-micron cutoff, subtending an FOV of 2.2×2.2 arcmin. In order to achieve the same FOV in the short-wavelength channel, four similar Hawaii-IIIRG detectors with 2.5-micron cutoff are arranged in a 2×2 configuration. This configuration is equivalent to a $4k \times 4k$ chip with a central gap between quadrants of about 5" or 160 pixels.

The filter wheel assemblies contain a large variety of the selectable optical elements that can be used in NIRCam observations (see Figure 1). Other elements support wavefront sensing, alignment, and instrument calibration. Figure 2 shows the system throughput associated with each filter. NIRCam also has a Lyot coronagraphic mode, enabled by an optical wedge at the pupil that brings a coronagraph optical mount with occulting spots and bars within the FOV of the arrays. Grisms in the long-wavelength channels also provide some slitless spectroscopic capability (e.g., for planet transits or search for line-emitting galaxies at very high redshift).



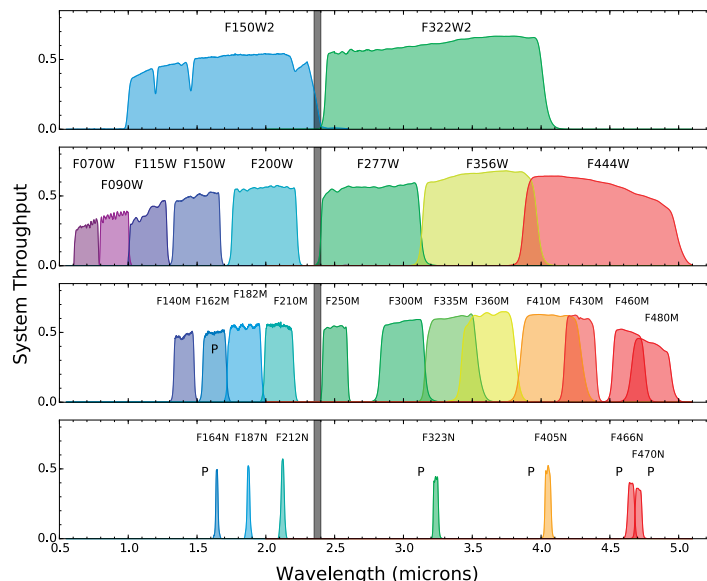


Figure 2: System throughputs for NIRCam filters. The vertical gray bar shows the division between the short- and long-wavelength channels; in most observing modes data is collected simultaneously in both channels. Filters marked with a 'P' indicate elements that are located in the pupil wheels. Coronagraphic elements in the pupil wheels include optical wedges with integral pupil masks that bring the coronagraph optical mount within the FOV of the arrays.

ISIM CV2

Extensive testing of NIRCam is essential to verify its required performance and to ensure its functionality within the full observatory. After undergoing “module level” testing in cryo-vacuum (CV) environments at Lockheed Martin ATC, NIRCam was delivered and integrated, together with the other *Webb* science instruments (SIs), into the Integrated Science Instrument Module (ISIM) at NASA Goddard. Then, using the Space Environmental Simulator (SES)—a large cylindrical vacuum chamber 9 meters in diameter by 13 meters tall—ISIM was tested in space conditions. An Optical Telescope Element Simulator (OSIM), which simulates the *Webb* optical assembly delivering both point-source and extended-source illumination, was also inserted into the SES. The first, short test campaign of ISIM in CV conditions was mostly aimed at characterizing the setup. The second campaign, CV2, ran from June to October in 2014, allowing the testing of all instruments in a flight-like configuration.

The goals for NIRCam testing during ISIM CV2 were manifold, and included an assessment of science capabilities and the acquisition of reference files. Dark exposures were taken to characterize the read noise, $1/f$ noise,¹ inter-pixel capacitance, cross-talk, and other detector features (see Table 1). Optical baseline tests, consisting of external flat fields, a through-focus exposure sweep, and a measurement of the pupil alignment of the SIs were performed in order to verify the optical alignment, image quality, plate scale, wavefront error, ghosting, vignetting, stray light, and orientation, among others.

The detector tests, carried out for the first time with the flight Sidecar ASICs devices, provided key data on the instrument performance. In the absence of the Poisson noise associated with an astronomical signal, the dominant noise sources are the dark current, read noise and the $1/f$ -noise. NIRCam requirements specify a dark current of $<0.01e^-/\text{sec}$, a read noise of $21e^-$ for correlated double sampling, and an effective noise in a 1000-sec integration of $<9e^-$, with multiple non-destructive samples. As is seen in Table 1, all detectors easily meet requirements with the exception of the long-wavelength (LW) detectors, which exceed the dark current requirement. Note that the effective noise after 1000 seconds for the LW detectors includes a significant contribution from the dark current—see Figure 3. Correcting for the dark current, the effective noise at 1000 seconds for the LW detectors reaches the same level as the short-wavelength (SW) detectors.

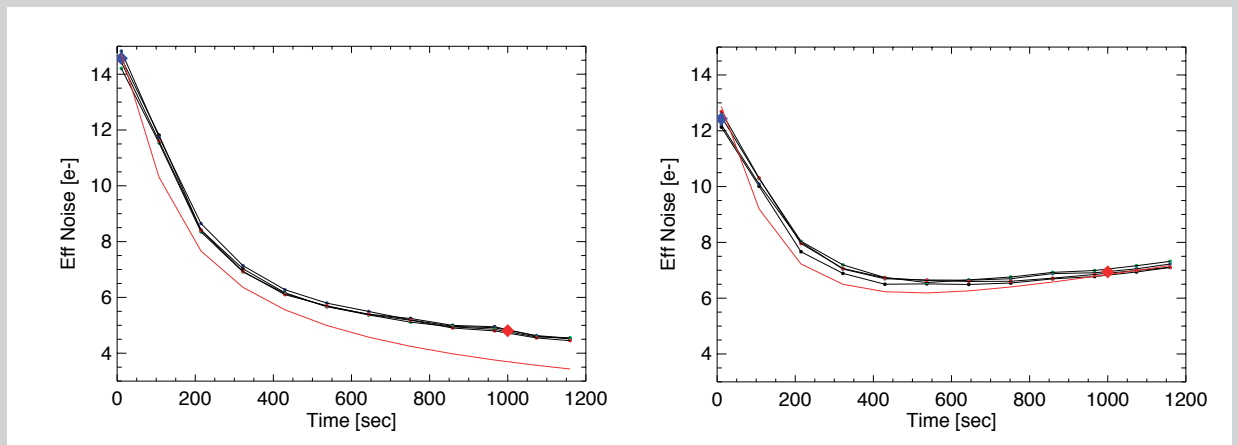


Figure 3: Examples of the measured noise as a function of integration for short- and long-wave NIRCcam detectors as measured in ISIM-CV2 (*left:* NRCB1-16991, *right:* NRCB5-17161). The black curves represent the noise measured on each output of the detector. The blue diamond represents the measured CDS noise (see Table 1) and the red diamond the effective noise at 1000 seconds. The red line represents the theoretical expectation of the noise as a function of integration time for non-destructive reads and has been computed assuming the read noise and dark current reported in Table 1. Note the contribution of the dark current to the measured noise on the LW detector.

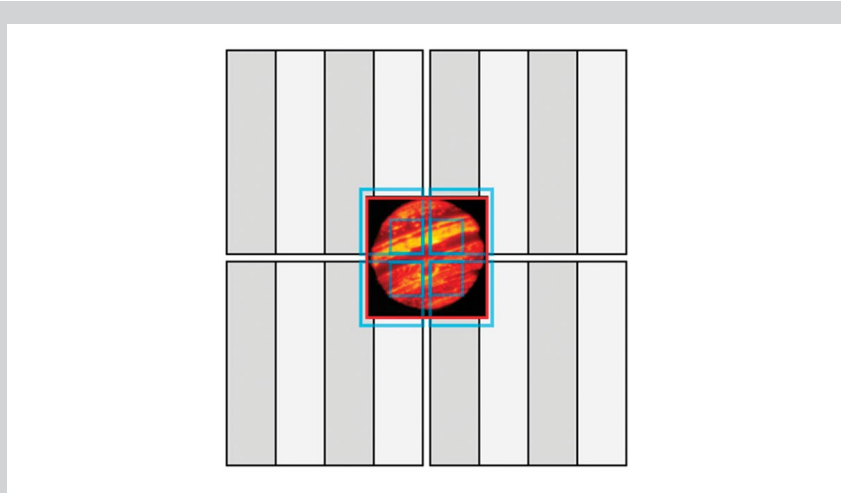


Figure 4: NIRCcam supports imaging of extended bright sources using subarrays. Subarray exposure times can be significantly shorter than those for full-frame images. For extended sources, 4 subarrays (blue squares) are clustered at the center of the short-wavelength focal plane (shown as the 4 squares split into 512×2048 readout sectors). A single subarray centered on the long-wavelength detector (red square) provides an overlapping field of view. Dither and/or mosaic motions can be used to fill in regions that fall in the gaps between the 4 short-wavelength detectors. The large blue squares and the red square show the FOV for the 640×640 pixel subarray configuration relative to the disk of Jupiter. Smaller blue rectangles show the 320×320 subarrays, which give a saturation limit $10\times$ brighter than can be observed in full-array mode. (The corresponding long-wavelength subarray is omitted for clarity). The smallest subarrays (160×160) increase the saturation limit by another factor of 4.

Detector	Detector ID	QE ¹	Dark Current (e ⁻ /sec)	σ_{RN} (e ⁻)	σ_{1000} (e ⁻)	Well Depth (10 ⁴ e ⁻)
A1	16989 ²	0.92	<0.001	11.5	6.1	10.8
A2	17023 ^{2,3}	0.92	N/A	N/A	N/A	10.9
A3	17024 ²	0.90	0.002	10.4	5.7	10.1
A4	17048	0.87	0.001	10.3	6.2	10.6
B1	16991	0.79	<0.001	12.1	5.5	10.5
B2	17005	0.92	<0.001	11.0	5.9	10.3
B3	17011	0.94	0.002	11.5	5.4	10.3
B4	17047	0.92	0.004	10.7	6.2	10.3
ALONG	17158	0.81	0.033	9.4	7.6	8.5
BLONG	17161	0.85	0.036	10.9	8.0	8.2

¹Quantum Efficiency (QE) measurements from Teledyne and are reported at 2.0 μm (short wavelength detectors) and 4.4 μm (long wavelength detectors)

²Replaced after ISIM-CV2. The replacement detectors (A1-17004, A2-17006, A3-17012) will be fully characterized with the flight system during ISIM-CV3.

³A2-17023 was turned off during ISIM-CV2 testing for instrument safety. Hence no ISIM-CV2 characterization data are available.

Table 1: *NIRCam detector characteristics. Read noise was determined for each pixel from a long series of CDS frames. The reported value is the centroid of a Gaussian fit to the distribution. The effective noise at 1000 seconds was determined from for each pixel from a series of 1000-second exposures. The reported value is the centroid of a Gaussian fit to the distribution. Pixel operability is >99% for all current NIRCam detectors.*

Template	Purpose	Description/Notes
Imaging	General-purpose direct imaging	<ul style="list-style-type: none"> Simultaneous images in 2 filters (one in each of the 0.6–2.3 μm and 2.4–5 μm channels) Mapping (dual 2.2' \times 2.2' fields of view) Point- and bright-source imaging (subarrays increase bright limits by ~ 4 mag, $\times 40$ in flux) Extensive, flexible mosaics, and dithers
Coronagraphy	High-contrast imaging	<ul style="list-style-type: none"> Round occulters optimized for 2.1, 3.35, and 4.3 μm wavelengths, extended structures Bar occulters optimized for wavelengths >1.8 μm, point sources Inner working angle $\approx 0.5''$ at 4 μm Contrast exceeding $\approx 10^{-5}$
Time Series	Exoplanet transits, stellar occultations	<ul style="list-style-type: none"> High-cadence (≤ 10 Hz) high-precision imaging and slitless spectroscopy Uninterrupted data collection for up to 48 hours Simultaneous data collection in both wavelength channels (0.6–2.3 μm and 2.4–5 μm)
Grism Imaging*	Slitless spectral imaging	<ul style="list-style-type: none"> Wide-field spectral imaging (dual 2.2' \times 2.2' FOVs) 2.5–4 microns or 3.9–5 microns Two grisms with orthogonal dispersion directions

Table 2: *NIRCam observing templates in APT.*

* Soon to be available

NIRCam observing templates in APT

The development of the ASTRONOMER'S PROPOSAL TOOL (APT) for *Webb* is reaching maturity, and numerous observing templates are available for all science instruments. Three NIRCam science templates are already available to the general user: Imaging, Coronagraphy, and Time-series Photometry. Grism Imaging will be available soon. Table 2 summarizes the science templates that will be available for Cycle 1 observers. As an example, we show in Figure 4 how subarray imaging has been implemented to enable imaging of bright sources, using the demanding case of Jupiter as a specific test case. With this observing template, it will be possible to acquire unsaturated full-disk imaging of Jupiter in most NIRCam medium-bandpass filters; only at the shortest wavelengths will one need to use smaller subarrays, due to the lack of medium-band filters shorter than 1.4 microns, as well as at the longest wavelengths, due to the Jupiter's bright thermal emission.

Look to the future

The final flight configuration of NIRCam includes three new detectors on module A. One was replaced following a high current state noticed in ISIM-CV2 test, while the other two were replaced when they failed a vibration test. With this new configuration, NIRCam is currently preparing for the final round of cryogenic ISIM testing in the fall. ISIM-CV3 represents the last chance to carefully characterize instrument performance before launch. Testing will be geared towards several tasks, e.g., optimize voltage biases for the new detectors on module A; characterize their performance in the flight system and verify the performance of all the detectors; confirm mechanism functionality; verify optical performance and wavefront stability through cryo cycles and ISIM re-integration; and test science observing scenarios.

At the end of CV3, NIRCam construction will be considered complete. The ISIM with all *Webb* instruments will be integrated in the spacecraft. After an extensive general system test in Houston, *Webb* will be prepared for launch in October 2018.

Trailblazing for Supernova Cosmology in the Early Universe

Steven A. Rodney, srodney@sc.edu, and Adam Riess, ariess@stsci.edu

The explosion of a star at the end of its life as a supernova (SN) is a spectacular and fascinating event. Starting with the pioneering work of Baade & Zwicky (1934), astronomers have spent eight decades trying to understand these remarkable objects. Today we are still wrestling with fundamental questions about the nature of their progenitor systems (Maoz, Mannucci & Nelemans 2014; Smartt 2015). Nevertheless, even with our incomplete understanding of these stellar explosions, Type Ia SNe in particular have become an indispensable tool for illuminating the structure and history of the Universe. With *Hubble Space Telescope* observations of distant Type Ia SNe, we are now opening up new avenues for testing dark energy models.

The empirical calibration of Type Ia SNe as standard candles (Phillips 1993) led in short order to the paradigm-shifting discovery of the accelerating expansion of the Universe (Riess et al. 1998; Perlmutter et al. 1999). The current challenge for SN cosmology is to constrain the so-called *dark energy* that drives this cosmic acceleration by testing its equation of state (the ratio of pressure to density, $w = p/\rho$). Over 1000 Type Ia SNe have been observed in this effort (Figure 1). These have come primarily from wide-field ground-based surveys, but *Hubble* has been a key contributor at the high-redshift end (e.g., Riess et al. 2007; Suzuki et al. 2012). In fact, all of the cosmologically useful Type Ia SNe at $z > 1.2$ have been discovered with *Hubble*. Most recently, with the CLASH and CANDELS SN surveys (Graur et al. 2014; Rodney et al. 2014) we have used the WFC3-IR camera to push the high-redshift frontier of Type Ia SN discovery to $z \sim 2$ (Rodney et al. 2012; Jones et al. 2013; Rodney et al. 2015).

Continued
page 50

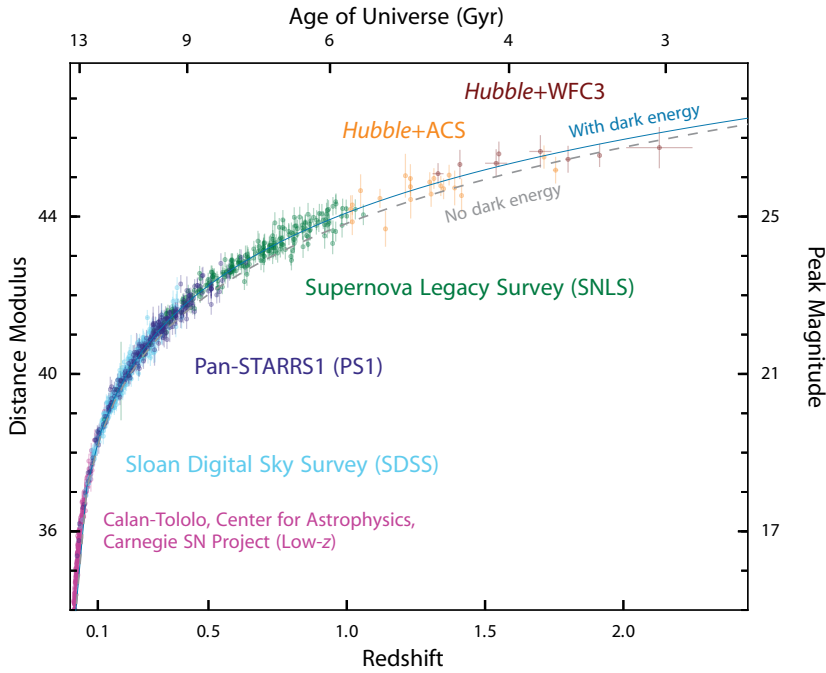


Figure 1: The Type Ia SN *Hubble* diagram in 2015, showing distance vs. redshift for ~1100 Type Ia SNe. At $z > 1.2$ all the SNe have been discovered and observed with *Hubble*, first using ACS (Riess et al. 2004; Suzuki et al. 2012; Rubin et al. 2013), and more recently with WFC3-IR (Rodney et al. 2012; Jones et al. 2013; Rodney et al. 2015). These SNe alone can clearly distinguish a Universe with no dark energy (dashed gray line) from the broadly accepted Λ CDM model that includes a dark energy component (solid blue line). Putting useful constraints on the dark energy equation of state, w , requires much greater precision and therefore demands a careful control of systematic uncertainties.

These high- z SNe exploded when the Universe was only 3–5 Gyr old, and this makes them especially valuable for testing *flexible* dark energy models, i.e., models that are not restricted by too many assumptions about how dark energy might change with time. As a first step toward constraining the dark energy equation of state, it is common to start with an uncomplicated framework for the behavior of w , and then test whether the available data can reject that simplified model. The simplest model presumes that w is a constant over the age of the universe—in which case the data support a value very close to $w = -1$, which is equivalent to a Universe where dark energy can be described by Einstein’s cosmological constant, Λ .

To allow a little more complexity, many investigations consider a simple parameterization, where w evolves linearly with the cosmic scale factor, a :

$$\begin{aligned} w &= w_0 + w_a (1 - a) \\ &= w_0 + w_a z / (1 + z) \end{aligned}$$

(Chevallier & Polarski 2001; Linder 2003). This is a very useful incremental step, especially given that current data are still unable to distinguish between such a minimally variable dark energy model and the cosmological constant (Figure 2). If this simple model for dark energy evolution were correct, then a small sample of high- z SNe collected with *Hubble* would have very little value as direct cosmological constraints. This is because the w_0, w_a parameterization effectively places a very strong *prior* on the behavior of dark energy. The model itself asserts that any evolution of dark energy is monotonic, so that if you measure how w changes from $z = 0$ to 0.5, then you would already know how it behaves from $z = 2$ to 2.5. However, there is really no reason to believe that the Universe is so well-behaved. That is, we have no theoretical motivation for assuming that the evolution of w should have such a conveniently simple form. When one allows a model with more flexibility—for example, expanding to a polynomial instead of a linear representation for $w(z)$ —then the Universe suddenly looks much wilder and unconstrained (Figure 2).

In this less rigid cosmological framework, even the small collection of *Hubble* SNe will be extremely valuable for taming the high- z tail of the dark energy equation of state. The addition of ~10 new high- z SNe from the CLASH and CANDELS sample will provide the next opportunity to examine flexible dark energy models (Riess et al., in prep.). Currently the entire sample at $z > 1.2$ comprises only ~20 SNe, but this number continues to grow, with new contributions to come from ongoing *Hubble* programs such as the Cycle 22 “See Change” survey (HST-ID:13677, PI:Perlmutter).

Following on the heels of these trail-blazing efforts, *Hubble* will soon pass the torch to new space observatories. First, *Webb* will extend the frontier by making it possible to discover SNe at $z > 2.5$, exploding just 1–3 Gyr after the big bang. Finally, we will begin to really populate this high-redshift territory with the *WFIRST* mission, which is designed to deliver several thousand Type Ia SNe to $z \sim 2$.

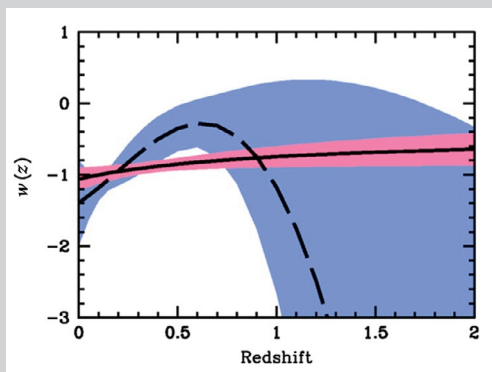


Figure 2: The effect of a strong prior on the apparent constraints for time-variable dark energy. Adopting a simple w_0, w_a parameterization (Equation 1) effectively builds in the assumption that dark energy was much weaker at $z > 1$ than it is today. With very few Type Ia SNe at those redshifts to challenge that assumption, the best-fit w_0, w_a model and uncertainty (solid line, red shading) would indicate that current data already put fairly tight restrictions on dark energy evolution. However, when adopting a more flexible parameterization such as a quartic polynomial, the best-fit model and uncertainty (dashed line, blue shading) are much less constrained. Moving beyond the simplistic linear parameterization for $w(z)$, we see that the high-redshift Type Ia SN sample still has a lot of room to surprise us (figure from Riess et al. 2007).

References

- Baade, W. & Zwicky, F. 1934, PNAS, 20, 254
 Graur, O., et al. 2014, ApJ, 783, 28
 Jones, D. O., et al. 2013, ApJ, 768, 166
 Maoz, D., Mannucci, F., & Nelemans, G. 2014, ARA&A, 52, 107
 Perlmutter, S., et al. 1999, ApJ, 517, 565
 Phillips, M. M. 1993, ApJL, 413, 105
 Riess, A. G., et al. 1998, AJ, 116, 1009
 Riess, A. G., et al. 2004, ApJ, 600, L163
 Riess, A. G., et al. 2007, ApJ, 659, 98
 Rodney, S. A., et al. 2012, ApJ, 746, 5
 Rodney, S. A., et al. 2014, AJ, 148, 13
 Rodney, S. A., et al. 2015 (submitted to ApJ)
 Rubin, D., et al. 2013, ApJ, 763, 35
 Smartt, S. J. 2015, PASA, 32, 16
 Suzuki, N., et al. 2012, ApJ, 746, 85

UV Astronomy with *Webb*: Star-Forming Galaxies at $z \gtrsim 9$

Emily M. Levesque, emsque@uw.edu

Landscape at $z \gtrsim 9$

High redshift ($z \gtrsim 9$) galaxies offer us windows into the early universe, only 400–500 Myr after the Big Bang. They serve as laboratories for studying cosmic reionization, the earliest generations of star formation, and a key formative phase in how galaxies have evolved from these early epochs to the diverse population of galaxies observed in the local universe. The galaxy luminosity function offers us a means of quantifying the ultraviolet luminosity of galaxies at these redshifts (and their subsequent role in reionization), as well as the efficiency of star formation as a function of cosmic time. The history of star formation, in turn, is critical for understanding metal production in the early universe. Finally, the young massive star populations produced in these galaxies are compelling in their own right, representing the extremes of metal-poor stellar evolution.

While EGSY8p7 currently holds the record for the most distant star-forming galaxy, with a spectroscopic redshift of $z \sim 8.7$ from the detection of Lyman-alpha (Zitrin et al. 2015), ongoing searches are assembling an ever-growing list of $z \gtrsim 9$ candidates using Lyman-break selection. This technique, focused on the redshifted photometric signature of the Lyman limit (where a photometric dropout is visible at $\lambda < 912 \text{ \AA}$ in the rest-frame; Steidel et al. 1996) and combined with increasingly deep

*Continued
page 52*

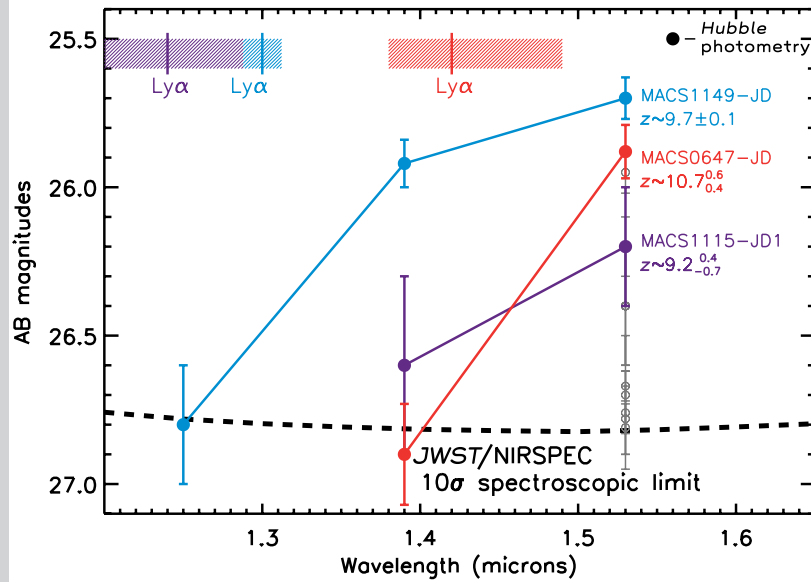


Figure 1: Comparison of the *Webb* NIRSpec limiting continuum magnitudes for $R = 100$ S/N ~ 10 spectroscopy (black dashed line; data from <http://www.stsci.edu/jwst/instruments/nirspec/sensitivity/>) to photometry of the $z \geq 9$ galaxy candidates MACS1115-JD1 (purple; Bouwens et al. 2014), MACS1149-JD (blue; Zheng et al. 2012, with redshift from Bouwens et al. 2014), and MACS0647-JD (red; Coe et al. 2013). For each candidate galaxy the expected observer-frame wavelength of the $\text{Ly}\alpha$ 1215 Å emission feature (with errors), is illustrated at the top of the plot. Additional $z \geq 9$ candidate galaxies observable with NIRSpec from Oesch et al. (2014), Bouwens et al. (2015), and Ishigaki et al. (2015) are shown in gray.

imaging capabilities, has continued to push detections of star-forming galaxies out to increasingly high redshifts. Today we have several dozen galaxy candidates at $z \geq 9$ (e.g., Bouwens et al. 2015); with the *Hubble* Frontier Fields initiative (e.g., Coe et al. 2015) and the continued identification of $z \sim 9$ –10 candidate galaxies in wide-field surveys (e.g., Trenti et al. 2012a; Oesch et al. 2013), this number will continue to grow.

Signatures of high-redshift star formation have been pushed even further with detections of long-duration gamma-ray bursts (LGRBs). GRB 090423, with a spectroscopic redshift of $z \sim 8.2$ (Salvaterra et al. 2009; Tanvir et al. 2009), and GRB 090429B, with a photometric redshift of $z \sim 9.4$ (Cucchiara et al. 2011), are both presumed to have formed from the core-collapse deaths of young, extremely massive stars. While the host galaxies of these two have not yet been detected (the host of GRB 090423 was undetected to $H_{160,AB} > 28.36$; Tanvir et al. 2012), detections of high- z LGRBs call our attention to sites of active star formation in the early universe.

Exploring the high-redshift universe with *Webb*

There are a number of open and exciting questions for us to address with $z \geq 9$ galaxies in the coming decade. Quantifying the nature of galaxy environments in the early universe, including the metallicity and ionizing conditions of the interstellar medium (ISM), is crucial for modeling the first epoch of star formation. Star-formation rate densities inferred from the discovery rate of high-redshift LGRB detections disagree with those determined from ultraviolet (UV)-selected galaxies (e.g., Trenti et al. 2012b; Robertson & Ellis 2012) and consequently lead to conflicting results on the steepness of the galaxy luminosity function. A larger sample of $z \geq 9$ observations, including deep multi-band photometry or even spectroscopy of these galaxies, would offer a wealth of information on the galaxies' star-formation rates, ISM properties, stellar populations, and contributions to the conditions of the early universe.

The launch and first light of *Webb* will mark the beginning of a new era in our study of high-redshift galaxies. The Near-Infrared Spectrograph (NIRSpec) will be capable of observing low-resolution ($R \sim 100$) spectra of galaxies up to a limiting magnitude of $H_{160,AB} \sim 26$ –27, yielding a S/N ~ 10 in the continuum at 1–3 μm with a 10^4 s exposure. As a result, in just a few years it will be possible to obtain rest-frame UV spectra of some of the most extreme sites of active star-formation in the early universe, including more than a dozen of the $z \geq 9$ galaxy candidates identified by current surveys (e.g., Zheng et al. 2012; Coe et al. 2013; Oesch et al. 2014; Bouwens et al. 2014, 2015; see Figure 1).

In addition, the Near-Infrared Camera (NIRCam) will push photometric detections of the most luminous galaxies into the $z \sim 12\text{--}15$ regime and make it possible to robustly sample the lower-luminosity population at $z \sim 5\text{--}10$, offering a wealth of information on the diversity and UV luminosities of galaxies in the epoch of reionization. Combining this larger high-redshift galaxy sample with detections or even upper limits on high-redshift LGRB hosts will also be extremely valuable for understanding the population sampled by LGRBs and the utility of these events as probes of early-universe star formation.

Counterpart UV/optical observations with *Hubble*

With *Webb* essentially serving as a UV instrument for the $z \gtrsim 9$ universe, it is particularly important that we take full advantage of the local UV capabilities of *Hubble* in the next few years. Building a library of UV spectra for star-forming galaxies in the local universe is vital if we wish to develop well-calibrated UV ISM diagnostics. Much of our current work on star-forming galaxies is being carried out in the rest-frame optical, and effective comparisons between the optical and UV regimes are crucial for placing future observations into context and forming a cohesive picture of how galaxy environments evolve with redshift (see Zetterlund et al. 2015). Using *Hubble* observations to improve current models of star-forming galaxies and stellar populations in the UV will also lay important groundwork for future interpretations of high-redshift UV spectra and photometry.

Beyond the UV, it is also important to continue work on LGRBs—these events serve as valuable beacons drawing us to sites of active star formation in the early universe, and a better understanding of their progenitors and host environments increases their efficacy. Ongoing improvements to our models of massive stellar evolution in extremely metal-poor environments will improve understanding of the key building blocks in these galaxies that contribute to ionization and the early stages of metal enrichment. Finally, continued searches for $z \gtrsim 9$ galaxy candidates with *Hubble* and other facilities will further increase our sample of candidates for future spectroscopic and multiband photometric observational campaigns.

A focus on these areas will help equip the astronomical community with the tools we need to take full advantage of the high-redshift frontiers opened up by *Webb*, allowing us to immediately begin probing the new corners of the universe that it will reveal.



Figure 2: This detail of high- z galaxies is taken from the *Hubble* Ultra Deep Field 2014 image, which is a composite of separate exposures taken from 2002 to 2012 in wavelengths ranging from near-infrared to ultraviolet. The observations come from *Hubble*'s Advanced Camera for Surveys and Wide Field Camera 3. From STScI press release STScI-2014-27. Image Credit: NASA, ESA, H. Teplitz and M. Rafelski (IPAC/Caltech), A. Koekemoer (STScI), R. Windhorst (Arizona State University), and Z. Levay (STScI).

*Continued
page 54*

References

- Bouwens, R. J., et al. 2014, ApJ, 795, 126 (arXiv:1211.2230)
Bouwens, R. J., et al. 2015, ApJ, 803, 34 (arXiv:1403.4295)
Coe, D., et al. 2013, ApJ, 762, 32 (arXiv:1211.3663)
Coe, D., et al. 2015, ApJ, 800, 84 (arXiv:1405.0011)
Cucchiara, A., et al. 2011, ApJ, 736, 7 (arXiv:1105.4915)
Ishigaki, M., et al. 2015, ApJ, 799, 12 (arXiv:1408.6903)
Oesch, P. A., et al. 2013, ApJ, 773, 75 (arXiv:1301.6162)
Oesch, P. A., et al. 2014, ApJ, 786, 108 (arXiv:1309.2280)
Robertson, B. E. & Ellis, R. S. 2012, ApJ, 744, 95 (arXiv:1109.0990)
Salvaterra, R., et al. 2009, Nature, 461, 1258 (arXiv:0906.1578)
Steidel, C. C., et al. 1996, ApJ, 462, 17 (arXiv:astro-ph/9602024)
Tanvir, N. R., et al. 2009, Nature, 461, 1254 (arXiv:0906.1577)
Tanvir, N. R., et al. 2012, ApJ, 754, 46 (arXiv:1201.6074)
Trenti, M., et al. 2012a, ApJ, 749, 38 (arXiv:1110.0468)
Trenti, M., et al. 2012b, ApJ, 749, 38 (arXiv:1202.0010)
Zetterlund, E., et al. 2015, ApJ, 805, 151 (arXiv:1504.00011)
Zheng, W., et al. 2012, Nature, 489, 406 (arXiv:1204.2305)
Zitrin, A., et al. 2015, ApJL, submitted (arXiv:1507.02679)

The Most Massive Extragalactic Evolved Stars

Rubab Khan, rubab.m.khan@nasa.gov

The recent identification of an emerging class of evolved self-obscured $25\text{--}60 M_{\odot}$ stars in galaxies at $\sim 1\text{--}4$ Mpc has for the first time created the opportunity to observationally investigate a statistically significant number of stars undergoing episodic mass loss. While our current efforts to identify these rare objects in a short-lived yet consequential evolutionary phase primarily rely on archival *Spitzer* IRAC ($3.6\text{--}8 \mu\text{m}$) and MIPS ($24 \mu\text{m}$) images, they can be studied far more optimally at $10 \sim 28 \mu\text{m}$ with the *Webb* taking advantage of MIRI's order-of-magnitude-higher resolution.

Episodic mass loss from evolved stars

Stellar mass loss determines the structure and terminal mass of evolved massive stars and the presence of circumstellar material. This in turn calibrates the energetics and observed properties of some of the highest energy phenomena in the universe such as core-collapse supernovae, gamma-ray bursts, neutrino bursts, and gravitational wave bursts. However, there are no good prescriptions on how to include large, episodic, mass-loss events into theoretical models. Such complicated objects are difficult to comprehend in a theoretical framework due to the computational complexities involved in modeling a dynamically unstable, short (decades to centuries) evolutionary phase in the ~ 10 million-year lifetimes of the most massive ($\gtrsim 25 M_{\odot}$) stars. Observationally, the overall small number of stars detected in this ultra-short, yet eventful, evolutionary phase limits us. Searching for these stars in the Galaxy is hard because of distance uncertainties, as well as having to look through the crowded galactic disk.

A full understanding of the evolution of these stars therefore requires exploring galaxies beyond the Milky Way. Surveys of nearby galaxies are better defined and when used to build larger samples of younger systems (having a shorter time since mass ejection), can be studied to better understand their evolution. At extragalactic distances, a self-obscured massive star would appear as a bright, red point source in IRAC images, with a relatively fainter optical counterpart due to self-obscuration. Its spectral energy distribution (SED) would generally have two peaks—an obscured optical peak, which could be absent altogether given enough absorption, and a mid-IR peak. In the *Spitzer* bands, the SED would be either flat or rising towards longer wavelengths, before turning over between 8 and $24 \mu\text{m}$ due to the presence of warm circumstellar dust. Our team concentrated on these properties to identify the extragalactic obscured massive stars.

An emerging class of self-obscured stars

In our pilot study of seven galaxies at <4 Mpc (NGC 6822, M33, NGC 300, M81, NGC 2403, NGC 247, NGC 7793), first we identified the candidate sources that are most likely to be evolved self-obscured stars. We selected sources that have a mid-IR luminosity of $>10^5 L_\odot$ in the IRAC (3.6–8.0 μm) bands, as well as a flat or rising SED in this wavelength range. Next we verified the stellar nature of the candidates utilizing ancillary multi-wavelength archival data from the *Spitzer* MIPS (24 μm), WISE, 2MASS, *Hubble* and other space- and ground-based observatories. We focused on identifying two telltale signatures of the SED of a luminous star obscured by warm circumstellar ejecta: signs of the SEDs turning over between 8 μm and 24 μm , and low optical fluxes or flux limits compared to the mid-IR peak. Finally, we determined the best fit to the verified obscured stars' SEDs by modeling radiation transfer (see Figure 1) through a spherical medium surrounding the star, which is also a good approximation for *unresolved* objects with a combination of non-spherical, patchy, and multiple shells.

This allowed us to estimate their bolometric luminosities and circumstellar ejecta mass. Surprisingly, we found that all the newly identified stars have bolometric luminosities within a narrow range of $\log L/L_\odot \approx 5.5$ –6.0, which roughly corresponds to initial stellar masses of ~ 25 –60 M_\odot . Stars enter this high optical depth phase at a rate that is consistent with all obscured stars at this mass for a negligible fraction of their ~ 3 –10 million years' post-main-sequence lifetimes, that is, at most a few thousand years. The number of such events a star experiences is also small: one or two, not ten or twenty. This implies that these events have to be associated with special periods in the evolution of the stars.

Extragalactic stellar astrophysics with the *Webb*

The primary limitation of the present search is *Spitzer's* angular resolution. The *Webb's* order-of-magnitude-higher spatial resolution will enable us to greatly reduce the problem of confusion and to expand the survey volume. Far more important will be the ability to carry out the search at $10 \sim 28 \mu\text{m}$, which will increase the post-eruption time over which we can identify expanding circumstellar dusty ejecta, significantly improving the statistics and our ability to study the long-term evolution of these systems.

When we expand the search with the *Webb* to include more distant star-forming galaxies, we will put to test the general post-main-sequence stellar evolution scenario described by Nieuwenhuijzen & de Jager (2000) and Smith et al. (2004). They proposed that the photospheres of blueward evolving red supergiants with $\log(L/L_\odot) = 5.6 \sim 6.0$ and $T_{\text{eff}} \approx 7000$ –12500 K become moderately unstable. This leads to periods of lower effective temperature and enhanced mass loss as the stars try to evolve into a “prohibited” region of the H-R diagram. With the *Webb*, we will verify if the obscured massive stars identified in a much larger number of galaxies reside in the same narrow luminosity range as the ones we identified in the pilot study of seven galaxies. This is the anticipated luminosity regime of

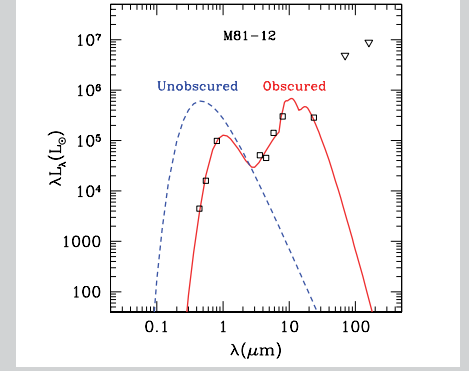


Figure 1: We determined the best fit to an obscured star's SED through radiative transfer modeling to estimate the bolometric luminosity and temperature of the underlying star as well as the mass, temperature and optical depth for the obscuring material. The solid red line shows the best-fit model of the obscured stellar SED of one of the newly identified stars in M81, while the dashed blue line shows the blackbody SED of the underlying, unobscured star.

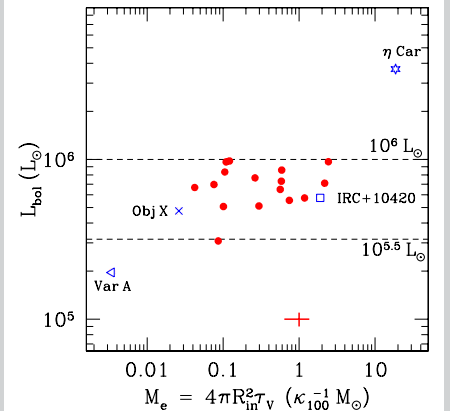
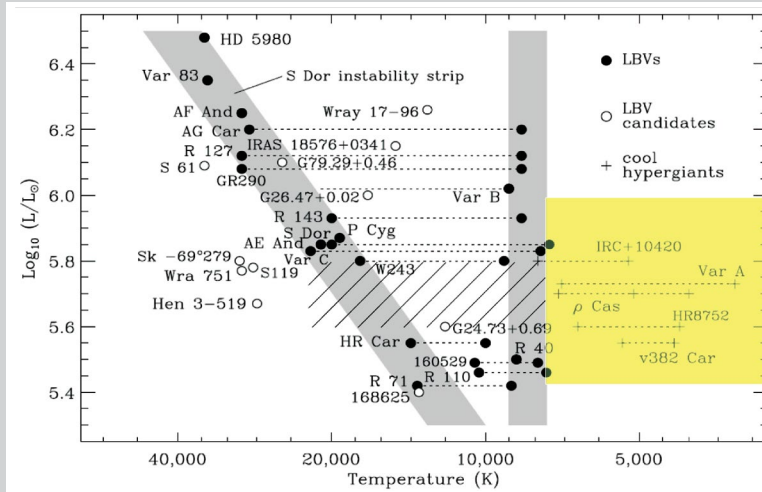


Figure 2: The evolved massive stars we found may be the “missing LBVs” (Smith et al. 2004) traversing the “Yellow Void” (Nieuwenhuijzen & de Jager 2000) like the Galactic star IRC+10420 (e.g., Tiffany et al. 2010). Smith et al. (2004) proposed that LBVs missing from the striped region on the upper H-R Diagram (*left* panel, adopted from their paper) reappear as cooler obscured giants in the yellow box. The *right* panel shows the luminosities of the sources that Khan et al. (2015) found, as a function of their estimated ejecta masses. The luminosity range enclosed by the dashed lines here is same as the yellow box on the *left* panel.

the “bistability jump” (Vink et al. 1999) in wind speeds driven by opacity changes, which can explain the “missing LBVs” and the existence of Yellow Hypergiants with high mass-loss rates (see Figure 2).

These extremely rare stars are by definition luminous in the 3.6–24 μm wavelength range, where the *Webb* will be most sensitive. They are rare laboratories of stellar astrophysics and will be very interesting extragalactic stellar targets for mid-IR spectroscopy with the MIRI. This will give us an unprecedented view of these most massive self-obscured stars, letting us to determine their evolutionary state and the chemical composition of their circumstellar ejecta.

References

- Khan, R., Kochanek, C. S., Stanek, K. Z., & Gerke, J. 2015, *ApJ*, 799, 187
Nieuwenhuijzen, H. & de Jager, C. 2000, *AAP*, 353, 163
Smith, N., Vink, J. S., & de Koter, A. 2004, *ApJ*, 615, 475
Tiffany, C., Humphreys, R. M., Jones, T. J., & Davidson, K. 2010, *AJ*, 140, 339
Vink, J. S., de Koter, A., & Lamers, H. J. G. L. M. 1999, *AAP*, 350, 181

Revealing Core-Collapse Supernova Explosions with *Webb*

Dan Milisavljevic, dmilisav@cfa.harvard.edu, and Robert A. Fesen, robert.fesen@dartmouth.edu

Core-collapse supernovae are the deaths of massive stars and among the most powerful explosions in the universe. They influence the energy balance, structure, and chemical make-up of galaxies (Dalla Vecchia & Schaye 2008), and produce a variety of exotic objects such as neutron stars, black holes, and some gamma-ray bursts (Woosley & Weaver 2002). Most importantly for us, supernova debris is rich in heavy elements that make planets like Earth and its life possible (Burbidge et al. 1957).

Hubble has already led in the exploration of several fundamental aspects of core-collapse supernovae (Smartt 2009; Van Dyk et al. 2011), but much of their nature, with respect to what types of stars explode and how they explode, remains unclear. The next breakthroughs require the capabilities of the *James Webb Telescope (Webb)*, which will enable transformative science in supernova progenitor systems, explosive nucleosynthesis, and dust formation.

3D reconstructions of supernova explosions

Extragalactic supernovae are unresolved even for *Hubble*, and this imposes severe limits on our understanding of their three-dimensional kinematic and chemical properties. One way around this is to examine young, nearby supernova remnants—the expanding remains of ancient supernovae—that encode valuable information about the core-collapse process in their debris. *Hubble* and *Spitzer* images and spectra have probed the Galactic and Magellanic Clouds’ supernova remnants in the optical and infrared with great success. However, *Webb*’s nearly two orders of magnitude increased sensitivity and unprecedented angular and spectral resolution will propel our understanding of these systems into uncharted frontiers.

One of the chief targets for *Webb* will be the supernova remnant Cassiopeia A (Cas A; Figure 1). It is the youngest Galactic core-collapse supernova remnant known (~335 yr; Fesen et al. 2006a), it is among the closest (3.4 kpc; Reed et al. 1995), and it is the only core-collapse remnant with a secure supernova classification (Type IIb; Krause et al. 2008). Three-dimensional optical and infrared Doppler reconstructions of Cas A have shown that the reverse-shocked gas is distributed in a quasi-spherical shell made up of intersecting rings (DeLaney et al. 2010; Milisavljevic & Fesen 2013), and recent near-infrared work has established that the faint, interior unshocked gas has large-scale coherent structure in the form of cavities or “bubbles” that connect with these rings (Figure 2; Milisavljevic & Fesen 2015).

Cas A’s interior emissions were poorly mapped for many years in large part because of substantial and non-uniform foreground interstellar extinction ($A_V = 5\text{--}8$ mag). This line-of-sight dust minimally

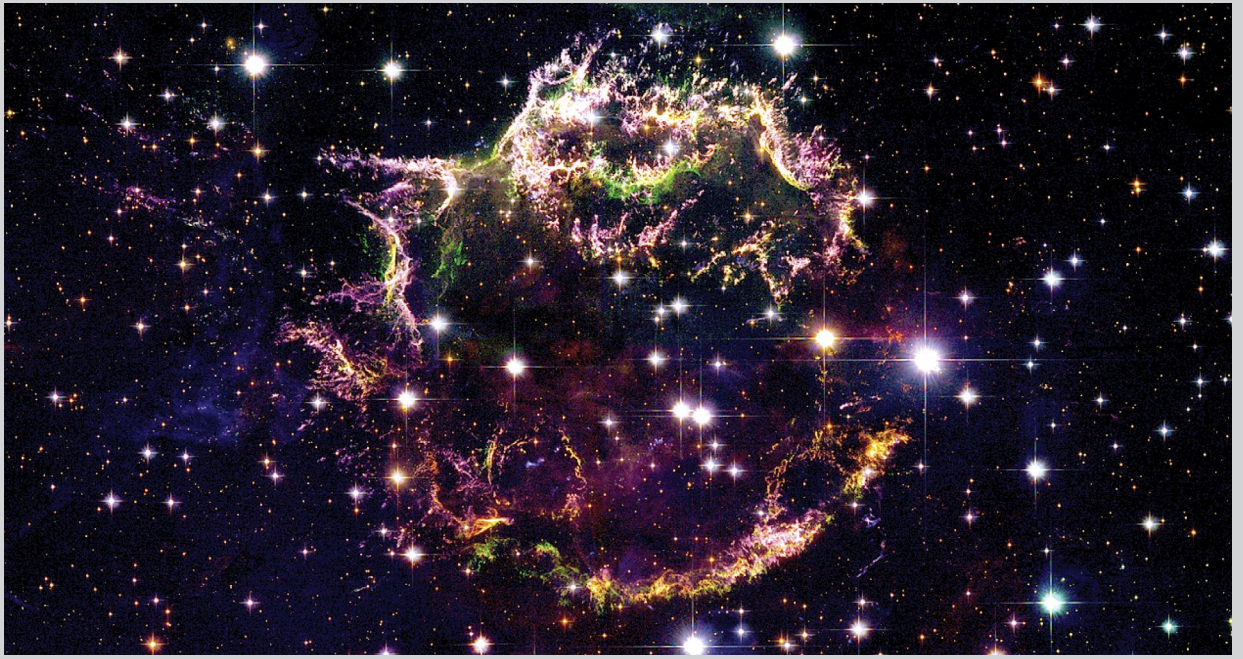


Figure 1: Color composite of *Hubble*/ACS/WFC images of Cas A sensitive to the remnant's oxygen and sulfur emissions [*Hubble* Heritage Archive. Credit: NASA, ESA, and the *Hubble* Heritage Team (STScI/AURA)].

affects the infrared, and thus *Webb* observations will be capable of probing a broad suite of unobscured ionized species (Figure 3). Near-Infrared Camera (NIRCam) images will locate interior emission with unprecedented resolution and depth, and guide spectroscopy of key regions of interest with Near-Infrared Spectrograph (NIRSpec) and Mid-Infrared Instrument (MIRI). The wide field of view of the NIRSpec micro-shutter assembly will make it fairly easy to combine the 0.6–5 microns spectroscopy with existing *Hubble* and ground-based optical data to create a detailed kinematic reconstruction of the entire remnant with information about chemical abundances.

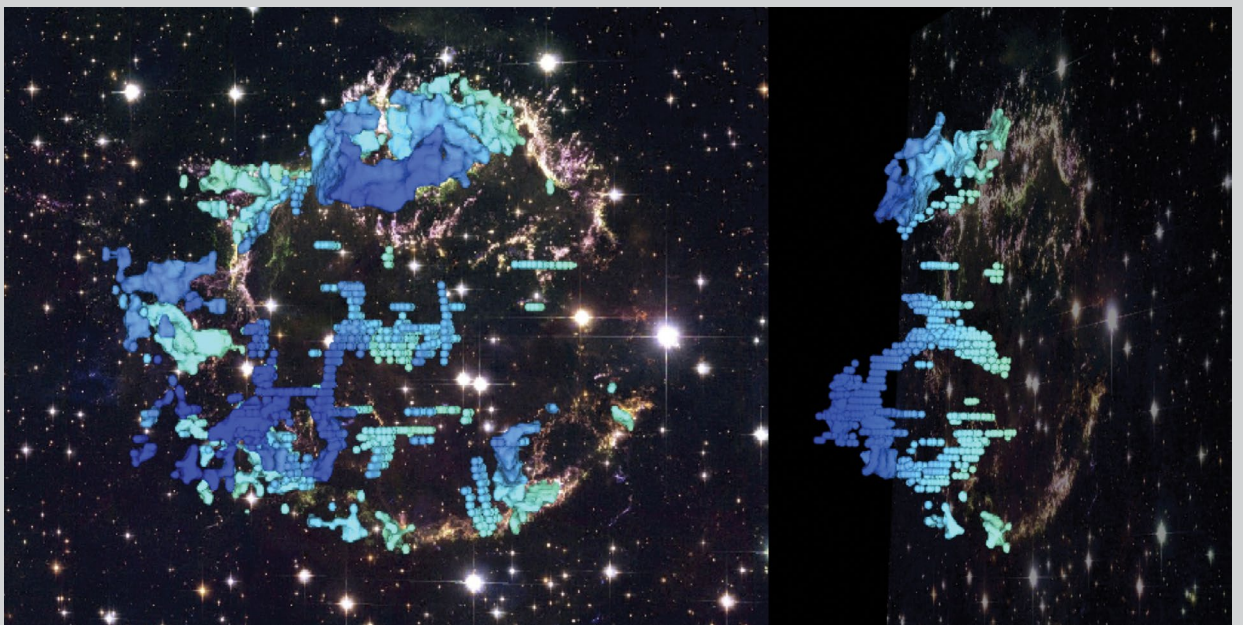


Figure 2: Doppler reconstruction of Cas A. Color gradient blue-to-red corresponds to Doppler velocities that range from -4000 to 6000 km s^{-1} . Two angled perspectives highlighting the south cavity are shown. The background is the same composite *Hubble* image shown in Figure 1. Adapted from Milisavljevic & Fesen (2015).

Missing iron?

The presence of large cavities in Cas A's interior may have been created early in the explosion from plumes of radioactive ^{56}Ni -rich ejecta that rose up through outer shells of lighter elements. Such nickel-rich material would have decayed into cobalt and iron, releasing energy that would cause the gas to expand and compress nearby non-radioactive material such as oxygen, sulfur, and argon into cavity walls (Li & McCray 1993). This picture, consistent with Chandra observations of Cas A's x-ray-emitting iron, shows most of it to lie nicely within the remnant's cavities (DeLaney et al. 2010; Milisavljevic & Fesen 2013).

The amount of Ni produced and its distribution in a supernova are fundamental properties of the explosion that inform us about the progenitor star's interior structure and explosion mechanism. State-of-the-art computer simulations of core-collapse explosions find that the bulk of the Ni mass should remain inside the remnant with velocities below 2000 km s^{-1} (Hammer et al. 2010). However, this is actually opposite to what we currently see in Cas A, where x-ray-bright Fe emission traces the original Ni distribution out to velocities of 4000 km s^{-1} . Thus, either the simulations are not adequately following the dynamics of mixing or more Fe remains to be detected in Cas A's interior. *Webb* has the potential to finally resolve this "missing iron" problem because the interior, cool iron should be emitting at wavelengths that NIRCams throughput and resolution are optimized for.

Surviving companion and the nature of the collapsed central object

A perennial question about Cas A concerns the possibility of a surviving companion (Podsiadlowski et al. 1992). Optical spectra of Cas A's light echoes associated with the original supernova explosion closely resemble those of the extragalactic SN 1993J (Krause et al. 2008; Rest et al. 2011). WFC3 and COS observations of SN 1993J show a UV spectrum consistent with contributions from a B2 Ia star (Fox et al. 2014), leading some to suspect that a companion star may also exist near the explosion center of Cas A. However, to date no surviving companion has been identified (Fesen et al. 2006b).

It may be that increased extinction at the very center of the remnant has prevented optical detection. The superior sensitivity and angular resolution of *Webb* in the infrared might finally uncover a surviving companion—should one exist. The proper motion of the binary companion would likely be $\sim 0.02''/\text{yr}$. In only 1.5 yr, this proper motion would already translate to a pixel shift on NIRCams, which would make it fairly easy to secure a firm identification in *Webb*'s expected lifetime.

Webb observations of Cas A's explosion center would also help in our understanding of its central compact object (CCO). *Chandra* first-light images of Cas A revealed a central x-ray point source that is likely the neutron star that formed from the collapsed core of the progenitor star (Tananbaum 1999), but no optical, infrared, or radio counterpart has ever been detected. These null detections leave considerable latitude in the interpretation of the CCO (see Fesen et al. 2006b). *Webb*/NIRCams offers

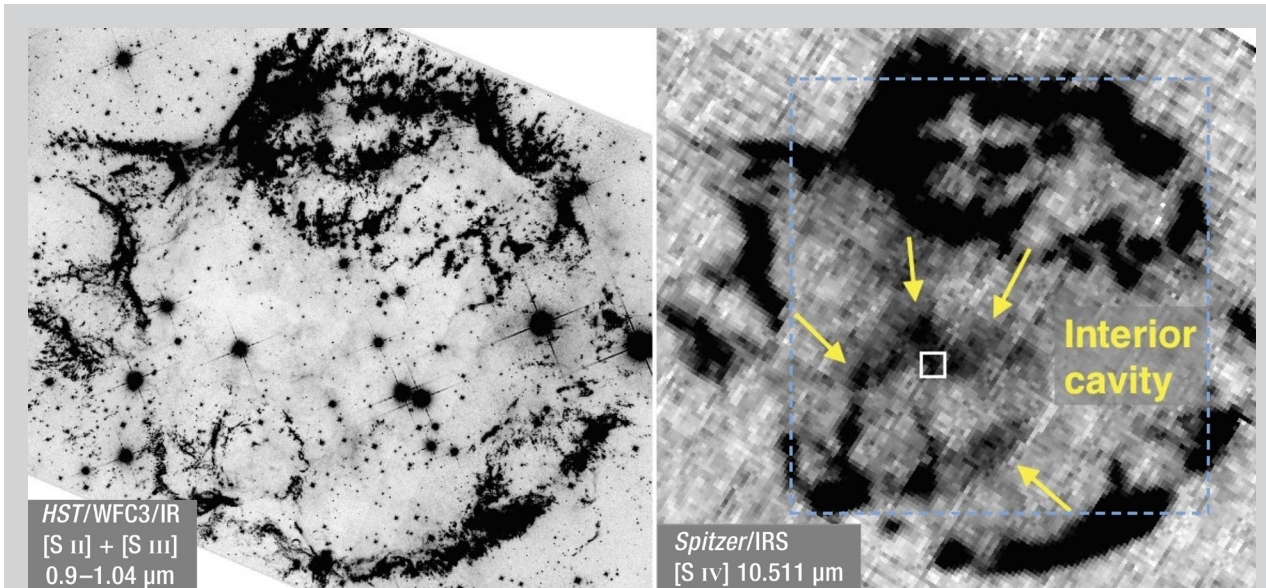


Figure 3: Hubble and Spitzer images of Cas A. Left: Hubble/WFC3/IR image sensitive to [S II] and [S III] line emission. The angular resolution is $0.1''$. Right: Spitzer IRS spectral map filtered to reveal [S IV] emission around 10.511 microns (Smith et al. 2009). The spectral resolution is $R \sim 100$, and the effective angular resolution is $2''$. *Webb* will be able to achieve Hubble's angular resolution and access this wavelength region of Spitzer with superior spectral resolution. NIRSpect, which has a large $3' \times 3'$ FOV (dashed blue box), will achieve up to $R \sim 1000$ between 0.6–5 micron, and up to $R \sim 2400$ between 5–29 micron. Regions of interest can be followed up in more detail with MIRI/Integral Field Unit observations (FOV $7.5'' \times 7.5''$; white box), which will permit medium resolution spectroscopy ($R \sim 3000$) over the wavelength range 5–28.3 micron.

a significant gain in infrared sensitivity over current missions and thus may be the instrument to finally make progress on the CCO's nature.

The work discussed here specifically for Cas A highlights some of the tremendous capabilities *Webb* will provide to answer many fundamental open questions about the physical processes that govern core-collapse supernovae. Undoubtedly, similar analyses applied to the many Galactic and Magellanic Clouds' remnants will also lead to major steps forward in our understanding of how massive stars explode, enrich the universe, and generate compact stellar remnants.

References

- Burbidge, E., et al. 1957, *Rev. Mod. Phys.*, 29, 547
Dalla Vecchia, C., & Schaye, J. 2008, *MNRAS*, 387, 1431
DeLaney, T., et al. 2010, *ApJ*, 725, 2038
Fesen, R., et al. 2006a, *ApJ*, 645, 283
Fesen, R., et al. 2006b, *ApJ*, 636, 848
Fox, O., et al. 2014, *ApJ*, 790, 17
Hammer, N., et al. 2010, *ApJ*, 714, 1371
Krause, O., et al. 2008, *Science*, 320, 1195
Li, H., & McCray, R. 1993, *ApJ*, 419, 824
Milisavljevic, D., & Fesen, R. 2012, *ApJ*, 751, 25
Milisavljevic, D., & Fesen, R. 2013, *ApJ*, 772, 134
Milisavljevic, D., & Fesen, R. 2015, *Science*, 347, 526
Pavlov, G., et al. 2000, *ApJ*, 531, 53
Podsiadlowski, P. 1992, *ApJ*, 391, 246
Reed, J., et al. 1995, *ApJ*, 440, 706
Rest, A., et al. 2011, *ApJ*, 732, 3
Smartt, S. 2009, *ARAA*, 47, 63
Smith, J., et al. 2009, *ApJ*, 693, 713
Tananbaum, H. 1999, *IAU Circ.*, 7246
Van Dyk, S., et al. 2011, *ApJ*, 741, L28
Woosley, S., & Weaver, T. 2002, *Rev. Mod. Phys.*, 74, 1015

The Biconical Outflow at the Center of the Milky Way: *A Hubble Space Telescope* Program to Explore the Galactic Center

Andrew Fox, afox@stsci.edu

Introduction

The nuclei of star-forming galaxies are energetic places. These are the powerhouses where supermassive black holes (SMBHs) collect interstellar gas from their surroundings, funnel it onto accretion disks, heat it to temperatures high enough to emit x-rays, and drive winds out into galaxy halos. Nuclear winds in external galaxies often show a distinctive biconical shape, as in the galaxies M82, NGC 3079, and Arp 220 (see Veilleux et al. 2005). In these galaxies, optical H α emission can be used to trace the outflow out to distances up to several kpc above and below the galactic center.

In the Milky Way, the rotating disk of interstellar gas and dust lying between the Sun and the Galactic Center (GC) complicates the identification and measurement of the nuclear outflow. This foreground material is opaque at optical wavelengths, making it essentially impossible to study the GC with visible-light telescopes. Observing in the infrared and other parts of the electromagnetic spectrum solves this problem. It is also possible to study the outflow in the ultraviolet (UV) by looking out of the Galactic plane, away from the obscuring disk.

*Continued
page 60*

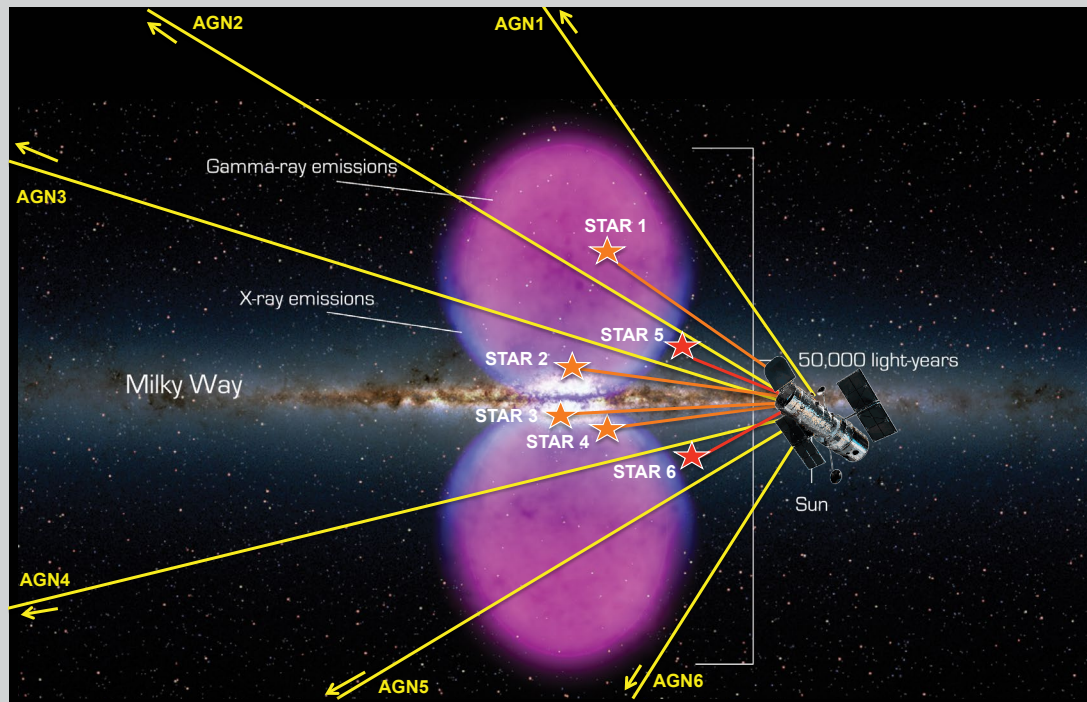


Figure 1: Illustration of the use of extragalactic (yellow) and stellar (orange) sightlines to bracket the Fermi Bubbles (pink). The graphic shows an artist impression of the Milky Way viewed from outside. Our full sample contains ten stellar directions and 24 extragalactic sightlines spread between the Northern and Southern Galactic hemispheres (courtesy NASA/GSFC).

Evidence for wind activity near the GC has emerged from recent multi-wavelength studies of diffuse emission above and below the GC. This emission is seen in microwaves (the *WMAP* haze; Finkbeiner et al. 2004), gamma-rays (the so-called “Fermi Bubbles”; Su et al. 2010), and polarized radio emission (Carretti et al. 2013). The Fermi Bubbles are two giant lobes extending ~ 10 kpc above and below the GC, covering a similar ~ 10 kpc range in Galactic longitude, but narrow at the waist (see Figure 1). It is debated whether the bubbles are powered by high-density nuclear star formation in the central 500 pc of the Galaxy, or by the central AGN (Crocker & Aharonian 2011).

While the multi-wavelength emission maps reveal the morphological properties and energetics of the gas in the nuclear outflow, they do not reveal how fast it is moving or its chemical composition. To measure these quantities, spectroscopic information is needed. We therefore designed a *Hubble Space Telescope* spectroscopic experiment in Cycle 21 to study the kinematics, spatial extent, and chemical abundances of the Galactic nuclear outflow.

Experimental design

We selected samples of UV-bright active galactic nuclei (AGN), lying within 30 degrees longitude of the GC in both the Southern and Northern Galactic hemispheres, including directions both inside and outside the Fermi Bubbles. These AGN act as lighthouses—each one illuminating the foreground gas along its line-of-sight to the Earth. The AGN must be bright in the UV since that is the richest part of the electromagnetic spectrum for measuring interstellar metal absorption lines.

We also identified a sample of halo stars at distances $d > 7$ kpc, distant enough to lie within the Fermi Bubbles. Each target was observed in the UV using one of *Hubble*’s spectrographs (the Cosmic Origins Spectrograph or the Space Telescope Imaging Spectrograph). By comparing the halo-star spectra with the AGN spectra, we placed limits along the line-of-sight where the absorption was occurring. Furthermore, by observing how the absorption properties depend on the latitude of the target, we studied the vertical behavior of the outflow. The outline of the geometry underpinning this experiment is shown in Figure 1.

Results and discussion

We searched for high-velocity ($|v| > 100$ km s $^{-1}$) metal absorption components in the spectrum of each target. One extragalactic direction, the sightline to the AGN PDS 456, caught our attention because of its location on the sky and the properties of its UV spectrum (Fox et al. 2015). This direction lies close to the GC at Galactic coordinates $l, b = 10.4^\circ, +11.2^\circ$, near the base of the northern Fermi Bubble (see Figure 2), within a region where biconical x-ray emission was detected from the *ROSAT* satellite (Snowden et al. 1997).

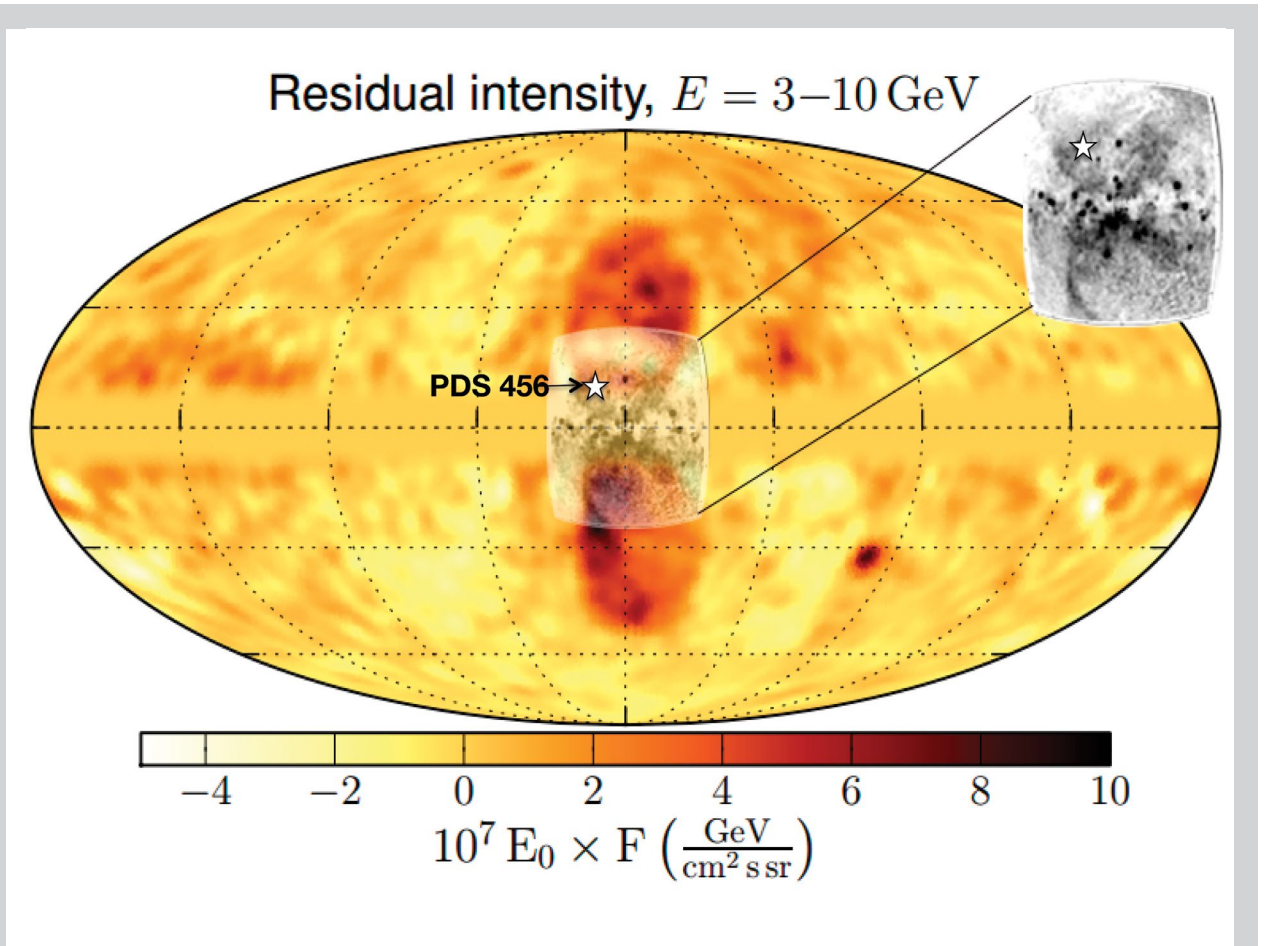


Figure 2: Collage of gamma-ray and x-ray emission showing the striking biconical nuclear structure intercepted by the PDS 456 sightline (Fox et al. 2015). The yellow/orange map is an all-sky *Fermi* image of the residual gamma-ray intensity in the 3–10 GeV range, in Galactic coordinates centered on the GC (Ackermann et al. 2014). The Fermi Bubbles are the twin lobes in dark orange at the center of the figure. Superimposed in grayscale is the *ROSAT* diffuse 1.5 keV emission map (Bland-Hawthorn & Cohen 2003). The inset on the right shows a zoom-in on the x-ray data.

The UV metal-line absorption profiles show three high-velocity components (see Figure 3). One (at $+130\text{ km s}^{-1}$) might be attributable to foreground gas in the disk of the Milky Way, but the other two (at -235 km s^{-1} and $+250\text{ km s}^{-1}$) are moving too fast to be located in the disk of the Galaxy. Particularly striking is that these two high-velocity components (HVCs) show velocities that are almost *symmetric* with respect to zero. This is exactly the observational signature expected if we are observing the front (blueshifted) and back (redshifted) sides of a biconical nuclear outflow (see Figure 4). Using kinematical modeling of the biconical wind, we inferred an outflow velocity of $900\text{--}1000\text{ km s}^{-1}$ —the first time the velocity of the Galactic nuclear wind has been determined (Fox et al. 2015).

There are several lines of evidence that favor the biconical outflow explanation over the alternative explanation in which the symmetric absorption components trace unrelated HVCs at other distances along the line of sight.

First, it is highly unusual to detect *two or more* HVCs with absolute velocities above 140 km s^{-1} ; Sembach et al. (2003) found only two such cases out of 100 sightlines in their survey of O VI absorption in HVCs (and one was a Galactic Center direction).

Second, the low latitude of the PDS 456 sightline makes the kinematics of high-velocity components hard to reproduce from unrelated HVCs, since the de-projected vertical velocities ($\sim 1000\text{ km s}^{-1}$) would be unusually high for “regular” (non-GC) HVCs.

Third, we know from x-ray emission maps that the PDS 456 direction passes through a biconical structure, which provides circumstantial support to the biconical outflow model.

Finally, the outflow velocity we infer for the Milky Way’s nuclear wind is in line with that seen from the nuclei of other star-forming galaxies (Veilleux et al. 2005). These results are discussed in more detail in Fox et al. (2015).

Continued
page 62

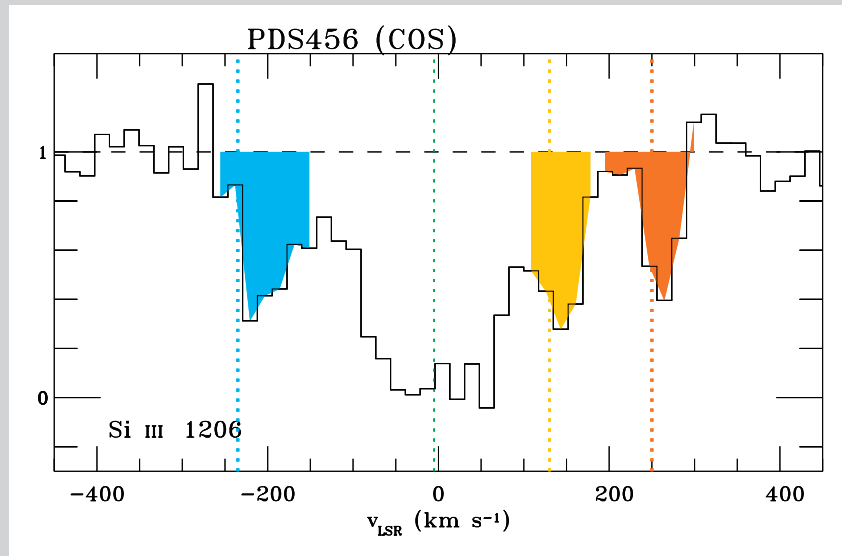


Figure 3: *HST/COS* spectra of Si III 1206 absorption toward the low-latitude AGN PDS 456. Normalized flux is plotted against LSR velocity. Along with the zero-velocity absorption from the disk of the Milky Way, three high-velocity components of absorption are seen, shaded blue, yellow, and orange. Whereas the component near $+100 \text{ km s}^{-1}$ (yellow) has a velocity consistent with Galactic rotation, the components at $\pm 250 \text{ km s}^{-1}$ (blue and orange) do not, and therefore require an alternative explanation. We favor an origin in the two sides of a biconical nuclear outflow (see Figure 4), with the negative-velocity component arising on the near-side and the positive-velocity component arising on the far-side of the cone.

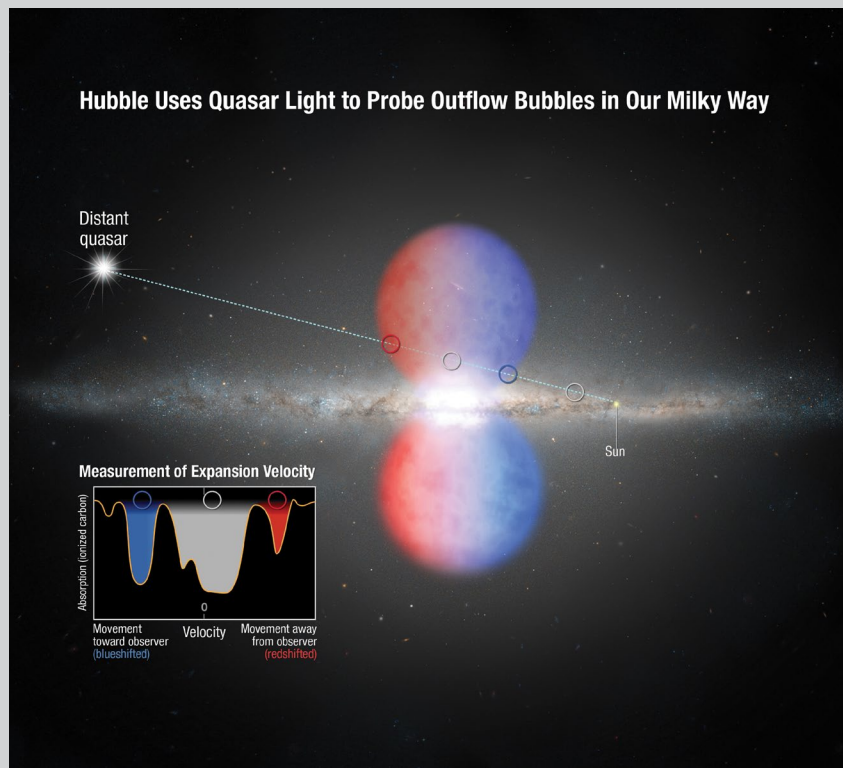


Figure 4: Illustration of the biconical outflow interpretation for our *Hubble* absorption-line data of quasar PDS 456. The line-of-sight from the Sun to the quasar intercepts gas in several locations: near the Galactic disk (close to zero velocity), the near side of the outflow (blueshifted), the center of the outflow (close to zero velocity), and the far side of the outflow (redshifted). From STScI Press Release 2015-03 (courtesy NASA, ESA, Ann Feild/STScI).

References

- Ackermann, M., et al. 2014, ApJ, 793, 64
Bland-Hawthorn, J., & Cohen, M. 2003, ApJ, 582, 246
Carretti, E., et al. 2013, Nature, 493, 66
Crocker, R. M., & Aharonian, F. 2011, PhRvL, 106, 101102
Finkbeiner, D. 2004, ApJ, 614, 186
Fox, A. J., et al. 2015, ApJ, 799, L7
Sembach, K. R., et al. 2003, ApJS, 146, 165
Snowden, S., et al. 1997, ApJ, 485, 125
Su, M., et al. 2010, ApJ, 724, 1044
Veilleux, S., et al. 2005, ARA&A, 43, 769

New Insights on Exoplanet Atmospheres

Jacob Bean, jbean@oddjob.uchicago.edu, and Jean-Michel Désert, desert@colorado.edu

The importance of exoplanet atmosphere observations

The multitude of recently discovered exoplanets presents both challenges and opportunities. The challenge is to understand these objects as part of a complete theory of planetary system cosmogony, which is one of the forefront topics of modern astrophysics and planetary science. The opportunity is the chance to study a large and diverse sample of planets, including solar system analogues in different physical regimes (e.g., hot Jupiters) and classes of planets with no solar system counterparts (e.g., super-Earths).

Now that we are getting tight constraints on the rate of planet occurrence from exoplanet surveys, a key next frontier for the field is atmospheric characterization. The fundamental themes of exoplanet atmosphere characterization are the measurements of compositions, thermal structures, energy budgets, and dynamics to understand planetary origins and physics. *Hubble* has been making groundbreaking contributions in this area for 15 years using transit observations. Furthermore, *Hubble* has maintained its forefront position with the installation of the WFC3 instrument during SM4, which enables accurate near-infrared spectroscopy, and the implementation of spatial scanning, which enables observations of bright stars so that the required high signal-to-noise levels can be reached efficiently.

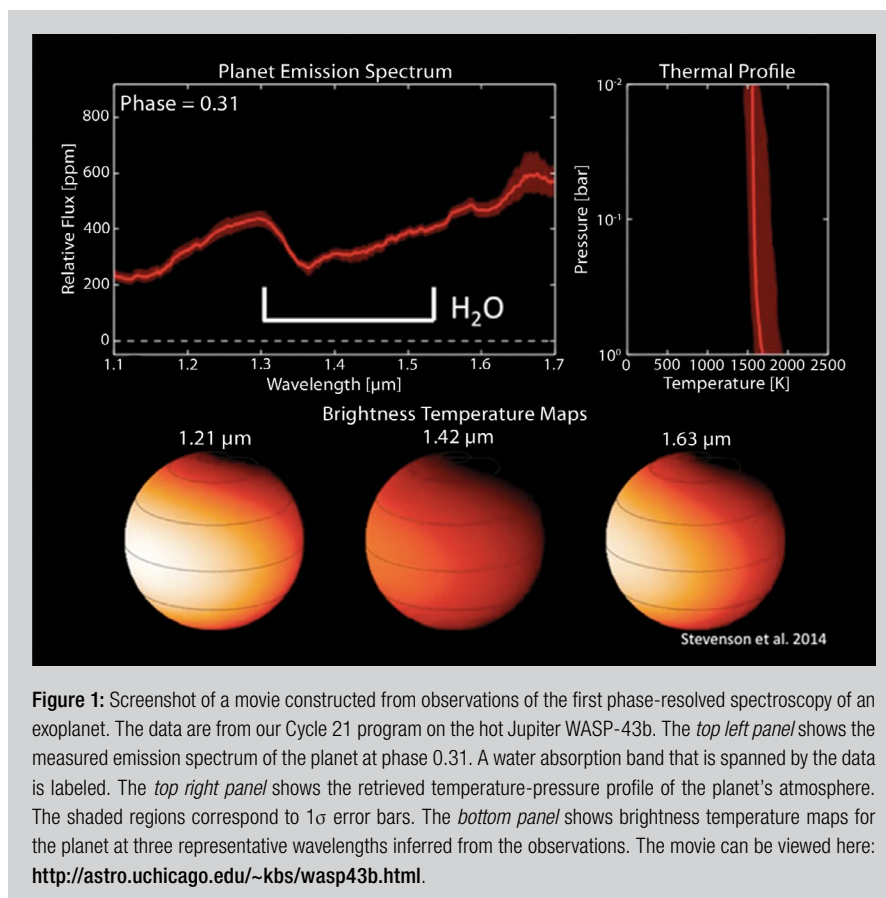
A new method to probe exoplanet atmospheres: phase-resolved spectroscopy

In this article we highlight two new results based on *Hubble* WFC3 transit spectroscopy observations that were carried out as part of a Large Treasury program in Cycle 21 (GO-13467). One of the exciting new developments is the demonstration of phase-resolved emission spectroscopy of exoplanets. The idea behind emission spectroscopy is that the effect of molecular absorption on the planet's thermal emission can be used to scan the temperature-pressure profile of the planet's atmosphere. For example, within a molecular band, where opacity is high, we probe the temperature structure higher in the atmosphere, while outside molecular bands where opacity is low, we probe deeper layers. This technique reveals the hemispheric average of the planet's dayside thermal structure when applied to secondary eclipse observations. Observations of an exoplanet as a function of its rotational phase enable necessary measurements of the thermal structure of the planet's atmosphere as a function of longitude.

Using *Hubble*, we performed the first phase-resolved emission spectroscopy of an exoplanet during our Cycle 21 program (Stevenson et al. 2014). We targeted the hot Jupiter WASP-43b for this demonstration. The observations spanned three complete orbits of the planet ($P = 19.5$ hr) using 14 continuous *Hubble* orbits for each planetary orbit. Our emission spectroscopy data set also included two observations centered just on the secondary eclipse. WASP-43b is likely tidally locked due to its close proximity to its host star. Therefore, there is a 1:1 correspondence between orbital phase and rotational phase for this planet.

Figure 1 is a screenshot of a movie that summarizes our phase-resolved measurements for WASP-43b. Previous exoplanet phase-curve observations were limited to broadband photometry (e.g., Knutson

Continued
page 64



et al. 2007), and the interpretation of such data has an inherent degeneracy between the atmospheric composition and thermal structure. Our spectroscopic observations enabled us to break this degeneracy and uniquely determine the composition and thermal structure of an exoplanet atmosphere as a function of longitude for the first time.

We have used the data for WASP-43b to confront 3D atmospheric circulation models (Kataria et al. 2015). We find that the models correctly predict the dayside spectrum of the planet, which is a major success. However, the models over-predict the flux measured from the night side, which suggests less efficient energy transport from the day-to-night side or the existence of thick clouds blocking our view to the deeper and hotter parts of the atmosphere.

The demonstration of phase-resolved spectroscopy with WFC3 opens the door to unique comparisons of the thermal structures, energy budgets, and dynamics of more exoplanet atmospheres. We anticipate that the application of this new technique will break new ground in understanding many exoplanet characteristics.

New constraints on exoplanet atmosphere compositions

A second recent development in *Hubble* transit spectroscopy studies is the demonstration of constraints on the carbon-to-oxygen ratios in exoplanet atmospheres. Oxygen and carbon are critically linked to the formation of planets because they are the third and fourth most abundant elements in the universe. Because of their dominance, the relative abundance of these elements sets the chemistry in planet-forming disks. There are roughly two oxygen atoms for every carbon atom in the Sun's photosphere, which is often used as the template abundance pattern in protoplanetary disks. The final carbon-to-oxygen ratio (C/O) in a planetary atmosphere is a result of the complex interplay between nebular gas and planetesimal accretion at the location in the disk where the planet formed. The carbon-to-oxygen ratio in the atmosphere of solar system giant planets is poorly known because the oxygen is locked up in water that has condensed out and is difficult to measure. However, close-in exoplanets are hot enough that volatile condensation does not deplete their atmospheres, and thus remote observations should yield an unbiased measurement of their carbon and oxygen abundances.

Nikku Madhusudhan and collaborators made a big splash in the field of exoplanet atmospheres in 2011 by showing that the hot Jupiter WASP-12b could have a non-solar C/O value (Madhusudhan et al. 2011). They suggested that the planet had a $C/O > 1$ based on observations and modeling of its dayside emission. This was important because it suggested a very different chemistry and formation

pathway than was commonly assumed for giant planets. However, the WASP-12b result was based on just broadband photometry rather than the robust spectroscopic identification of molecules that would only be present in a high C/O atmosphere. Therefore, the high C/O result remained a hypothesis rather than a definitive conclusion.

We have measured a precise transmission spectrum for the planet WASP-12b using during our Cycle 21 program to test the high C/O hypothesis for this planet (Kreidberg et al. 2015). In addition to using the now-standard G141 grism ($\lambda = 1.1$ to $1.7 \mu\text{m}$), which is mainly sensitive to water vapor, we also observed transits for the first time using the G102 grism ($\lambda = 0.8$ to $1.1 \mu\text{m}$) to gain sensitivity to a wider variety of molecules. The resulting spectrum is shown in Figure 2.

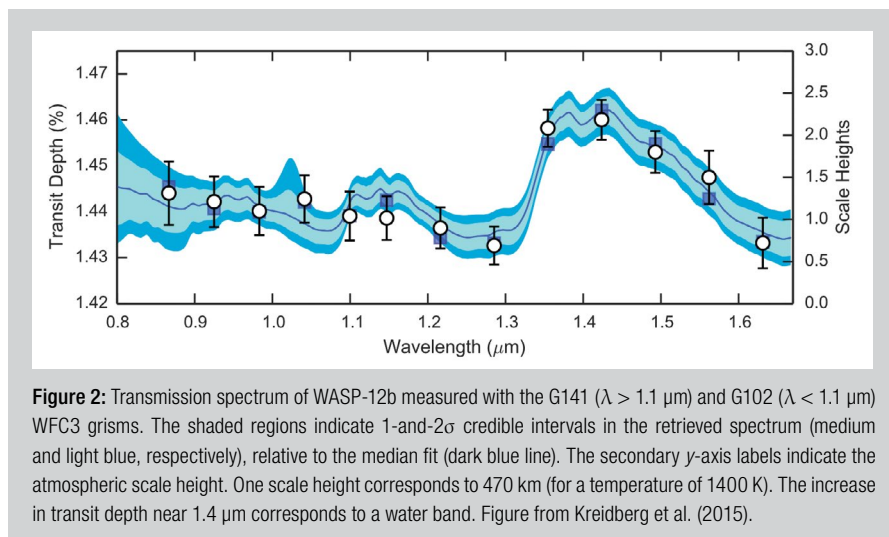


Figure 2: Transmission spectrum of WASP-12b measured with the G141 ($\lambda > 1.1 \mu\text{m}$) and G102 ($\lambda < 1.1 \mu\text{m}$) WFC3 grisms. The shaded regions indicate 1-and-2 σ credible intervals in the retrieved spectrum (medium and light blue, respectively), relative to the median fit (dark blue line). The secondary y-axis labels indicate the atmospheric scale height. One scale height corresponds to 470 km (for a temperature of 1400 K). The increase in transit depth near $1.4 \mu\text{m}$ corresponds to a water band. Figure from Kreidberg et al. (2015).

We detect water absorption in the WASP-12b transmission spectrum at 7σ confidence. Our detection is the first spectroscopic identification of a molecule in this benchmark planet's atmosphere. However, our goal for these measurements was not simply to detect molecules, but rather to measure their abundances precisely enough to constrain the composition. This was the motivation for our intensive observing campaign, which utilized 30 *Hubble* orbits to measure three transits of the planet with each of the two grisms.

The strength of the water absorption in our measured spectrum implies a water-rich composition for WASP-12b's atmosphere. This is surprising given that water would not be abundant in a $\text{C/O} > 1$ atmosphere. The reason for this is that all of the oxygen atoms would be locked up in CO due to the overabundance of carbon for the region of the atmosphere being probed. Figure 3 illustrates how the measured water abundance is inconsistent with this prediction. Detailed modeling of the transmission spectrum by collaborator Michael Line constrains the C/O of the atmosphere to be less than 1.0 at more than 3σ confidence assuming chemical equilibrium. For this inference, the lack of detection of the other molecules that would be expected in a high C/O atmosphere is just as important as the detection of water.

There has also been an independent effort to model our WASP-12b data together with WFC3 transmission spectra of seven other hot Jupiters that show evidence of water absorption (Benneke 2015). The main conclusion of this work is similar to our findings: the data for all eight planets are consistent with solar C/O values and there is no evidence of unusual abundances. Thus the high C/O hypothesis for WASP-12b and other planets may need revision. Speaking more generally, the agreement between two independent modeling efforts for the WASP-12b spectrum demonstrates that unambiguous results can be obtained for exoplanet atmospheres if enough observing time is invested to make high precision measurements.

Looking to the future with *Webb*

The *James Webb Space Telescope* is expected to revolutionize the field of exoplanet atmospheres (Beichman et al. 2014). The results discussed here suggest that given its design capability, *Webb* will be instrumental in complete planet characterization studies. Transiting planets offer multiple atmospheric diagnostics: transmission, dayside emission, and phase-resolved emission spectroscopy. These multiple diagnostics are needed to break modeling degeneracies and untangle the complexity of exoplanet atmospheres. A special handful of planets are within reach for the full complement of transit spectroscopy measurements with *Hubble*, and these measurements will be feasible for many more planets with the increased power of *Webb*.

Continued
page 66

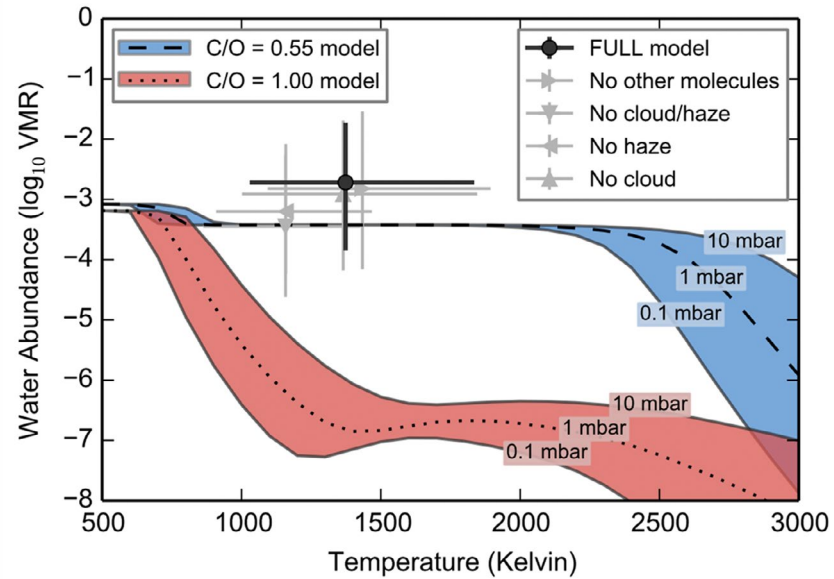


Figure 3: Measurement of the water abundance and scale height temperature for WASP-12b (points) compared to equilibrium chemistry predictions of the water content for different atmospheric compositions (lines and shading). The black point indicates the water abundance and temperature measurements from the main model fit to the WFC3 spectrum. Results from other nested models are shown in gray. The black dashed line and blue shading correspond to water abundance predictions for a solar C/O composition (0.55), and the black dotted line and red shading correspond to C/O = 1. Both models have solar metallicity. For each model composition, the shading shows the span of predicted water abundances over pressures ranging from 0.1–10 mbar. The black lines correspond to 1 mbar, which is the typical pressure level probed by our observations. Figure from Kreidberg et al. (2015).

References

- Beichman, C., et al. 2014, *PASP*, 126, 1134
 Benneke, B. 2015, *ApJ* submitted, arXiv:1504.07655
 Kataria, T., et al. 2015, *ApJ*, 801, 86
 Knutson, H., et al. 2007, *Nature*, 447, 183
 Kreidberg, L., et al. 2015, *ApJ*, 814, 66
 Madhusudhan, N., et al. 2011, *Nature*, 469, 64
 Stevenson, K. B., et al. 2014, *Science*, 346, 838

Planetary Systems Around White Dwarfs

Boris Gänsicke, boris.gaensicke@warwick.ac.uk

The vast majority of all known planet-hosting stars, including the Sun, will eventually evolve into red giants, lose a significant fraction of their mass as a planetary nebula, and finally end their lives as white dwarfs: extremely dense Earth-sized stellar embers that slowly consume their thermal heat content, monotonously cooling for billions of years. Only close-in planets will be devoured during the red-giant phase, whereas all surviving planetary bodies will see their orbits widening due to the mass loss of the host star.

In the solar system, Mars, the asteroid belt, and all the giant planets will escape evaporation, and move out by about a factor of two. Given the ubiquity of planets around main-sequence stars, it is certain that many of the known white dwarfs were once hosting planets, and it is very likely that a fair fraction of them still have remnants of their planetary systems. These systems offer a glimpse into the future of the solar system, and provide insight into the bulk composition of exo-planetesimals, as well as the frequency of rocky planetary systems around A-type stars.

Signposts of evolved planetary systems

The strong surface gravity of white dwarfs ($\sim 40,000$ stronger than that of the Sun) causes metals to sink out of the atmosphere on time-scales much shorter than their cooling ages (the time since the formation of the white dwarf), leading unavoidably to pristine hydrogen or helium atmospheres. Therefore any metals detected in the atmosphere of a white dwarf imply recent or ongoing accretion.

The existence of metal-polluted white dwarfs has been a conundrum for nearly a century, as accretion from the interstellar medium could explain neither the frequency, nor the composition of these stars (Friedrich et al. 2004; Farihi et al. 2010). The detection of an infrared excess around the white dwarf G29-38 (Zuckerman et al. 1987) was interpreted by Graham et al. (1990) as a dusty debris disk formed from the destruction of an asteroid or comet, years before the discovery of the first exoplanet.

Such a circumstellar reservoir of debris provides a natural explanation for the origin of the metals identified in optical and ultraviolet *Hubble*/FOS spectra of G29-38 (Koester et al. 1997). Asteroids approaching a white dwarf to $\approx 1 R_{\odot}$ will be tidally disrupted (Jura 2003), and the compact geometrical scale of the debris disks has been dynamically confirmed (Gänsicke et al. 2006). The existence of planets in these systems, scattering asteroids towards the white dwarf, is implied by simulations (Debes et al. 2012), however, the direct detection of white dwarf planets remains observationally challenging.

The frequency of white dwarfs with planetary systems

Given that the detection of metals in the atmospheres of white dwarfs is the unmistakable signpost of planetary debris accretion, the frequency of evolved planetary systems can be directly measured from spectroscopic surveys. Ground-based observations are almost exclusively sensitive to the Ca H/K lines in relatively cool and old white dwarfs. Using Keck and Very Large Telescope (VLT) high-resolution spectra, Zuckerman et al. (2003) detected Ca H/K absorption in $\approx 25\%$ of a sample of 87 stars with a median cooling age of ≈ 1 Gyr.

In younger, hotter white dwarfs, the Ca H/K lines become very weak as Ca II is ionized to Ca III. Probing the incidence of debris pollution at younger white dwarfs therefore requires far-ultraviolet spectroscopy, as this wavelength range is extremely rich in strong metallic transitions, in particular the Si II 1260/65 Å doublet.

Throughout Cycles 18/19, we carried out a COS survey of a representative sample of 85 white dwarfs with cooling ages of 20–200 Myr, and detected traces of heavy elements in 56% of these stars (Figure 1). Accounting for the effects of radiative levitation, i.e., the momentum of outgoing photons being absorbed in atomic transitions, we conclude that at least 27% of the stars in our sample must be currently accreting planetary debris (Koester et al. 2014).

Thus, so far there seems to be little evidence of an evolution in the rate of debris accretion as a function of cooling age, and the fraction of white dwarfs that host evolved planetary systems is overall comparable to the fraction of main-sequence stars with planets. Moreover, as many white dwarfs descend from $2\text{--}3 M_{\odot}$ progenitors, this study also demonstrates the efficient formation of planetary systems around A-type stars.

Many simulations predict a peak in the dynamical activity of evolved planetary systems around 100 Myr cooling age (Debes et al. 2012, Mustill et al. 2014), though instabilities may occur in closely packed planetary systems even at very late stages in the evolution (Veras & Gänsicke 2015). We are now extending this study in an ongoing Cycles 22/23 COS survey to provide a seamless measure of the incidence of debris over the range 5–300 Myr.

Continued
page 68

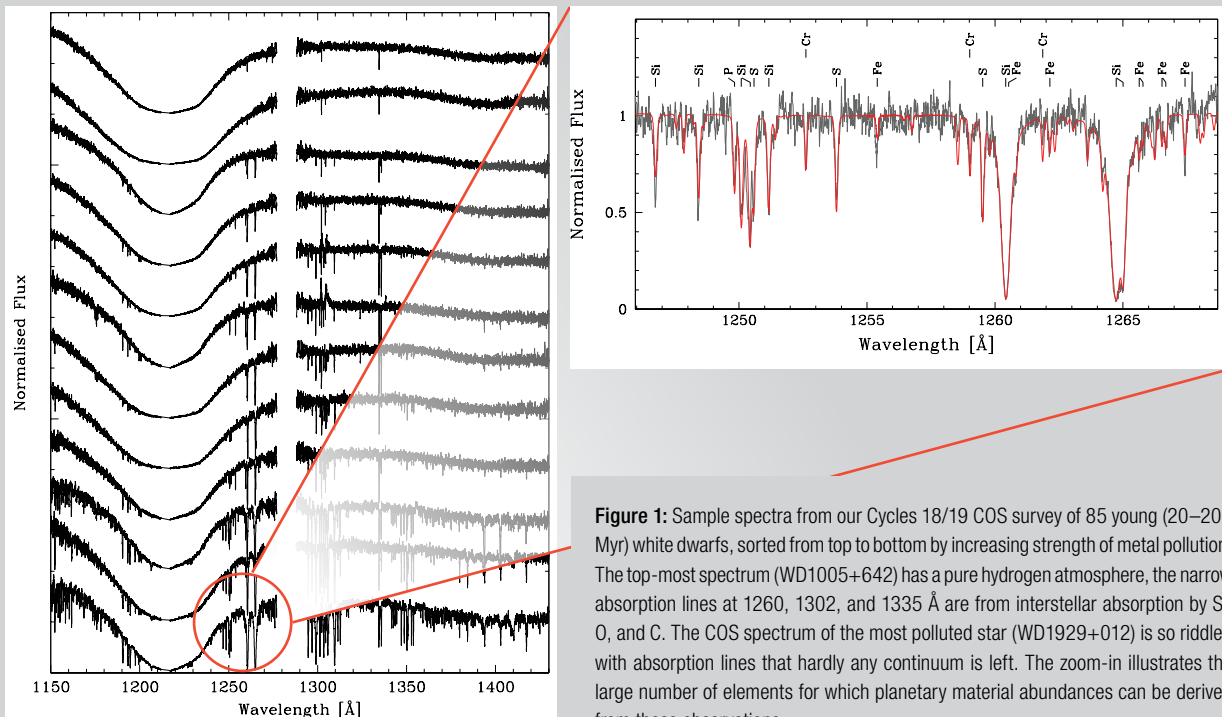


Figure 1: Sample spectra from our Cycles 18/19 COS survey of 85 young (20–200 Myr) white dwarfs, sorted from top to bottom by increasing strength of metal pollution. The top-most spectrum (WD1005+642) has a pure hydrogen atmosphere, the narrow absorption lines at 1260, 1302, and 1335 Å are from interstellar absorption by Si, O, and C. The COS spectrum of the most polluted star (WD1929+012) is so riddled with absorption lines that hardly any continuum is left. The zoom-in illustrates the large number of elements for which planetary material abundances can be derived from these observations.

The bulk composition of exoplanetary systems

The known population of exoplanetary systems is growing at a breath-taking pace, and the focus is shifting from discovery to characterization. A property of key importance to our understanding of the formation of planetary systems is their bulk composition. In a pioneering paper, Zuckerman et al. (2007) realized that determining the photospheric abundances of debris-polluted white dwarfs is entirely analogue to learning about the abundances of planetary bodies in our solar system from the analysis of meteorites—“rocks that fell from the sky.”

Taking into account the different velocities with which the various accreted elements diffuse through the white dwarf atmosphere (Koester 2009), it is possible to directly and accurately infer the bulk composition of extra-solar planetesimals from the measured photospheric abundances of the debris-polluted white dwarfs. The far-ultraviolet wavelength range is fundamental to these studies, and several groups have used *Hubble*/COS from Cycles 17 to 21 to analyze more than 15 metal-polluted white dwarfs. In zeroth approximation, the abundance patterns measured so far are overall similar to those of the terrestrial planets in the solar system, dominated by the major rock-forming elements (Si, Fe, Mg, and O), and volatile-depleted (Jura et al. 2012; Gänsicke et al. 2012).

At a closer look, the compositions measured in individual systems show a diversity similar to that of the different meteorite groups in the solar system, including Fe/Ni-rich differentiated parent bodies (Wilson et al. 2015), and collisional blending of asteroids (Xu et al. 2014). Our COS observations also identified debris from a water-rich planetesimal, that in its bulk composition resembles Ceres—the largest asteroid in the solar system (Farihi et al. 2013). Such planetary bodies may play an important role in the delivery of water onto rocky planets that formed dry.

Moving from the analyses of individual systems to ensemble studies of exoplanetary chemistry will provide important constraints for models of planet formation (Carter-Bond et al. 2012). *Hubble* and its ultraviolet spectrographs remain essential for this research over the coming years, and the increased sensitivity of large-aperture mission such as *HDST* has the potential to obtain accurate compositions for a few hundred planetary systems.

White-dwarf debris disk studies in the era of *Webb*

Spitzer played a key role in identifying the current sample of nearly 40 dusty debris disks around white dwarfs (Rocchetto et al. 2015). Infrared spectroscopy of the brightest disks shows a mixture of minerals dominated by silicates (Reach et al. 2009; Jura et al. 2009). *Webb* will be able to obtain high-quality mid-IR spectra for tens of white-dwarf debris disks, for which abundances measurements of the metal-polluted atmospheres will be already available from *Hubble* ultraviolet observations.

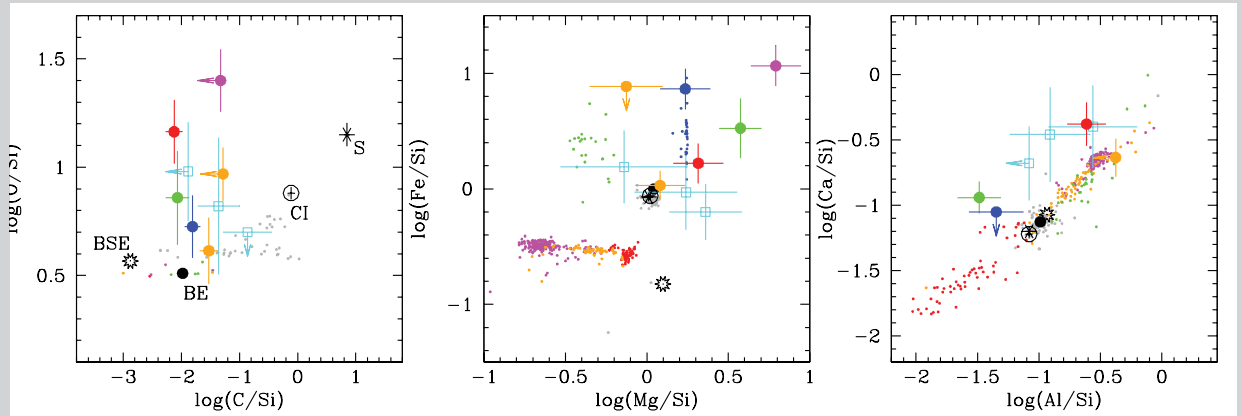


Figure 2: The three panels illustrate a range of metal-to-Si number abundance ratios for several debris-polluted white dwarfs (big dots with error bars, from Gänsicke et al. 2012; Jura et al. 2012; Xu et al. 2013, 2014), compared to different families of meteorites (small dots, Nittler et al. 2004); the bulk Earth (BE) and bulk silicate Earth (BSE; McDonough 2000); the Sun (S; Lodders 2003); and CI chondrites (CI; Lodders 2003). The chemical abundances of planetary debris are, overall, similar to those of the inner solar system, being volatile-depleted (low C/Si ratio, *left panel*). The major rock-forming elements (Si, Fe, Mg, and O) show a wide range of relative abundances (*left and middle panel*), indicating thermal and collisional processing, with some evidence for differentiation. The relative ratio of the Ca and Al, which are confined to planetary crusts, remains unaltered by post-nebular processing.

The diagnostic potential of these combined data sets is enormous, as it enables the detailed mineralogical modelling of the circumstellar dust, constrained by the precise knowledge of its bulk composition. The results from these studies will provide a wealth of observational insight into the formation and composition of rocky planets.

References

- Debes, J. H., Walsh, K. J., & Stark, C. 2012, *ApJ*, 747, 148
- Farihi, J., Barstow, M. A., Redfield, S., et al. 2010, *MNRAS*, 404, 2123
- Farihi, J., Gänsicke, B. T., & Koester, D. 2013, *Science*, 342, 218
- Friedrich, S., Jordan, S., & Koester, D. 2004, *A&A*, 424, 665
- Gänsicke, B. T., Koester, D., Farihi, J., et al. 2012, *MNRAS*, 424, 333
- Gänsicke, B. T., Marsh, T. R., Southworth, J., & Rebassa-Mansergas, A. 2006, *Science*, 314, 1908
- Graham, J. R., Matthews, K., Neugebauer, G., & Soifer, B.T. 1990, *ApJ*, 357, 216
- Jura, M. 2003, *ApJ*, 584, 91
- Jura, M., Farihi, J., & Zuckerman, B. 2009, *AJ*, 137, 3191
- Jura, M., Klein, B., Koester, D., & Zuckerman, B. 2012, *ApJ*, 750, 69
- Koester, D. 2009, *A&A*, 498, 517
- Koester, D., Gänsicke, B.T., & Farihi, J. 2014, *A&A*, 566, 34
- Koester, D., Wolff, B., Jordan, S., & Dreizler, S. 1997, *A&A*, 320, 57
- Lodders, K. 2003, *ApJ*, 591, 1220L
- McDonough, W. 2000, in *Earthquake Thermodynamics and Phase Transformation in the Earth's Interior*, Teisseyre R., Majewski E., eds. (San Diego: Academic Press), p. 5
- Mustill, A. J., Veras, D., & Villaver, E. 2014, *MNRAS*, 437, 1404
- Nittler, L. R., McCoy, T. J., Clark, P. E., et al. 2004, *Antarctic Meteorite Research*, 17, 231
- Reach, W. T., Lisse, C., von Hippel, T., & Mullally, F. 2009, *ApJ*, 693, 697
- Rochetto, M., Farihi, J., Gänsicke, B. T., & Bergfors, C. 2015, *MNRAS*, 449, 574
- Veras, D., & Gänsicke, B.T. 2015, *MNRAS*, 447, 1049
- Wilson, D. J., Gänsicke, B. T., Koester, D., et al. 2015, *MNRAS*, 451, 3237
- Xu, S., Jura, M., Klein, B., et al. 2013, *ApJ*, 766, 132
- Xu, S., Jura, M., Koester, D., et al. 2014, *ApJ*, 783, 79
- Zuckerman, B., & Becklin E. E. 1987, *Nature*, 330, 138
- Zuckerman, B., Koester, D., Melis, C., et al. 2007, *ApJ*, 671, 872
- Zuckerman, B., Koester, D., Reid, I. N., & Hünsch, M. 2003, *ApJ*, 596, 477

Vulcanism on Io with Aperture Masking Interferometry on *Webb*'s NIRISS

Deepashri Thatte, thatte@stsci.edu, Anand Sivaramakrishnan, anand@stsci.edu,
and John Stansberry, jstans@stsci.edu

Vulcanism on Jupiter's innermost Galilean moon, Io, presents a solar system science opportunity for the Aperture Masking Interferometry (AMI) mode of the Near Infrared Imager and Slitless Spectrograph (NIRISS) on *Webb*. Precise determinations of the positions of unresolved volcanic eruptions will be possible. NIRISS' F380M, F430M, F480M or F277W filters are well matched to emission from Io's lavas, which have temperatures of 500 K–2000 K. Accurate, high-cadence photometry of the eruptions in some or all filters will provide uniquely powerful insights into short-term variability, eruption temperatures and active areas, and long-term trends in activity for individual calderas on Io. These data could also provide new measurements of the global distribution of vulcanism on Io, improving constraints on the depth and location of tidal heating in the interior.

AMI is enabled by a seven-hole non-redundant aperture mask (NRM). The mask generates an interferogram in the image plane, turning the full aperture of the telescope into an interferometric array with an angular resolution of $0.5 \lambda/D$, rather than full aperture resolution of $1.22 \lambda/D$. We explore this capability by creating simulated observations of volcanic features on Io as observed with the NRM and F430M filter.

When Io is observable with *Webb* it will be at distances between 4.6 and 5.3 AU, and its 3642 km diameter will typically span 16 NIRISS pixels with pixel scale of approximately 65 mas. It can be placed at four different dither positions on the 80×80 pixel fast readout subarray designated for the AMI mode. The dithers are separated by 36 detector pixels (about $2.36''$), to mitigate against persistence and other detector and calibration noise sources (Greenbaum et al. 2015). This strategy also reduces the effect of flat-field errors (which we include in our simulations) and bad pixels.

We have simulated NIRISS AMI data for Io, including the effects of read noise, Poisson noise, dark current, sky background, and dither-position uncertainties (predicted to be 15 mas^1 single axis rms) and jitter (7 mas single axis rms). The dithers are randomly located within a pixel because of these placement errors, which may help mitigate against the effects of inter-pixel capacitance (re-distribution of signal due to capacitive coupling between pixels).

We create a count-rate image of the disk of Io including the contributions from reflected sunlight (IR albedo assumed to be 0.5) and from volcanoes calculated for assumed temperatures and radii. Loki, the largest volcanic feature on Io, is assumed to have a near-IR emitting area 20 km in radius with a temperature of 500K. Our so-called "Big event" has a radius of 4 km with a temperature of 1700 K, and our "Typical event" is only 1 km in radius, with a temperature of 1000 K.

Our simulated images are oversampled by a factor of 11 relative to the NIRISS pixels scale; even so, the volcanoes only occupy a fraction of the pixel, so we treat them as point sources. With NRM and F430M we estimate the count rate of Io disk to be 25,000 photons/sec/pixel, the count rate of Loki to be 5.4×10^5 photons/second, the count rate from bright events 2.8×10^6 photons/second and the count rate from typical event as 4×10^4 photons/second. We convolve the count rate images with NIRISS PSF created with *Webb* PSF simulation tool WebbPSF (Perrin et al. 2014) and introduce the noise and other effects mentioned above. For observations with Loki being the only active volcanic feature, the exposure time at each of the four dither positions is set to 29.5 seconds. Observations involving bright events are much shorter, with an exposure time set to 8 sec at each of the four dithers.

The FITS file containing the exposure at each dither position is made up of slices, one for each integration, and each such integration is made up of multiple non-destructive frames. In practice each non-destructive frame samples the signal every 75 milliseconds in the 80×80 AMI subarray, and the count rate can be accurately measured even for sources that would saturate in less than one second.

Figure 1 illustrates the results of our data modeling for a case with four active eruptions on Io. The NRM produces a PSF that has a sharp peak and an extended structure made up of coherent fringe patterns overlaid across one another. When convolved with the model input image, both Io's sunlit disk and emission from volcanic sources is visible. Emission from the eruptive centers is more readily

¹ milli-arcsecond

apparent in disk-subtracted images, as shown in the bottom panels of the figure, including emission from the fainter sources. Note that the simulated data (panel *d*) shown here is for a single AMI integration of 0.45 seconds and for our simulations each exposure is made up of 18 such integrations. To explore the ability of NIRISS AMI to resolve closely spaced eruptions, we simulated a bright event and Loki at separations of 88 mas and 177 mas respectively from each other. The results are equally

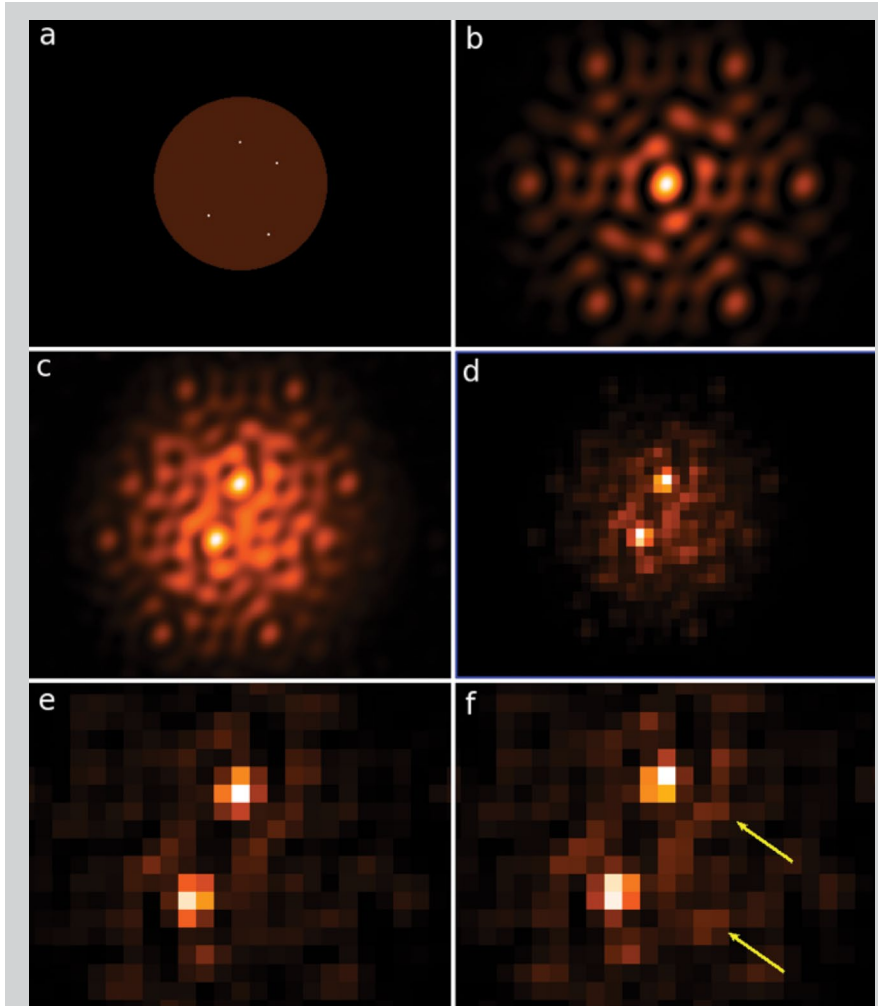


Figure 1: Panel *a* shows count rate image of Io with Loki, two bright events and one typical event that is used as an input image, Panel *b* is the NRM PSF of a point source created using WebbPSF for F430M filter. Panel *c* shows the convolution of input image with NRM PSF and Panel *d* is the simulated data (one integration). Panels *e* and *f* are the difference images obtained by subtracting simulated Io image without volcanoes from simulated Io image with volcanoes. To pinpoint the location of two fainter volcanoes, we first simulated the data with two bright events (Panel *e*) and then with two bright and two fainter events (Panel *f*). A comparison of Panels *e* and *f* reveals the location of two fainter volcanoes that are indicated by arrows in Panel *f*. The dimensions of Panels *a*, *b* and *c* are in 11× oversampled pixels and are displayed with linear stretch. Panels *d*, *e* and *f* are binned to the NIRISS pixel scale and are displayed using a squared stretch.

encouraging to those shown above. Even closely spaced eruptions appear to be resolvable in the raw model images where the disk of Io has been subtracted. Using deconvolution or other more advanced techniques, it should be possible to retrieve much clearer images reflecting a wealth of detail across the disk of Io. SO₂ frost, with an absorption at about 4.1 μm, is also of interest. While NIRISS lacks an appropriate filter in AMI mode, both NIRCam and NIRSspec could be used to characterize SO₂, albeit at lower spatial resolution. Nevertheless, NIRISS has the potential to acquire remarkable and unique data constraining vulcanism on Io.

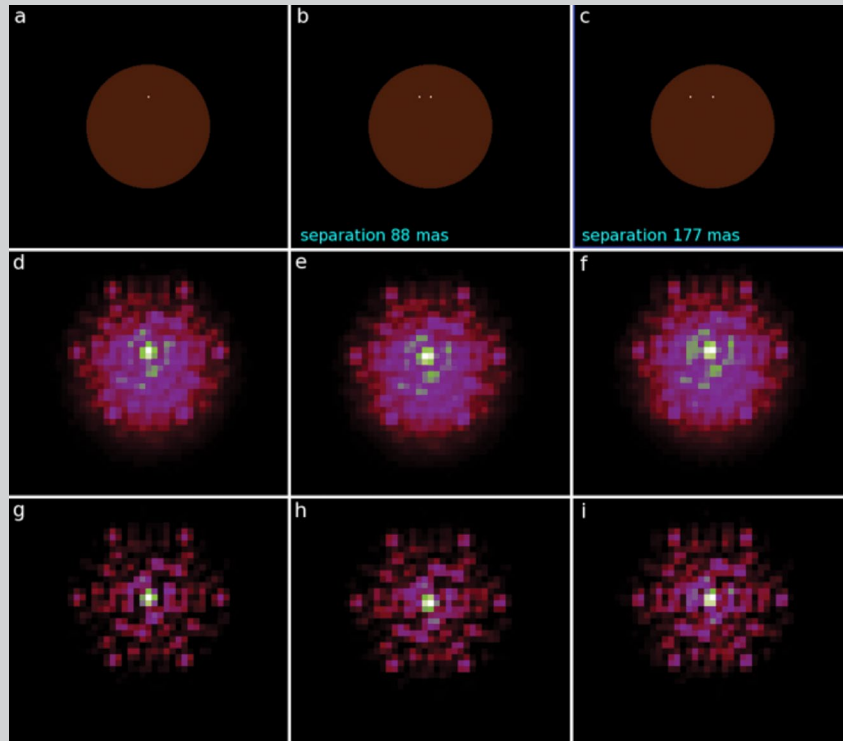


Figure 2: Panels *a*, *b*, and *c* show input model count-rate images with one bright event (Panel *a*), a bright event and Loki separated by 88 mas (Panel *b*), and a bright event and Loki separated by 177 mas (Panel *c*). A 65 mas NIRISS pixel spans about 246 km on Io at an Io-JWST separation of 5.2 AU. Panels *d*, *e*, and *f* show one integration of the simulated data based on the models in *a*, *b*, and *c*, respectively. Panels *g*, *h*, and *i* are the difference images obtained by subtracting a simulated Io image without volcanoes from the images in *d*, *e*, and *f*, respectively. The images in Panels *a*, *b*, and *c* are in 11× oversampled pixels and are displayed using a linear stretch; Panels *d* to *i* are binned to the NIRISS pixel scale and are displayed using a squared stretch. Subtle differences between *h* and *g*, and between *i* and *g*, suggest that deconvolution methods should allow the retrieval of fluxes and locations for even closely spaced eruptions from AMI observations of Io.

Conclusions

Our initial efforts at modeling AMI observations of Io volcanism are very promising. The volcanic emission from even fairly typical eruptions is visible in the raw simulated images for exposures of only a few 10s of seconds. Scattered light from Jupiter may be an issue for such observations, but can be mitigated directly by choosing appropriate filters. We hope to explore this application of AMI further by modeling scattered light gradients across the scene, and applying deconvolution to retrieve images that reflect more clearly the ~65 mas spatial resolution that should be achievable from the data.

References

- Greenbaum, A. Z., Pueyo, L., Sivaramakrishnan, A., & Lacour, S. 2015, *ApJ*, 798, 68
Perrin, M., et al. 2014, *Proc. of SPIE*, Vol. 9143, 91433X-1

Barbara A. Mikulski Archive for Space Telescopes

Anton Koekemoer, koekemoer@stsci.edu, for the MAST team

The Barbara A. Mikulski Archive for Space Telescopes (MAST) is one of NASA's premier astronomy data centers, along with the High Energy Astrophysics Science Archive Research Center (HEASARC) and the NASA/IPAC Infrared Science Archive (IRSA). MAST is the primary archive repository for data from several large, active space missions (*Hubble*, *Kepler*, *XMM-OM* and *Swift*-UVOT), legacy data from past missions (*GALEX*, *FUSE*, *IUE*, *EUVE*, and others), planned data from future missions, such as *James Webb Space Telescope*, and all-sky surveys such as VLA-FIRST, GSC and DSS.

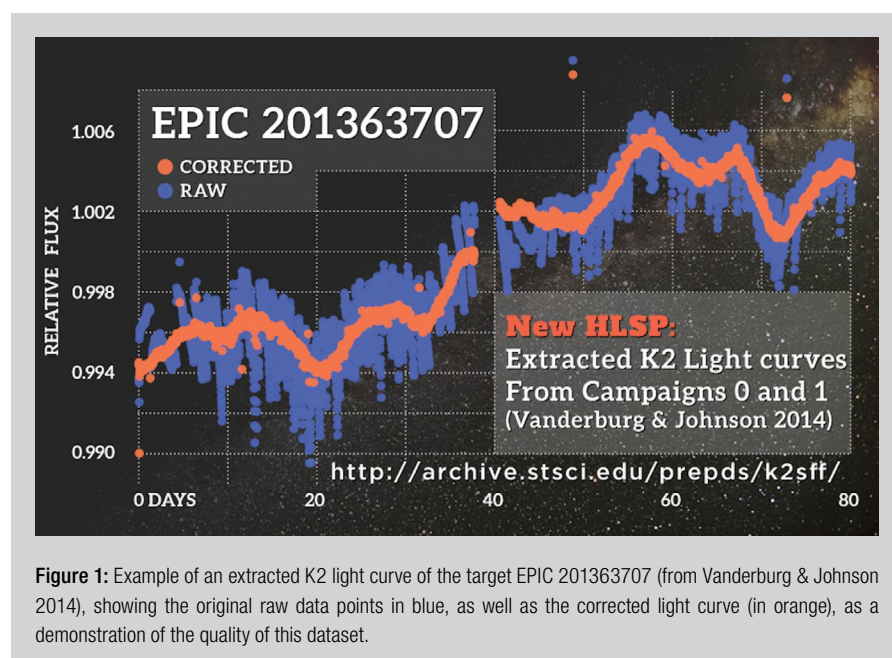
MAST supports the scientific research carried out by the astronomical community by facilitating access to its collections, offering expert user support and software for calibration and analysis, and providing value-added scientific data products. These include high-level science products (HLSPs) such as mosaics, catalogs, and spectra delivered to MAST by science teams, as well as enhanced products accessible via the *Hubble* Legacy Archive (HLA) and the *Hubble* Source Catalog. Current MAST news and updates are posted on our main archive website (<http://archive.stsci.edu>) and on social media, including Facebook (<https://www.facebook.com/MASTArchive>) and Twitter (https://twitter.com/MAST_News). MAST also makes available HLSPs from Treasury, Archival Legacy, and Large programs (see <http://archive.stsci.edu/hst/tail.html>).

Products from *Kepler* K2 Campaigns 0 to 4 now available at MAST

New K2 high-level science products (HLSPs) include extracted light curves! Courtesy of Vanderburg & Johnson (2014, 2015), long-cadence targets now have de-trended, extracted light curves available at MAST, including 20 different photometric apertures. There is a MAST Classic Search Interface providing access to light curves based on target IDs, coordinates, fluxes from the EPIC catalog, and other related quantities. An interactive plotter is also available to zoom and explore the light curves using any of the photometric apertures before downloading the FITS files. Further details are available at: <http://archive.stsci.edu/prepds/k2sff/>.

Kepler K2 Variability Catalog ("K2VARCAT")

Armstrong et al. (2015) have created a technique to correct for the pointing-dependent nature of the pixel-level fluxes. The team has released its extracted light curves (using a photometric aperture defined by the brightness of the target), as well as three plots of the resulting light curves: extracted, de-trended, and phase-folded. The light curves are stored in FITS files with binary tables in the first extension. The header also includes information on the aperture size used and the coordinates of the aperture center. The team has also released a catalog of variability statistics and object classification.



Continued
page 74

The catalog values are also available in the Search Form output results and are linked to the individual target pages in the output results. For more details, please see: <https://archive.stsci.edu/prepds/k2varcat/>.

gPhoton: A time-tagged database of over one trillion photon events observed by GALEX

MAST is pleased to announce the initial release of gPhoton (Million et al. 2015; Fleming et al. 2014): a time-tagged database of nearly 1.1 trillion photon events observed in the ultraviolet by the *Galaxy Evolution Explorer* (GALEX) spacecraft during its ten-year mission. A python-based software suite allows users to query this database and construct calibrated light curves and images at user-specified temporal and spatial scales. The gPhoton project enables UV variability studies over short time-domains (seconds to minutes), and simplifies the creation of new GALEX images across mission phases. This is an initial release. We continue to improve the software, update documentation, and add new features. We encourage anyone interested to install the open-source software, ask questions, and provide feedback. User documentation, installation instructions, and a few quick examples of how to use the software are available here: <https://archive.stsci.edu/prepds/gphoton/>.

New products delivered by “GLASS” (Grism Lens-Amplified Survey from Space)

GLASS (Treu et al. 2015) is a Cycle 21 Large Program, consisting of 140 primary and 140 parallel orbits, targeting 10 massive galaxy clusters (including the 6 Frontier Fields clusters) using *Hubble* WFC3 and ACS grisms. The primary goal of the project is to obtain spectra of faint galaxies with unprecedented sensitivity and angular resolution. Data of the first galaxy cluster has now been released at MAST (MACS 0717.5+3745). The data at MAST include processed and extracted spectra of targets in the field, source catalogs, redshift measurements, and a wealth of diagnostic plots. For a complete description of the project and to access the data, please visit: <https://archive.stsci.edu/prepds/glass/>.

New WISP survey products now available at MAST

The WFC3 Infrared Spectroscopic Parallel Survey (WISP; Atek et al. 2010) is a *Hubble* parallel survey using the WFC3 to collect images, grism spectra, and generate source catalogs in nearby areas of the sky while other *Hubble* instruments are in use. The primary science drivers include measuring the star-formation rate of galaxies across 10 billion years of cosmic time, studying galaxy clustering on Mpc scales between redshifts $1 < z < 2$, constraining dust extinction/metallicity, and searching for $z > 6$ Lyman-alpha emitters. MAST is pleased to announce new data products, including images, extracted grism spectra, and source catalogs, for 136 parallel fields. For further details, please visit: <https://archive.stsci.edu/prepds/wisp/>.

New mosaics of M83 available at MAST

The M83 mosaic project has delivered new mosaic images (Blair et al. 2014) spanning seven fields across M83, using 15 filters from WFC3-UVIS and WFC3-IR. In addition to the mosaics from each filter (and a combined F547M+F555W version), we also provide access through our Interactive Displays, where you can combine any of the files to form custom three-color versions to preview. More details are available at: <https://archive.stsci.edu/prepds/m83mos/>.

Hubble Legacy Fields (HLF) Data Release 0.5

The *Hubble* Legacy Fields team (led by G. Illingworth) has released v0.5 products, consisting of three deep ACS/WFC3 regions (HLF-HUDFP2, HLF-HUDFP3, and HLF-HUDFP4). The release combines exposures from *Hubble*'s two main workhorse cameras, the Advanced Camera for Surveys Wide Field Channel (ACSWFC) and the Wide Field Camera 3 InfraRed Channel (WFC3IR), obtained over more than a decade, between mid-2002 to the end of 2014. For further details and access to the data, please visit <https://archive.stsci.edu/prepds/hlf/>.

Ultraviolet UDF (UVUDF) v2.0 release

The Ultraviolet Ultra-Deep Field (UVUDF) team (Teplitz et al. 2013) has released v2.0 mosaics in F225W, F275W and F336W of the data obtained in epoch 3 (see Rafelski et al. 2015). In this release, all the UVIS data have been fully recalibrated and re-reduced using a combination of standard and custom calibration scripts and reference files, to improve the low-level noise structure in the final images. In addition to the image mosaics, an aperture-matched PSF-corrected photometric catalog is also made available, including photometric and spectroscopic redshifts in this field. Please see <http://archive.stsci.edu/prepds/uvudf/> for more details and for the full products.

Hubble Frontier Fields high-level science products available in MAST

The *Hubble* Frontier Fields program (PI: J. Lotz/M. Mountain) has completed observations of the first four clusters, Abell 2744 MACS J0416.1-2403, MACSJ0717.5+3745 and MACSJ1149.5+2223, and have released v1.0 mosaics of all of these, for a total of 560 orbits to date (140 orbits per cluster, divided between two epochs, covering both the cluster and parallel field using ACS in the F435W, F606W

and F814W filters, and WFC3 in the F105W, F125W, F140W and F160W filters. The observations for the final two clusters (Abell 370 and Abell S1063) are scheduled from late 2015 until mid-2016. All products are (and will be) available at: <https://archive.stsci.edu/prepds/frontier/>.

The MAST Data Discovery Portal

We encourage all users to try the latest version of MAST Data Discovery Portal (accessible at <http://mast.stsci.edu/explore>) which enables graphical browsing and queries of images, catalogs and other data from all the missions currently available through MAST, as well as direct queries of other datasets available *via* the Virtual Observatory. The latest features include support for overlaying catalogs, interactive spectral previews, a time series/light curve viewer for *Kepler*/K2 data, and cross-matching data on a given target using different instruments and telescopes. Since early 2015, we have also provided access to the *Hubble* Source Catalog, both as a searchable database and as a resource against which to cross-match other source lists.

Hubble Legacy Archive (HLA) and Hubble Source Catalog (HSC)

The HLA (<http://hla.stsci.edu>) has made available Data Release 8.1, which includes interface enhancements to support the release of version 1 of the HSC. The HSC version 1 release (Budavari & Lubow 2012) includes updated WFC3 source lists that now go deeper than the previous version, and contains members of the WFPC2, ACS/WFC, WFC3/UVIS and WFC3/IR SOURCE EXTRACTOR source lists from the HLA. The cross-matching process involves adjusting the relative astrometry of overlapping images so as to minimize positional offsets between closely aligned sources in different images. Access is available through the MAST Discovery Portal, as well as through CASJobs for larger, more complex queries. For more details and for access to the entire catalog, please visit: <http://archive.stsci.edu/hst/hsc/>.

As always, please feel free to contact the MAST help desk (archive@stsci.edu) with questions, or contact us through Facebook (**MASTArchive**) or Twitter (**@MAST_News**) to provide suggestions on how we can improve our sites and services.

References

- Armstrong, D., et al. 2015, A&A, 579, 19
- Atek, H., et al. 2010, ApJ, 723, 104
- Blair, W., et al. 2014, ApJ, 788, 55
- Budavari, T., & Lubow, S. 2012, ApJ 761, 188
- Fleming, S., et al. 2014, AAS, 224, 322.04
- Million, C., et al. 2015, in preparation
- Rafelski, M., et al. 2015, AJ, 150, 31
- Teplitz, H., et al. 2013, AJ 146, 159
- Treu, T., et al. 2015, ApJ, accepted, arxiv:1509.00475
- Vanderburg, A., & Johnson, J. A. 2014, PASP, 126, 948
- Vanderburg, A., et al. 2015, ApJ, 800, 59

Mocking the Universe: Better Science through Data Simulation

Molly S. Peeples, molly@stsci.edu

As observational facilities and surveys continually increase in complexity and required precision, so too have the demands for realistic mock universes—and mock observations of those fake universes. In the past, data simulations have predominantly been used in the context of large surveys: characterizing contamination and completeness, understanding biases and covariances, and testing pipelines. These applications transitioned to *planning* future surveys and instruments. These end-to-end “life of a photon” pipelines require not only robust models of astrophysical sources and systematics, but also detailed models of how telescopes and instruments turn photons into observed data.

For many ongoing and upcoming facilities (e.g., *Webb*, *WFIRST*, *Euclid*, SDSS, Large Synoptic Survey Telescope [LSST], PanSTARRS, Dark Energy Survey [DES], the Extremely Large Telescopes [ELTs], *Gaia*, ALMA, etc.) simulated data is playing an integral role in both the planning and data interpretation stages. The timeliness of these topics motivated the Institute to host a workshop on astronomical data simulation at the end of July 2015. The conference was co-sponsored by the Infrared Processing and Analysis Center (IPAC), which together with the Institute, is performing *WFIRST* pre-formulation studies that include development of data simulation tools.

“Mocking the Universe” spanned two-and-a-half days with 8 invited talks, 24 contributed talks, 10 contributed posters, and many active discussion sessions. With nearly 70 participants from 10 countries, the workshop brought together for the first time many experts working on similar problems but from different angles. The program can be found at the Institute’s webcast archive (<https://webcast.stsci.edu/webcast/searchresults.xhtml?searchtype=20&eventid=225&sortmode=1>); the workshop also generated much discussion on Twitter from both local and remote participants (<https://storify.com/astronomolly/mocking-the-universe>). SOC members Greg Snyder and Josh Peek joined me for a Hubble Hangout (<https://www.youtube.com/watch?v=eMvHRTCQnFg>) hosted by Tony Darnell, Carol Christian and Scott Lewis the day after the workshop concluded.

It was evident throughout the workshop that data simulation blurs the lines between theory, observation, and instrumentation. The workshop opened with a pair of invited talks outlining the need for mock data. Risa Wechsler described how simulations, specifically when used to simulate full surveys such as the DES, can be used to not only predict physics, but also to fully understand the systematics—both astrophysical and data-based—of real datasets.

Mario Jurić then introduced the need for mock data from the perspective of designing and building the LSST. In particular, Jurić called out the tendency for mocks to be very “survey-specific,” and gave the workshop participants a list of questions to consider for the week: How do we avoid duplication of effort? How do we usefully share mocks? How do we verify mocks and communicate the limits of mock data? These themes carried through the rest of the workshop; one of the take-away messages for the meeting is that the individual pieces of mock data pipelines need to be more modular, with outputs that are standardized enough to be used as input in other data simulation pipelines.

Several themes pervaded the workshop. Philosophically, the questions asked were not the traditional “Do our simulations match reality?” but instead, “What can our simulation teach us about reality?” and, perhaps more significantly, “How do we observe our simulations like we do reality?” Scientifically, most of the talks related to galaxy evolution and cosmology.

Many talks focused on how to go “from models to mocks” for a wide range of models: hydrodynamic simulations (Snyder, Wise, Camps, Ceverino), semi-analytic models (Ascaso, Lemson, Norberg), and empirical models (Bruderer). The issues raised by these speakers—that better mocking requires faster computers with more memory, improved algorithms, multiscale simulations, better analysis of existing simulations, and easily accessible shared telescope models—continually recurred throughout the conference.

Marcia Rieke, the PI for *Webb*’s NIRCam instrument, described how data simulation guided the filter selection for NIRCam, and Sarah Kendrew discussed how pushing mock data through a full instrument model drives instrument development, specifically for integral field spectrographs for *Webb* and the European Extremely Large Telescope. Another session addressed dust (Baes, Chevallard, and Narayanan), with a particular focus on how necessary 3-D radiative transfer is for accurately capturing galaxy spectral-energy distributions including the effect of dust—which are in turn crucial for realistically modeling large galaxy surveys.

Data simulation is a powerful tool for simultaneously testing physical models and improving observational measurement methods. Andrea Font presented a method for detecting stellar streams in the Milky Way's halo; by using this method in both simulated data and *Gaia* data, the detections of streams from *Gaia* are both more robust *and* provide a direct comparison to the simulated stream properties. This approach was reiterated in talks on how to determine the “initial conditions” for galaxy mergers (Mortazavi), how to characterize satellite galaxies and their debris (Hendel, Wheeler), and fully exploiting information from both strong (Coe, Metcalf) and weak (Dawson, Mandelbaum) gravitational lensing.

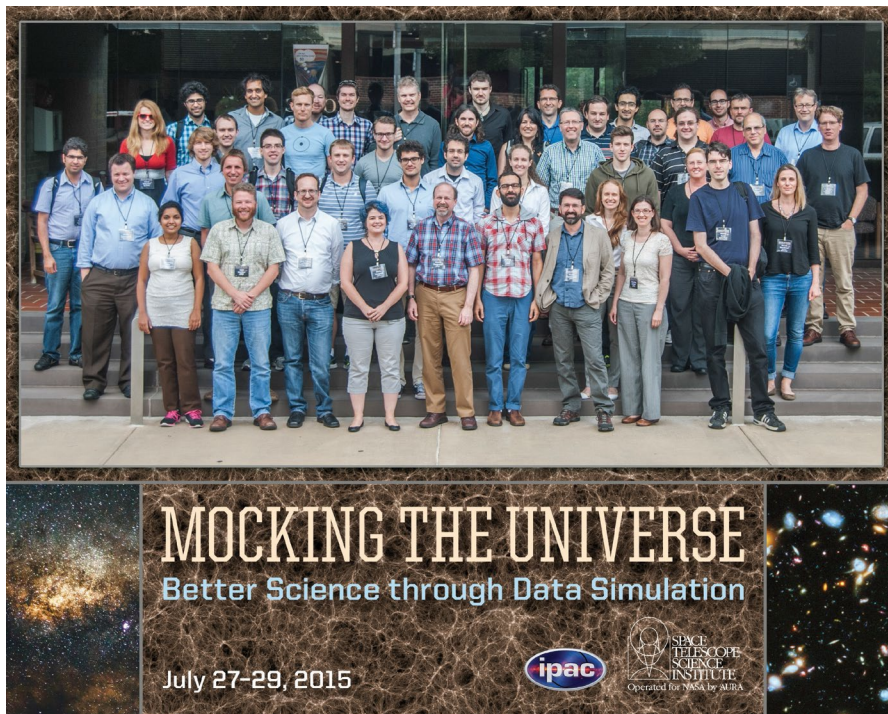
The gravitational lensing community has long been using realistic simulated images as inputs for “data challenges.” Central to these challenges are realistically simulated data with some well-defined signal that participants are challenged to measure. In her invited talk, Rachel Mandelbaum laid out the many lessons learned from the third Gravitational Lensing Accuracy Testing (GREAT3) data challenge, the most recent effort by the weak lensing community to compare how different codes are able to measure cosmic shear's subtle alteration of galaxy shapes—and to characterize the different biases inherent in different approaches. Mandelbaum pointed out that the way to best construct and execute a data challenge depends on its goal, e.g., to test existing pipelines or encourage new ones.

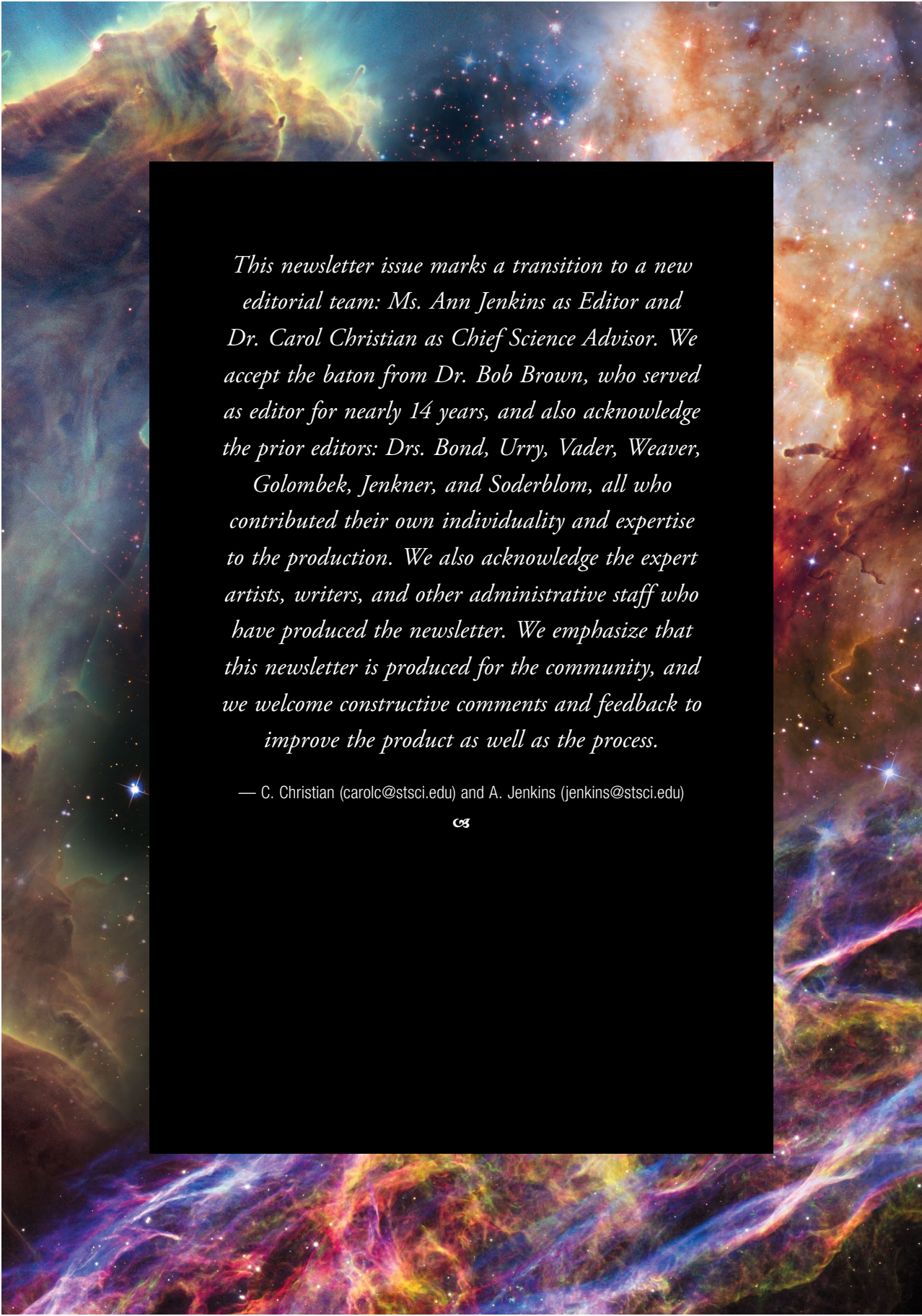
Long discussion sections were a central component of the workshop. The biggest take-away message from the meeting was that software engineering is becoming as crucial to our understanding of the universe as hardware engineering—and software certainly is crucial to fully capitalizing on the community's investment in instrumentation and new facilities. In this vein, astronomical data simulation software needs to be open source; this point was particularly well made by invited speaker Matt Turk when presenting the open-source software-analysis software, γT . But “open source” is not enough: the code needs to be well documented in order to be useable.

Moreover, the software needs to be modular so that different users with different needs and applications can use the pieces that are relevant for their purposes. As Josh Peek put it, while it is useful pedagogical exercise to reinvent the wheel, we should not all have to reinvent the internal combustion engine. But as the many talks at this workshop demonstrated, the current lay of the land is such that individual groups are continually reinventing which part of the life-of-a-photon pipeline they need for their own purposes, with data formats and code snippets that are very much *not* plug-and-play for other groups.

As astronomical data become larger, we have seen an increase in platforms that allow users to interact with and analyze data remotely on supercomputers, rather than downloading datasets onto their local machines. Simulated data need a similar platform, and this need will only increase as the size of simulations increase.

The meeting concluded with the consensus that “Mocking the Universe” merely helped get the necessary conversations started, with several participants expressing the desire for a data simulation workshop series. So, stay tuned for “Look Who's Mocking Too,” to be hosted by Matthew Turk at the National Center for Supercomputing Applications on the campus of University of Illinois in Urbana-Champaign in 2016.

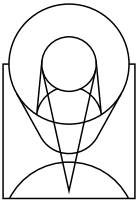




This newsletter issue marks a transition to a new editorial team: Ms. Ann Jenkins as Editor and Dr. Carol Christian as Chief Science Advisor. We accept the baton from Dr. Bob Brown, who served as editor for nearly 14 years, and also acknowledge the prior editors: Drs. Bond, Urry, Vader, Weaver, Golombek, Jenkner, and Soderblom, all who contributed their own individuality and expertise to the production. We also acknowledge the expert artists, writers, and other administrative staff who have produced the newsletter. We emphasize that this newsletter is produced for the community, and we welcome constructive comments and feedback to improve the product as well as the process.

— C. Christian (carolc@stsci.edu) and A. Jenkins (jenkins@stsci.edu)





Contact STScI:

The Institute's website is: **<http://www.stsci.edu>**

Assistance is available at *help@stsci.edu* or 800-544-8125.

International callers can use 1-410-338-1082.

For current *Hubble* users, program information is available at:

http://www.stsci.edu/hst/scheduling/program_information.

The current members of the Space Telescope Users Committee (STUC) are:

Michael Cushing (Chair), University of Toledo, *Michael.Cushing@utoledo.edu*

Jane Charlton, Penn State University

Hsiao-Wen Chen, University of Chicago

Jenny Greene, Princeton University

J. Christopher Howk, University of Notre Dame

Søren Larsen, Radboud University Nijmegen

Andrea Prestwich, Smithsonian Astrophysical Observatory

Brian Siana, University of California – Riverside

David Sing, University of Exeter

Ann Zabludoff, University of Arizona, Steward Observatory

The Space Telescope Science Institute Newsletter is edited by Ann Jenkins, *jenkins@stsci.edu*, who invites comments and suggestions.

Chief Science Advisor: Carol Christian, *carolc@stsci.edu*

Contents Manager: Sharon Toolan, *toolan@stsci.edu*

Design: Pam Jeffries, *jeffries@stsci.edu*

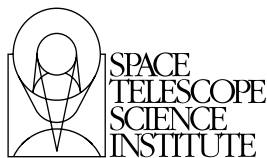
To record a change of address or to request receipt of the Newsletter, please send a message to *address-change@stsci.edu*.

Contents:

<i>Hubble's 25th Anniversary and Beyond</i>	1
From Cosmic Birth to Living Earths	4
<i>Hubble</i> Cycle 23 Proposal Selection	6
Lyman- α :	25
A Third Lifetime Position for COS/FUV	28
The Third COS/FUV Lifetime Position	32
Preparing for <i>JWST</i> Science	35
Small-Grid Dithers	40
NIRCam Ready for the Next Cryo Test	44
Supernova Cosmology in the Early Universe	49
Star-Forming Galaxies at $z \gtrsim 9$	51
The Most Massive Extragalactic Evolved Stars	54
Core-Collapse Supernova with <i>Webb</i>	56
The Biconical Outflow	59
New Insights on Exoplanet Atmospheres	63
Planetary Systems Around White Dwarfs	67
Vulcanism on Io with <i>Webb's</i> NIRISS	70
Barbara A. Mikulski Archive	73
Mocking the Universe	76

Calendar

<i>Hubble</i> Fellow Selection Committee Meeting	January 14–15, 2016
<i>Hubble</i> Fellows Symposium	March 14–16, 2016
Bahcall Lecture, Goddard Space Flight Center “Zooming in on the planet-forming zones of disks: Sweet results from ALMA” Ewine van Dishoek, Leiden University	March 29, 2016
Bahcall Lecture, Bahcall Auditorium, STScI 3:30pm - 4:30pm “Zooming in on the planet-forming zones of disks: Sweet results from ALMA” Ewine van Dishoek, Leiden University	March 30, 2016
2016 Spring Symposium: “What Shapes Galaxies? Rewriting the Hubble Sequence”	April 25–28, 2016
STUC Meeting	May TBD, 2016
<i>JWST</i> Advisory Committee Meeting	TBD May/June 2016
Workshop: “Mysterious Connection Between Superluminous Supernovae and Gamma-Ray Bursts”	May 23–25, 2016
<i>Hubble</i> Cycle 24 TAC	June 5–10, 2016
Exoplanets and Disks Workshop	September 12–14, 2016



3700 San Martin Drive
Baltimore, Maryland 21218

www.nasa.gov

NP-2015-11-360-GSFC

NON PROFIT
U.S. POSTAGE
PAID
PERMIT NO. 8928
BALTIMORE, MD